ABSTRACT

Title of Dissertation:	PHOTO-GUIDED SHAPE TRANSFORMATION OF COMPOSITE HYDROGEL SHEETS
	Hongyu Guo, Doctor of Philosophy, 2018
Dissertation Directed By:	Professor Zhihong Nie, Department of Chemistry and Biochemistry

Shape-changing hydrogel material has numerous potential applications in biomimetics, soft robotics, biomedicine, etc. Light as a clean energy source can be remotely delivered to material with high spatial and temporal resolution, which brings new controllability to shape-transformation of hydrogel material. However, the current strategy of using light to control deformation of hydrogel is limited. This dissertation aims to develop new approaches to program shape-transformation of hydrogel material by using light.

First, I developed a simple and efficient approach to re-program shape-transformation of composite hydrogel sheet with homogeneously distributed silver nanoparticle. By modulating light irradiation pattern, the same hydrogel sheet transformed to multiple distinct geometries, which were verified by finite element method.

Secondly, I developed a simple and reliable approach to pattern various types of photo-thermal converting nanoparticles in hydrogel sheet. The approach enables nanoparticle patterning in both lateral and thickness-direction of hydrogel, which cannot be readily achieved by other approaches such as microcontact printing and photo-lithography.

Thirdly, I explored shape transformation of composite hydrogel sheet with spatially patterned plasmonic gold nanoparticles fabricated by using the approach mentioned above. The same patterned composite hydrogel sheet can be designed to exhibit distinct shape transformation modes, highly depending on light irradiation direction, which has not been reported before.

Fourthly, I studied shape transformation of composite hydrogel sheet spatially patterned with erasable and rewritable iron oxide nanoparticles. The same hydrogel sheet was re-programmed to exhibit various distinct shape transformations by changing nanoparticle pattern. This provides a new method to reprogram shape transitions of hydrogel material by using external light source. In addition, a hydrogel tube was also readily patterned with iron oxide nanoparticles and its deformation was studied as well.

Lastly, I developed a simple and general approach to fabricate multifunctional composite hydrogel tube. The hydrogel tube was formed via self-rolling of 2D hydrogel sheet after releasing stress introduced during photo-polymerization. The introduced magnetic nanorod brought multi-functionality to the hydrogel tube. The self-rolled tube was used to load, transport and release cargo manipulated by capillary force, magnet and light, respectively.

This dissertation provides a new, simple and efficient toolset to program and re-program shape transformation of composite hydrogel material by using external light. It is believed that the toolset and concept developed in this dissertation can be applied to other light-responsive hydrogel material.

PHOTO-GUIDED SHAPE TRANSFORMATION OF COMPOSITE HYDROGEL SHEETS

by

Hongyu Guo

Dissertation submitted to the Faculty of the Graduate School of the
University of Maryland, College Park, in partial fulfillment
of the requirements for the degree of
Doctor of Philosophy
2018

Advisory Committee:
Professor Zhihong Nie, Chair
Professor Jeffery Davis
Professor Teng Li
Professor Paul Paukstelis,
Professor Gregory Payne, Dean's Representative

Dedication

To my parents, sister, brother-in-law, niece and nephew

Acknowledgements

There are many people to whom I would like to express my gratitude for their help and support during this journey.

First and foremost, I would like to thank my advisor, Dr. Zhihong Nie. It was him who taught me how to conduct independent research with his great patience and encouragement. It was him who guided me in writing articles and response letters for reviewers in a precise, concise and logical manner. It was also him who pointed out new research topic to me when my proposed research was not working well. He often said to me "think creatively". All in all, I owe him a lot and thank you, Dr. Nie.

Secondly, I want to thank my colleagues and friends. Ben and Jianying helped me get started with research by teaching me how to synthesize and assemble nanoparticles and how to fabricate light-responsive hydrogels. Yang and Guangyu gave good advice on analyzing data and polishing figures for publication. Yi helped me on resolving my concern when there was an issue with reproducibility in experimental result. Marcus and Kyle helped me in my dissertation writing. There are many other colleagues and friends with whom I ate and played. We discussed research, talked about concerns and shared happiness in life. Thank you, guys.

Thirdly, I would like to say thank you to people from our department. Working as teaching assistant for Dr. Friedman and Dr. Julin has been beneficial. I got tips from Dr. Friedman for organic synthesis. Dr. Julin's way of teaching inspired me and he often said to me "think about it". I also want to say thank you to Dr. Paukstelis who helped on my 3D printing which served an important tool for me to finish my dissertation.

Fourthly, I would like to thank my collaborator Professor Teng Li and his student Jian Cheng from Department of Mechanical Engineering. We discussed a lot about potential projects. It has been nice working with Jian Cheng. I learned from him that the description of a system should be and can be very precise, which helped me slow down and carefully design my following experiments. I also would like to thank Dr. Srinivasa R. Raghavan from Chemical Engineering Department for help on modulus measurement of my hydrogel samples.

Last but not least, I would like to express my great gratitude to my parents for raising me up, for educating and supporting me endlessly. I want to say thank you to my sister and brother-in-law who expressed their pure love for me. I also want to say thank you to my uncle and aunt who helped me get where I am now. Thank you, dear family.

Table of Contents

List of Figures

Chapter 1: Introduction

1.1 Shape-transformations in nature and artificial world

Shape transformation is ubiquitous in nature such as the coiling of a plant's tendril,[1] the snap-buckling of a Venus flytrap,[2] the unfolding of an ice plant seed capsule,[3] the wrinkling of plant leaves,[4-5] the opening of a pine cone,[6] and the twisting of a seedpod,[7] etc. (Figure 1.1). The remarkable self-shaping phenomena in nature has fascinated and continued to inspire artists, architects and research scientists for materials discovery. During the past decades, tremendous efforts have been devoted to understanding shape transformations in nature and engineering synthetic materials and structures to benefit mankind. [8-16] Recently, many types of self-shaping materials have been investigated, spanning a wide range from electroactive polymer/elastomer,[17-19] metallic films/alloy,[20-21] ceramic,[22] molecular crystal,[23-24] semiconductor nanomembrane,[25-26] graphene,[27-30] shape memory polymer,[31-33] liquid crystal polymer/elastomer,[34-37] polymer/elastomer film,[38-40] gels[41-45] to supramolecular assemblies,[46-47] colloid,[48] vesicles,[49] self-assembled nanoparticle membrane,[50-52] etc. (Figure 1.2). This dissertation will focus on advancing the potential of photo-responsive biocompatible hydrogels for shape transformations. Hydrogel material offer vast medical applications due to its biocompatibility, large volume change, and highly scalable nature. More importantly, self-shaping hydrogel has huge dimensional and geometric space that can be explored in order to design materials for possible applications in drug delivery, artificial muscle, biomedical device, tissue engineering, soft robots, microfluidics, adaptive optics and many others.[53-56]

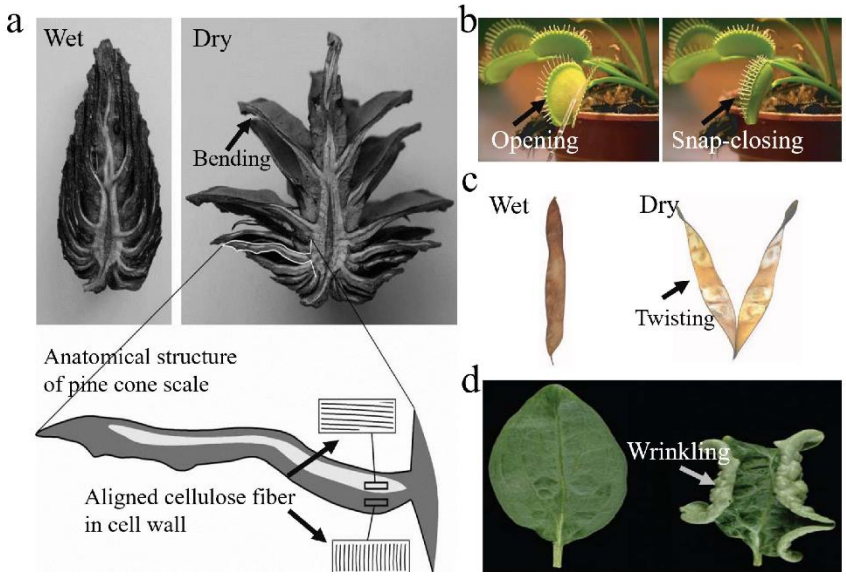

Figure 1.1 Shape transformations in nature. a) the opening/closing of a pine cone;[6] b) the snap-through buckling of a Venus flytrap;[2] c) the twisting of a seed pod;[7] d) the wrinkling of a plant leave during its growth.[4]

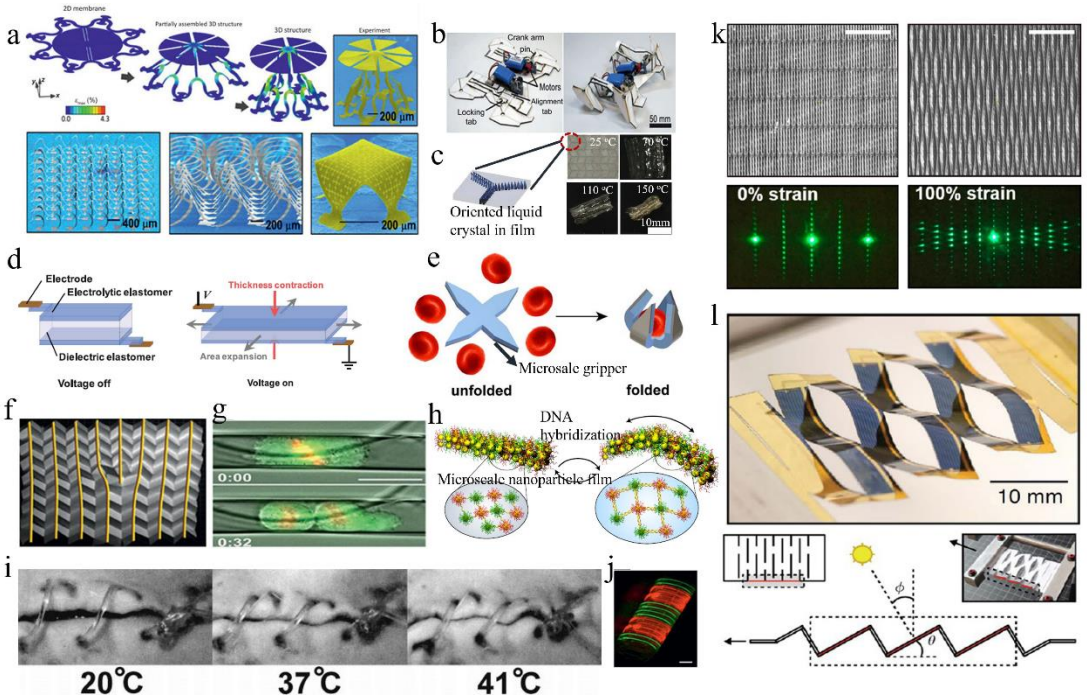

Figure 1.2 Shape transformations in artificial world. a) Buckling of device-grade semiconductor silicon nanomembrane from elastomeric substrate;[13] b) Self-folded soft robot enabled by shape-memory material;[13] c) Temperature-driven Miura-ori-type collapsing of liquid crystal elastomer film with patterned twisted nematic region in the film;[36] d) Voltage-driven expansion/contraction of electroactive dielectric elastomer with ionic hydrogel as the electrode;[57] e) Self-folded single-cell gripper based on strained SiO/SiO_2 thin film;[58] f) Miura-ori-type metamaterial with complex defect structure by folding a paper sheet;[13] g) Dynamics of an entrapped dividing HeLa cancer cell in self-rolled-up microtube device;[13] h) Self-folding of self-assembled microscale gold nanoparticle film driven by DNA hybridization;[51] i) Biodegradable shape-memory polymer suture for wound closure;[59] j) Self-rolling 3D microfluidics with dual fluidic channels filled with red and green dyes, respectively (scale bar: 500 μm);[13] k) Kirigami-based light diffraction grating made of Cr/Parylene C nanocomposite;[14] l) Kirigami-based solar tracking system.[14]

1.2 Shape-transformation of hydrogel material

Among shape-changing materials, hydrogels are unique due to their water-swollen networks. Hydrogel has long been studied as biological material due to its water-rich nature.[60-61] Recently, hydrogels are investigated as smart actuation materials since it changes its volume appreciably under environmental stimuli, such as temperature,[62-64] pH,[65] ionic strength,[66] enzyme,[67] DNA,[68] ions,[69] humidity,[70-71] light[28, 72-73] and external field,[74-75] etc. Generally speaking, differential swelling is needed in the hydrogel material in order to have out-of-plane deformation, such as bending (rolling), folding

and buckling.[16, 53, 55] Many approaches have been developed to achieve differential swelling in hydrogel material. These approaches usually utilize one of the two typical strategies to introduce differential swelling in the hydrogel material: i) generating a "layered" hydrogel system when stimulus is present, in which there is differential swelling in the thickness-direction of the material (Figure 1.3a); ii) generating differential swelling in lateral direction of the hydrogel material in the presence of stimulus, while the swelling state is homogeneous in its thickness-direction (Figure 1.3b). Representative examples in each strategy are given below.

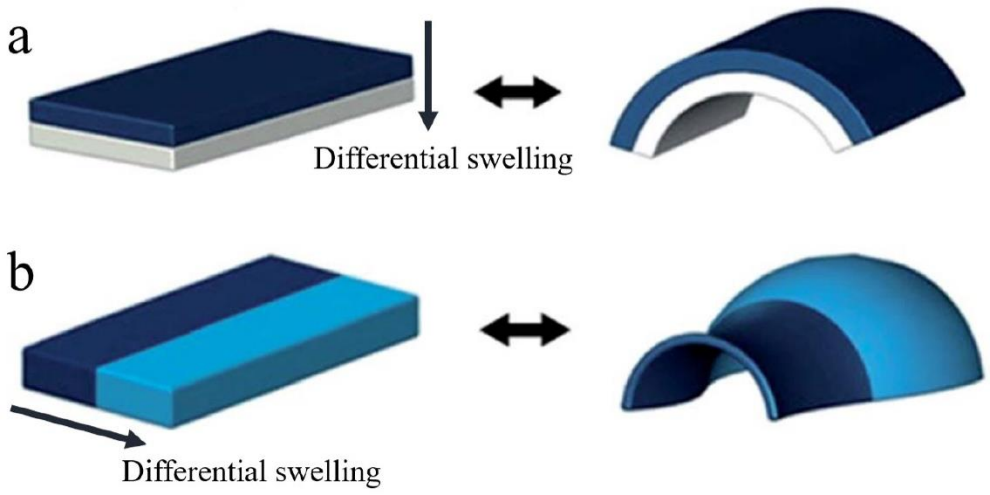

Figure 1.3 Two typical strategies to induce shape transformation of hydrogel material.[55] a) Differential swelling is introduced in thickness direction of hydrogel material; b) differential swelling is introduced in lateral direction of hydrogel material.

1.2.1 Shape-transformation of hydrogel with differential swelling in thickness direction

The differential swelling in hydrogel's thickness direction is the most used approach for shape transformation. Combining two materials that have different swelling ratios under stimulus is the most frequently used methods to introduce differential swelling in the thickness-direction of the hydrogel material. In this case, the hydrogel material usually has a bilayer structure composed of two different materials with distinct swelling extents.[76-77] For example, Stoychev *et al.* fabricated a bilayer hydrogel composed of poly(N-isopropyl acrylamide) (PNIPAM) layer which swelled in water and poly(ε-caprolactone) (PCL) layer that did not swell in water.[78-79] In the presence of water, the volumetric change of PNIPAM layer due to swelling generated stress in the interface between the two layers, causing the hydrogel to roll up from the substrate. The advantage of using a bilayer structure to introduce differential swelling is that the material in each layer can be greatly customized for targeted application. For example, Breger *et al.* fabricated a thermo-responsive gripper that folded up at physiological temperature and was used to capture and extract sample tissue.[80] In this work, the lower critical solution temperature (LCST) of the active layer was purposely tuned to a physiological temperature so that the bilayer hydrogel folded due to shrinkage of the active layer after being introduced to tissue. The passive layer was purposely chosen to enhance mechanical property of the gripper to aid in the tissue sampling. In the above examples, the thickness of the bilayer polymer hydrogel film were at microscale. Recently, Xu *et al.* fabricated an ultrathin (several nanometer) polymer-graphene composite film.[29] A thermo-responsive polymer, poly(N-isopropyl

acrylamide, PNIPAM), was grafted onto polydopamine-modified monolayer graphene sheet. At elevated temperature, the shrinkage of PNIPAM polymer induced the bending deformation of ultrathin graphene sheet. In addition to using temperature, many other biological signals, such as pH,[81-83] ion,[84] DNA,[68] etc. can be used as the stimulus in shape transformation of bilayer hydrogel.

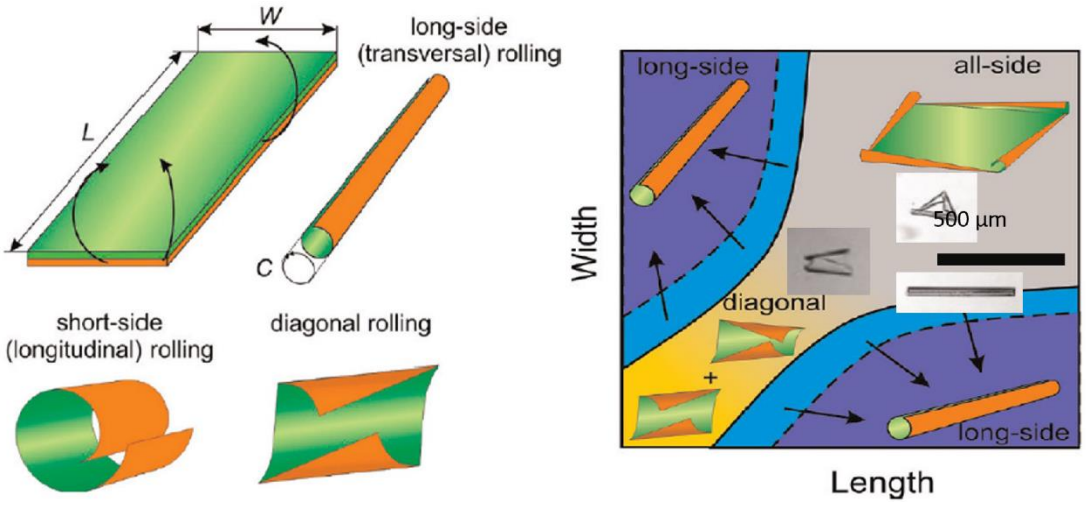

Figure 1.4 Shape-transformations of bilayer hydrogel sheet. The sheet exhibits different rolling modes depending on aspect ratio.[78]

In contrast to the global shape transformations of hydrogel in the examples mentioned above, localized bending can be achieved by introducing bilayer structure locally in the hydrogel material. For example, Na *et al.* introduced open areas in the passive layers in the fabrication of a trilayer sheet composed of a middle active layer (PNIPAM) and two passive layers (polystyrene) to generate localized bilayer structure.[85] These bilayer areas acted as local "hinges" in the subsequent folding of the

hydrogel sheet which aided in generation of mountains and valleys in the transformed geometry. By designing the position of the bilayer structure in the hydrogel, well-defined complex origami structures were achieved from the hydrogel sheet.

Bilayer hydrogel can also have well-tunable shape transformation by introducing preferential swelling direction in each layer of the bilayer hydrogel (Figure 1.5). For example, Erb *et al.* introduced microplates, structure-reinforcing elements, in hydrogel.[86] The microplates were aligned in the hydrogel in a certain angle with respect to the long axis of the hydrogel sheet. When the angle was 0^o, the composite hydrogel swelled or shrunk preferentially in the short axis direction, while when the angle was 90^o, the composite hydrogel swelled/shrunk preferentially in the long axis direction. When a bilayer hydrogel was constructed with microplates aligned differently in each layer, the bilayer hydrogel bent globally as well. The advantage of this approach is that the alignment direction of microplates with respect to long axis of the hydrogel sheet can be well tuned by magnetic field during hydrogel fabrication. Therefore other type of shape transformation such as helical transformation can be readily achieved from the bilayer hydrogel (Figure 1.5g-j).

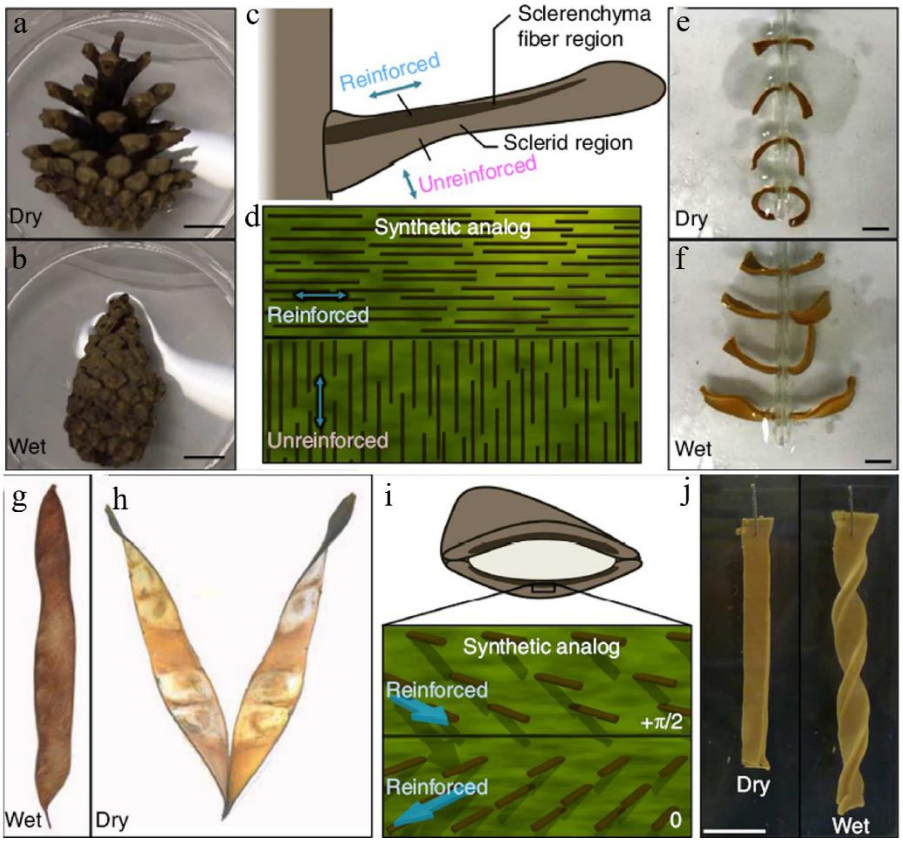

Figure 1.5 Shape transformations of bilayer hydrogel sheet with integrated preferential swelling direction in each layer by using structure-reinforcing element.[86] a,b) Opening and closing of pine cone scale; c) Structure of pine cone scale. Certain region in the scale is reinforced by aligned cellulose fiber; d) Synthetic analog of pine cone scale; e,f) Opening and closing of synthetic bilayer hydrogel sheet with structure-reinforcing element oriented in the sheet as shown in d; g,h) Twisting of seed pod; i) Synthetic analog of seed pod with structure-reinforcing element oriented with an angle to axis of the hydrogel sheet. j) Twisting of bilayer hydrogel sheet with structure shown in i).

Recently, Gladman *et al.* used 3D printing technique to generate layered hydrogel with aligned cellulose fibril in each layer.[87] Orientation direction of the fibril in the

hydrogel was determined by the printing path. Various complicated, controllable and predictable shape transformations were readily achieved from the hydrogel material.

Bilayer structure can be introduced in the hydrogel material on demand as well in addition to generating bilayer structure during hydrogel material fabrication. As an example, metal ions were locally introduced into ionic hydrogel which added ionic cross-linking in the hydrogel causing its local shrinkage.[69, 88] By modulating ion diffusion depth in hydrogel's thickness direction, a "bilayer" type structure was generated in the hydrogel, causing it to bend. Electric field was also used to drive ion movement to one side of the ionic hydrogel, generating bilayer structure on demand which induced bending deformation of the hydrogel.[89-90] Light was used to introduce bilayer structure in the hydrogel on demand as well. For example, Takashima *et al.* fabricated a covalently cross-linked hydrogel with host (adamantane) and guest (azobenzene) molecules grafted on the polymer network.[91] In the as-fabricated hydrogel, the host-guest interaction between adamantane and azobenzene added non-covalent cross-links in the network. When the hydrogel was subject to light, however, the molecular conformation change of azobenzene molecule caused dissociation of host-guest complex, which reduced hydrogel's cross-linking density and increased its swelling extent. By varying light penetration depth through hydrogel's thickness direction, a local bilayer type structure was generated in the material driving the bending deformation. In another example, graphene oxide was integrated in a thermo-responsive peptide hydrogel sheet.[73] When the composite hydrogel sheet was irradiated by near-infrared (NIR) light, the peptide hydrogel shrunk due to the heat generated by graphene oxide under NIR light irradiation. By varying light penetration depth through

the peptide hydrogel's thickness direction, local bilayer structure was generated which caused bending deformation of the composite hydrogel sheet. Humidity gradient was also used to generate bilayer structure in the hydrogel material to trigger its shape transformation.[71, 92-93]

1.2.2 Shape-transformation of hydrogel with differential swelling in lateral direction

Integrating differential swelling in hydrogel's lateral direction is another powerful strategy to guide shape transformation of hydrogel (Figure 1.6). The first experimental demonstration of shape transformation of hydrogel material by using this strategy was carried out by Klein *et al.*.[94] In this work, a polymer chain concentration gradient was integrated in the radial direction of a thermo-responsive disc-shape hydrogel by modulating hydrogel precursor concentration in the hydrogel fabrication process. At elevated temperature, the disc-shape hydrogel either transformed to a dome structure or transformed to a geometry with wavy edges in water due to laterally non-uniform shrinkage (Figure 1.6a). The authors proposed a theoretical model to explain the shape transformations and studied shape transformation of a tubular hydrogel with lateral swelling difference as well.

Later, Kim *et al.* developed a halftone lithography technique to generate two-dimensional swelling patterns in the hydrogel sheet by varying cross-linking density of the hydrogel film in 2D space.[95] This approach greatly increased the complexity of transformed 3D geometries (Figure 1.6b).

Wu *et al.* introduced lateral differential swelling in the hydrogel by locally generating a second polymer network in the pre-formed single-network hydrogel

sheet.[66] The double network region had distinct swelling property as compared to the single network region under stimulus. By varying location and orientation of the second network with respect to long axis of the hydrogel sheet, a wide variety of distinct transformed geometries can be designed (Figure 1.6c). Later on, the same group programmed the same hydrogel sheet to have multiple shape transformations.[96] This was achieved by integrating multiple polymer networks that responded to different stimuli into the pre-formed single hydrogel network. The same hydrogel sheet transformed to multiple 3D geometries triggered by different stimuli.

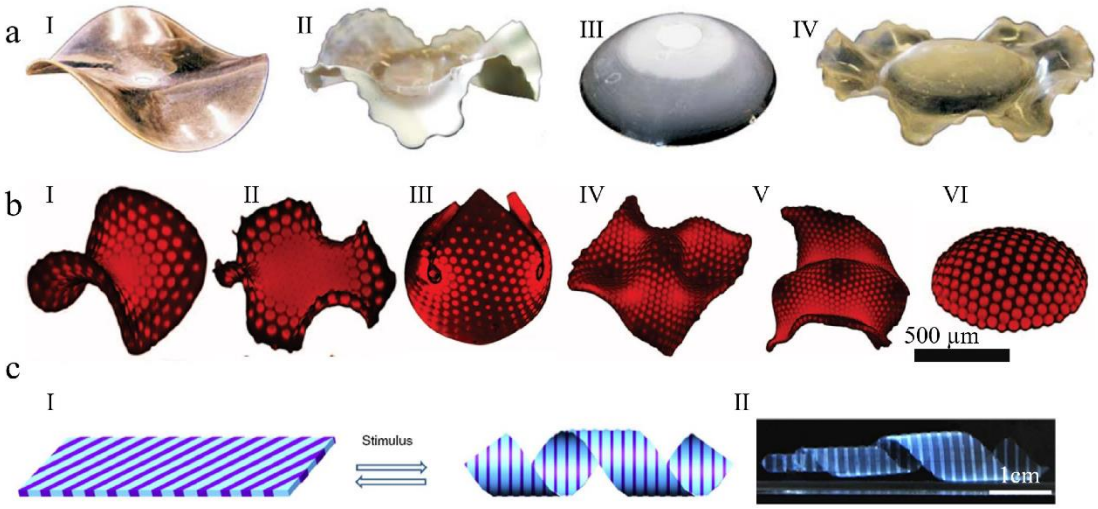

Figure 1.6 Shape transformations of hydrogel sheet with differential swelling in its lateral direction. a) shape transformation of hydrogel disc with radial gradient of monomer concentration during fabrication;[94] b) shape transformation of hydrogel disc with patterned high and low swelling regions;[95] c) shape transformation of hydrogel sheet with periodic stripes of different compositions, passing at an oblique angle with respect to the long axis of the sheet.[66]

As seen from above examples in sections 1.2.1 and 1.2.2, hydrogel material is often programmed to have one or several specific type of shape transformation upon stimuli. Achieving reprogrammable shape transformation from hydrogel material remains a challenge.

1.3 Shape transformation of photoactive material

Using light to control shape transformation of material has many advantages. First, light is a clean energy source. It can be remotely delivered to the material without contacting the material with high spatial and temporal resolution.[97] Second, various parameters such as light intensity, wavelength, polarization, irradiation time, irradiation pattern, etc. can be readily tuned to guide shape transformation of photoactive material.[98-99] A wide range of shape-changing photoactive material has been studied including elastomer,[100] vitrimer,[101] biopolymer film,[102] shape memory polymer,[103-104] molecular assembly,[105] liquid crystal polymer/elastomer[106-109] and gel.[110-115] Various types of light-responsive units have been integrated into photoactive material. Under light irradiation, the photo-responsive unit undergoes property change (such as hydrophobic-to-hydrophilic change,[113, 115] order parameter change,[106-107] dimerization content change,[104] etc.), which changes the swelling state or volume of the material resulting in its shape transformation. Or the photo-responsive unit generates heat (photo-thermal) under light irradiation,[110, 112, 116] which causes volumetric change of the material to achieve shape transformation. Usually, the light-responsive units are homogeneously integrated in the material which limits the type of

shape transformation achieved by light. Achieving reprogrammable shape transformations from photoactive materials by using light remains a challenge as well.

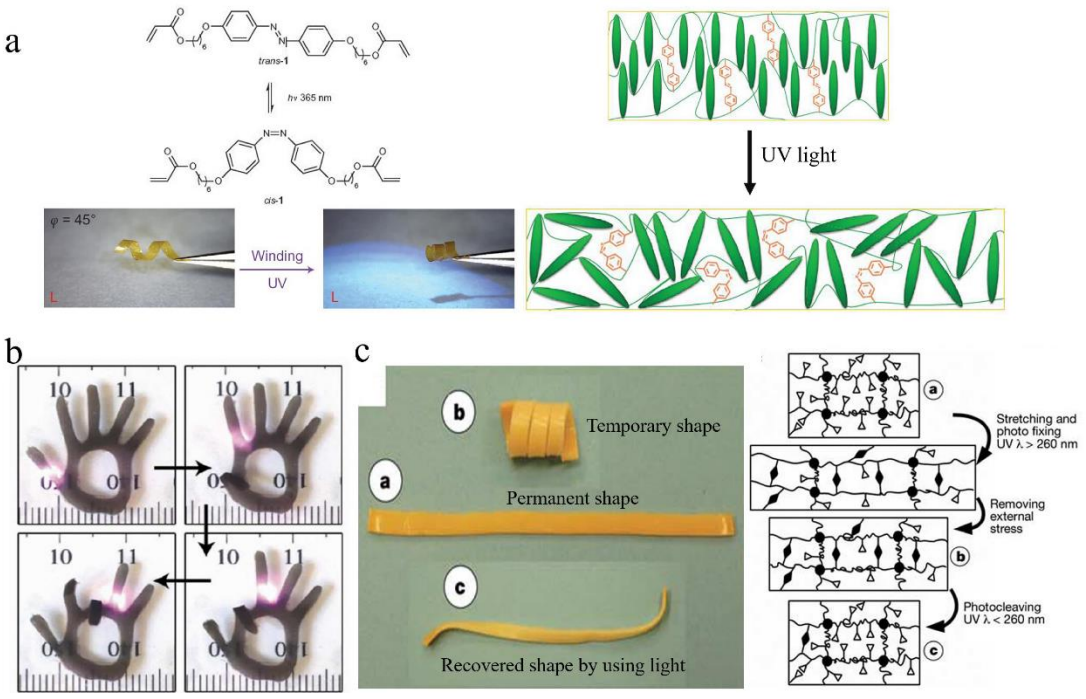

Figure 1.7 Shape transformation of photoactive material. a) Shape transformation of azobenzene-based liquid crystal film;[117] b) Bending of graphene-elastin peptide composite under near-infrared light irradiation;[73] c) light-induced shape memory polymer: the polymer was stretched and the shape was fixed by UV light (wavelength>260nm); the permanent shape was recovered when irradiated by UV light with wavelength< 260nm.[103]

1.4 Shape transformation of photoactive hydrogel material

As discussed in section 1.3, the study of photoactive shape-changing material is broad. As one of them, photo-responsive self-shaping hydrogel material has attracted increasing attention. A frequently used strategy is to integrate photo-thermal converting

agents into hydrogel material. Under light irradiation, the light energy is converted to thermal energy (photo-thermal mechanism), which increases temperature in the hydrogel. The increased temperature induces shrinkage of hydrogel, resulting in its shape transformation.[56] This photo-thermal mechanism was also used in mediating motion of a soft micromachine through remote control of its shape deformation. For example, Huang *et al.* integrated magnetic nanoparticle into a thermo-responsive hydrogel to prepare a swimming flagellum-type micromachine.[118] The magnetic nanoparticle was aligned in a certain angle with respect to axis of the material. Under rotating magnetic field, the soft material had directional movement in a viscous fluid. The swimming behavior of the soft micromachine, such as speed, could be controlled by transforming its body shape by using light via photothermal mechanism of the magnetic nanoparticle. In another example, photo-responsive azobenzene-based molecular unit was integrated in a humidity-responsive hydrogel material.[93] Motion behavior of the hydrogel material under humidity gradient was controlled by light which changed material's shape through light-induced molecular conformation change of azobenzene unit.

Up to date, most photo-thermal converting agents, such as graphene oxide, magnetic nanoparticle, plasmonic nanoparticle, carbon nanotube, etc. are homogeneously distributed in the hydrogel material. So far spatially patterning photo-thermal converting agents in shape-changing hydrogel material has rarely been explored. A recent study done by Zhu *et al.* patterned two types of plasmonic nanoparticles in hydrogel material through a layer-by-layer self-assembly approach.[119] The hydrogel material demonstrated two types of shape transformations under light

irradiation of different wavelengths. The shape transformations achieved by using this approach are far less complex than those accessed in liquid-crystal-film-based system.[34, 36] Integrating complex pattern of photo-thermal converting agents in hydrogel material is expected to bring in rich shape transformation modes to the material.

1.5 Application of shape-transforming hydrogel material

Shape-transforming material is a broad field and has potential applications in such as manufacturing, architecture, automotive, aerospace, packaging, soft robotics, actuator, biomedicine, artificial muscle, tissue engineering, optics, electronics, microfluidics, etc.[9, 13-14, 54] For shape-transforming hydrogel material, its usually weak mechanical property has limited its many applications. However, significant progress has been made to advance shape-transforming hydrogel to applications in such as biomedicine, soft robots, microfluidics, etc. over the past decades.

1.5.1 Application of shape-transforming hydrogel in biomedicine

Shape-transforming hydrogel, created using conventional photolithography techniques, has been studied in the microscale region as cell or drug carrier. For example, Shim *et al.* fabricated a pH-responsive bilayer hydrogel made of biocompatible polymer materials.[120] The bilayer hydrogel had a planar snowman shape in acidic conditions but folded into microcapsule in basic conditions (Figure 1.8a). This work made an important step towards drug delivery by using self-shaping material in that the microcapsule formed through folding of the hydrogel material was tight in this work, which eliminated drug leakage as compared with previous drug carrier using

self-shaping material. After delivering the microcapsule to site of interest (acidic area), the microcapsule opened up and released drugs in response to environmental change.

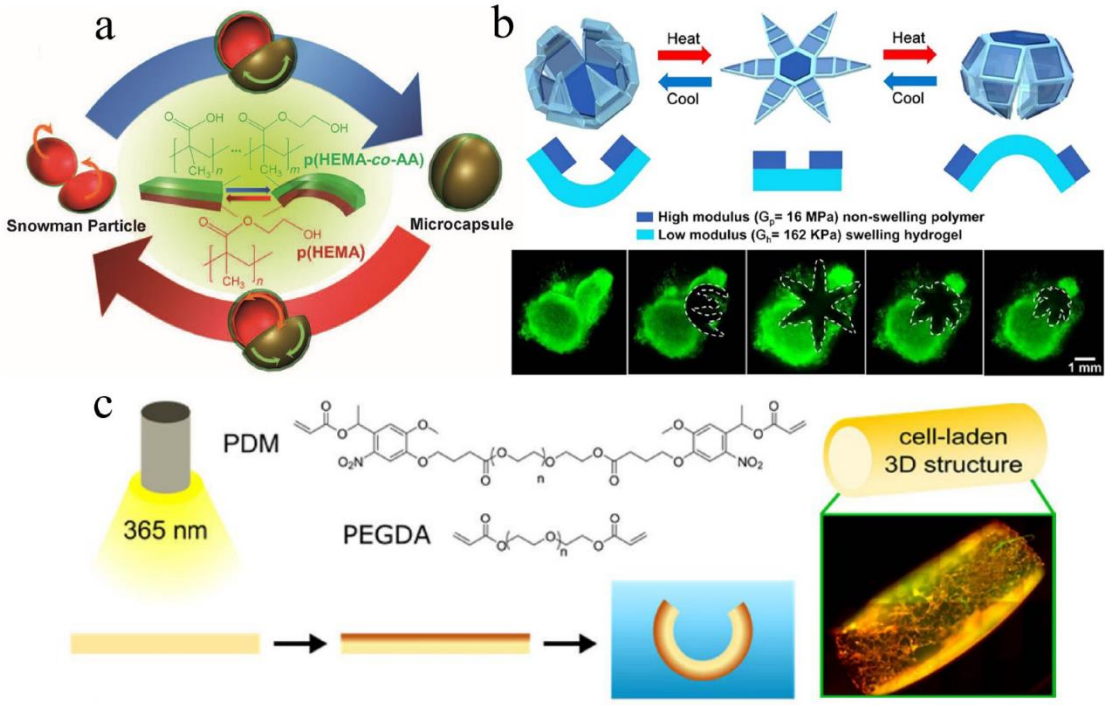

Figure 1.8 Application of shape-transforming hydrogel in biomedicine. a) Structural transformation of a microscale bilayer hydrogel composed of poly(hydroxyethyl methacrylate) gel layer and poly(hydroxyethyl methacrylate-co-acrylic acid) gel layer, depending on pH;[120] b) Shape-changing hydrogel made of a soft poly(N-isopropylacrylamide-co-acrylic acid) gel layer patterned with stiff polymer layer (Polypropylene fumarate) to enhance hydrogel's mechanical property to aid in extracting sample tissue at physiological temperature;[80] c) UV-light-triggered shape-change of cell-seeded planar poly(ethylene glycol diacrylate)-based hydrogel film with ortho-nitrobenzyl (o-NB)-based photodegradable polymer incorporated in the film.[121]

Another interesting work done by Breger *et al.* used self-shaping hydrogel material as a microsurgical tool to extract sample tissue.[80] In this work, a conventional polymer layer was used as swellable layer whose swelling extent was mediated by temperature (Figure 1.8b). On top of this layer, a non-swellable stiff polymer was segmentally cross-linked with bottom layer to form a bilayer structure. A six-sided star shape hydrogel was fabricated that folded up above physiological temperature. The introduction of stiff non-swellable polymer layer remarkably enhanced the mechanical property of the hydrogel gripper to make it grip on tissue tightly and excise the tissue later. The hydrogel gripper could be transported through tissue remotely with the help of magnetic field due to the presence of magnetic nanoparticle introduced in the hydrogel during its fabrication.

Shape-transforming hydrogel material can be used as a biological scaffold for cell culture. For example, Kapyla *et al.* fabricated a planar polymer hydrogel sheet seeded with cells.[121] The folding of the hydrogel sheet was triggered by subjecting the sheet to UV light irradiation which changed cross-linking density of the hydrogel by degrading ortho-nitrobenzyl (o-NB) moieties in the cross-linked network (Figure 1.8c). The important aspect of this work is that folding of the cell-seeded hydrogel sheet can be initiated on demand by using light which is in contrast with previous work in which the folding of the hydrogel sheet occurred after being introduced in the cell culture medium.

1.5.2 Application of shape-transforming hydrogel in soft robotics

Shape-transforming hydrogel has long been regarded as candidate in soft robotics in that it can sense its environment, transform its shape to generate motion and perform certain task. For example, Ma *et al.* fabricated a strong and flexible humidity-responsive polymer composite film with dynamic polyol-borate network that expanded or contracted in response to environmental moisture change.[71] The polymer film generated rapid continuous motion in the presence of water gradient which was used in a piezoelectric system to generate alternating voltage signal that was later stored in a capacitor. In addition, the polymer film could generate large contractile stress (up to 27 MPa) during water desorption and the film was used to lift up and transport load much heavier than its own weight. In another work, Mu *et al.* fabricated a light- and humidity-responsive graphene-based paper.[28] The un-reduced graphene oxide domain in the paper expanded and contracted in response to humidity change in the environment. Due to heat generated by graphene under light, the water content in the paper was controlled remotely by light as well. The graphene paper was designed to grip and release object, swim in a pipe, walk and make turns. Arazoe *et al.* fabricated a thin film consisting of a carbon nitride polymer that generated autonomous motion in an ultrafast manner (tens of milliseconds) in response to adsorption and desorption of a minute amount of water.[70] The film jumped high when heated or under light irradiation and it could be designed to exhibit unidirectional walking as well. Another interesting work utilized a completely different mechanism to construct self-walking hydrogel device.[122] In this work, cofacially oriented electrolyte nanosheet was introduced to the thermo-responsive poly(N-isopropyl acrylamide, PNIPAM) hydrogel. The expansion and

contraction of the hydrogel were modulated by the electrostatic repulsion between the nanosheets mediated by temperature, in sharp contrast with expansion or contraction of hydrogel modulated by swelling change. The composite hydrogel was designed to exhibit unidirectional walking by on-off switching of the stimulus. Self-walking hydrogel device based on on-off switching of electric field[75, 90] or based on Belousov–Zhabotinsky reaction has been demonstrated as well.[123]

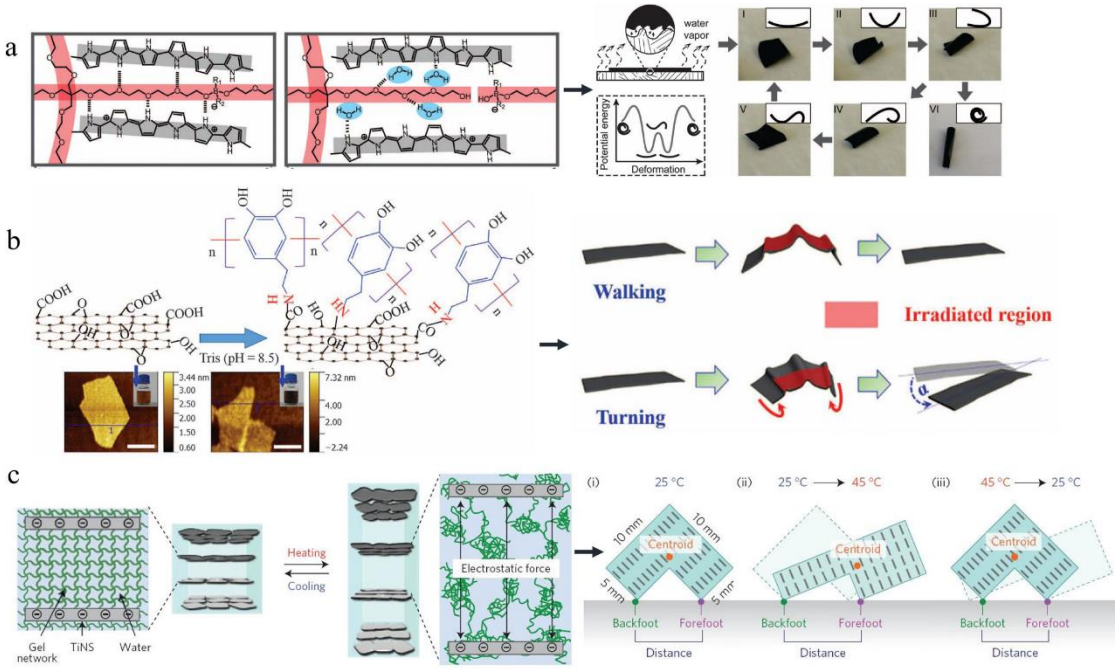

Figure 1.9 Application of shape-transforming hydrogel in soft robotics. a) Cyclic motion of humidity-responsive polymer composite film with dynamic polyol-borate network on moistened paper;[71] b) Light-guided walking and turning of graphene-based sheet;[28] c) Self-walking of composite hydrogel under cyclic heating and cooling.[122] The expansion and contraction of the hydrogel was due to electrostatic interaction change

between incorporated titanate nanosheet (TiNS), which was mediated by temperature-induced permittivity change in gel network.

In addition to self-walking hydrogel device as mentioned above, shape-transforming hydrogel was also used as microswimmer. For example, Kwon *et al.* fabricated electroactive hydrogel aquabot with a diverse range of functionality, such as swimming, sensing, catching, moving and releasing cargo, etc. mediated by electric control signal.[124] As another example, Huang *et al.* fabricated a magnetically-powered soft hydrogel microswimmer.[118] A folding axis is introduced in the hydrogel by aligning magnetic nanoparticle in a certain direction during fabrication. Upon swelling in water, the planar hydrogel transforms its shape to flagella morphology mimicking microorganism. The motion of the microswimmer was mediated by magnetic field direction as well as by changing the body shape by using light irradiation. The first autonomous entirely soft hydrogel robot was recently demonstrated by Wehner *et al.* in which soft controller, fuel reservoir (on-board power source), actuation mechanism, etc. were integrated in the hydrogel robot.[125]

1.5.3 Application of shape-transforming hydrogel in microfluidics

Shape-transforming hydrogel can also be integrated with microfluidics to manipulate flow.[126] For example, Yu *et al.* integrated two pH-responsive straight bilayer hydrogel strips within a microfluidic channel.[127] In basic conditions, the two bilayer hydrogels bent toward each other forming a check valve. The forward flow pressure opened the valve so that flow could pass while the back pressure closed the valve, preventing backflow. By treating the bilayer hydrogel strip with acidic solution,

the bilayer hydrogel strip recovered its straight shape and the valve was open, allowing fluid to pass in both forward and backward directions. By subjecting the bilayer hydrogel to basic condition, the two bilayer hydrogel strips reformed the check valve, recovering flow manipulation. In another work, Jamal *et al* fabricated a 3D microfluidic device through shape-change of a planar polymer film after solvent treatment.[128] Though the polymer film used to drive deformation of the device is not hydrophilic, the concept may apply to hydrogel-based 3D microfluidic which may have its own advantage. For example, hydrogel-based 3D microfluidic will allow transportation of nutrients through permeable wall of the channel.

1.6 Scope and organization of dissertation research

This dissertation aims to develop versatile approaches to reprogram shape transformation of photoactive hydrogel material. It also aims to develop simple and effective approaches to pattern photo-responsive units in hydrogel material to achieve complex shape transformation under light. The dissertation research is organized as follow: Chapter 2 discusses the development of a simple approach to reprogram shape transformation of photoactive hydrogel material with homogeneously distributed light-responsive units. Chapter 3 presents a general approach to pattern inorganic nanoparticles (NP) in hydrogel material. The inorganic nanoparticles include platinum NP, palladium NP, gold NP and iron oxide NP (Fe_3O_4 NP). Chapter 4 explores the shape transformations of photoactive hydrogel spatially patterned with gold NP using the approach developed in Chapter 3. Chapter 5 studies the reprogrammable shape transformation of photoactive hydrogel patterned with Fe_3O_4 NP. Fe_3O_4 NP can be

erased and re-integrated in the hydrogel. Chapter 6 examines a general one-step approach to fabricate self-rolled photoactive tubular hydrogel material. Chapter 7 concludes the dissertation and proposed future research work.

Chapter 2: Reprogrammable ultra-fast shape-transformation of macroporous composited hydrogel sheets

Chapter overview

In this Chapter, we reported a simple and effective approach to reprogram shape transformation of composited thermo-responsive poly(N-isopropyl acrylamide) (PNIPAM) hydrogel sheet with homogeneously distributed plasmonic nanoparticle (AgNP). By varying irradiation patterns, multiple (unlimited in theory) shape transformations were achieved from same hydrogel sheet. The shape transformations arose from the localized shrinkage of the hydrogel sheet under laser irradiation due to photothermal heating of AgNP. The shape transformations were verified by FEM analysis. I performed experiments in this Chapter and our collaborator Jian Cheng conducted the FEM analysis.

This chapter was adapted from the manuscript published in the following article: Guo, H. Y., Cheng, J. (co-first author), Wang, J. Y., Huang, P., Liu, Y. J., Jia, Z., Chen, X. Y., Sui, K. Y.*, Li, T.*, and Nie, Z. H.*, Reprogrammable ultra-fast shape-transformation of macroporous composite hydrogel sheets, *J. Mater. Chem. B*, **2017**, 5, 2883-2887

2.1 Introduction

Nature is replete with self-adaptive phenomena. Examples include humidity-mediated opening of plant organs, leaf wrinkling, tendril coiling, Venus flytrap, etc..[1-3] Inspired by nature, researchers have made great efforts to design and fabricate adaptive polymeric hydrogel materials that are capable of transforming in response to environmental stimuli, such as temperature, pH, ions, electricity, humidity, external

field and light, to name a few.[53, 55] Self-shaping hydrogel materials have found a wide range of applications in such as soft robotics, artificial muscles, biomedicine, microfluidics, actuators, etc..[53-54, 129] Generally, a stimuli-induced differential swelling within the hydrogel is required for it to bend, twist and fold.[53] As an example, a hydrogel sheet with a bilayer structure can bend upon temperature change due to the mismatch in the extent of swelling between the two layers.[63-64, 79] Among various environmental stimuli, light is particularly attractive as it can be implemented without contacting the material and can be remotely controlled.[73, 130-131] Light has been used to actuate liquid crystal films,[101, 117, 132] bend reduced-graphene-oxide-elastin composite,[73] and transform polymer-inorganic hybrid network[119] and carbon-nanotube-doped polymer film, etc..[101, 133]

It is truly amazing that in nature octopus can transform to adapt almost arbitrary shapes in order to survive.[134] The ability to mimic octopus's morphing strategy and design self-shaping hydrogel materials that are capable of transforming into rich shapes is needed. At present, most self-shaping hydrogel materials are designed to acquire one or few specific pre-determined shapes through preprogrammed shape transformations in response to external stimuli.[66, 78, 85, 95] In this case, one or more responsive components are patterned in the hydrogel sheet and the types of target shapes are often predetermined at the stage of patterning. Kumacheva and coworkers recently reported that the same hydrogel sheet patterned with multiple responsive components can be transformed into three different shapes upon exposure to different stimuli.[96] The state shapes that can be transferred from the pre-patterned hydrogel, however, is restricted by the limited number of responsive components that can be integrated in the sheet and

interference between these components in response to a specific stimulus. Recently, Hayward et al. demonstrated that the shape transformation of light-responsive composited hydrogel can be modulated to produce multiple shapes by controlling light irradiation patterns.[135] It is striking that the configurations that can be achieved from the same piece of these hydrogel sheets are infinite in theory. In their work, a characteristic response time of $\tau \approx 2\text{-}3$ s was found for their composited hydrogel with a thickness of 25 μm. However, since the gel shape-transforming rate (τ) increases quadratically with the thickness (h_o) of the hydrogel film as $\tau \sim h_o^2$, the transformation of a thicker hydrogel sheets would be rather slow. As an example, it would take up to fifteen minutes to reach equilibrium state in shape when the thickness is approximately 500 μm.[135] Previous studies suggest that introducing pores within self-shaping hydrogels can greatly increase the shape-transforming rate of hydrogels due to enhanced mass transport.[64, 73] However, to date a fast on-demand transforming hydrogel with macropores has never been demonstrated.

Here we report the design of a macroporous hybrid hydrogel sheet that can undergo an ultra-fast shape-transformation and acquire at least five (unlimited number in theory) well-defined geometric configurations in response to near-infrared (NIR) light (Figure 2.1). The macroporous hybrid hydrogel sheet is composed of thermo-responsive polymer, poly (N-isopropyl acrylamide) (PNIPAM) embedded with silver nanoparticles (AgNPs) that are capable of converting absorbed light to heat (so-called photothermal effect). Both our experimental and computational studies showed that the light-triggered shape transformation arises from the combination effect of the photothermal heating of AgNPs and thermo-responsiveness of PNIPAM. The

representative shapes obtained from the same hydrogel sheet include helical, boat-like, hoof-like, and saddle-like structures. The presence of macropores in the sheet significantly enhanced the transport of water molecules when it underwent swelling or shrinkage,[136] thus enabling the rapid reversible shape transformation of the hydrogel sheet. The shape transformations reached maximum on the order of seconds while it usually takes minutes or even hours for a macroscale nonporous hydrogel of similar thickness to reach its maximum transformation.[96] There are several important features of the design, which distinguish this work from others, including: i) the hydrogel bears macropores and hence the shape transformation is extremely fast; ii) the hydrogel material is reprogrammable and multiple well-defined shape transformations (at least five) are obtained from the same 2-D sheet; iii) light as a stimulus can be remotely controlled. iv) NIR light is less harmful than UV and visible light, and has a larger penetration depth to biological tissues.

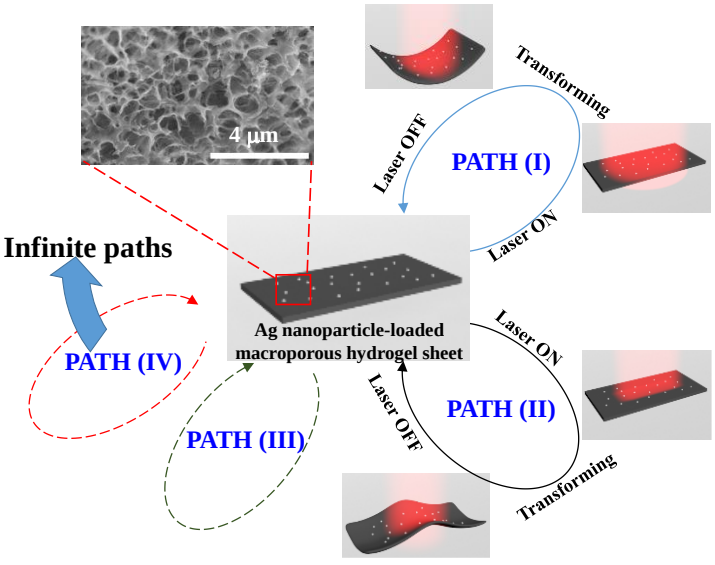

Figure 2.1 Schematic illustration of a hybrid hydrogel sheet that can transform into different geometries in response to near-infrared (NIR) light. The hybrid

hydrogel sheet consists of macroporous PNIPAM hydrogel embedded with silver nanoparticles (AgNPs) capable of converting absorbed light into heat. When subjected to NIR laser irradition with different patterns, the same hydrogel sheet can transfer into different geometries; and it recovers its orignal flat shape when the laser is off. SEM image in inset shows the macroporous feature of the hydrogel sheet.

2.2 Experiments

2.2.1 Materials

N-Isopropylacrylamide (NIPAM), N,N'-Methylenebisacrylamide (BIS), silver nitrate ($AgNO_3$), sodium borohydride ($NaBH_4$), ascorbic acid, sodium hydroxide, poly(ethylene glycol) (PEG, MW 6000), 2-hydroxy-2-methylpropiophenone (photo-initiator) were purchased from Sigma-Aldrich (USA) and used as received.

2.2.2 Synthesis of macroporous PNIPAM hydrogels

0.1785 g NIPAM monomer, 0.0575 g PEG (MW 6000) and 0.0226 g BIS were dissolved in 1 mL Nanopure water in a glass vial. 2.25 μL photoinitiator (2-hydroxy-2-methylpropiophenone) was then added. The vial was shaken by hand to make a homogeneous solution mixture. Two pieces of glass slides were separated by parafilms with a thickness of 0.5 mm, which was used as a holder for the monomer solution. The monomer solution and the holder were kept in a refrigerator (4 ℃) for 30 minutes. Then the monomer solution was injected to the holder. The polymerization was conducted by using a hand-hold UV lamp with 254 nm as the excitation wavelength. During the

polymerization, the holder was kept on a glass petri dish which floated on the surface of an ice-water bath. After the polymerization, the hydrogel was immersed in a large amount of water for at least 1 day to leak out the unreacted chemicals, non-cross-linked polymers and PEG. Then the hydrogel was cut into a rectangular shape (length: 1.70 cm; width: 0.85 cm) or other shapes (star, stripe, disk, etc.) for the fabrication of PNIPAM-AgNPs hybrid hydrogels.

2.2.3 Synthesis of PNIPAM-AgNPs hybrid hydrogels

The silver nanoparticles (AgNPs) were grown in situ within the macroporous PNIPAM hydrogel sheet. Briefly, the macroporous PNIPAM hydrogel sheet was immersed in 2 mL $AgNO_3$ solution (0.04 mg/mL) for 30 minutes. It was then transferred to a plastic petri dish and 5 mL freshly-prepared $NaBH_4$ (0.4 mg/mL) was added to reduce the silver nitrate within the hydrogel for 30 minutes to obtain silver (Ag) seeds. The Ag-seed-containing hydrogel sheet was put in water to remove excess $NaBH_4$ on its surface and then immersed in 2 mL $AgNO_3$ growth solution (1.7 mg/mL) in a glass vial for 30 minutes. A 200 μL of ascorbic acid (17.6 mg/mL) was then added to the growth solution, followed by the quick addition of 200 μL sodium hydroxide (40 mg/mL) while gently shaking the vial. After 5 minutes, the vial was put in a 29 ℃ water bath for 2 hours. Finally the hybrid hydrogel sheet was put in 29 ℃ water which slowly cooled down to room temperature. Before doing light-mediated shape transformation, the hybrid hydrogel sheet was immersed in a large amount of water for at least 24 h for the AgNPs to stabilize in the hydrogel. We point out that the hybrid hydrogel sheet can be kept in water for two years without losing the ability in shape transformation when

subject to NIR light. For the control experiments, we fabricated macroporous hydrogel but without loading AgNPs. We also synthesized non-porous hydrogel without using PEG, the pore-forming reagent. Then we loaded AgNPs in the non-porous hydrogel in situ by using the same experimental conditions as that for macroporous hybrid sheet. These hydrogels were also subject to NIR light irradiation. We found that the pristine macroporous hydrogel sheet without AgNPs barely deformed (Figure 2.S1). We also found that the non-porous hybrid sheet slowly and slightly deformed under NIR irradiation (Figure 2.S2).

2.2.4 Light-triggered shape transformations

An 808 nm laser (MDL-N-808, Changchun New Industries Optoelectronics Technology Co., Ltd, China) was used as the light source and it worked at 5 watts throughout the experiments. During the experiments, the hybrid hydrogel was immersed in 100 mL water in a glass petri dish. Aluminum foil was used to make the photo mask which was attached onto a glass slide. The distance between the laser and the glass slide was adjusted to make sure the light spot took on the shape indicated by the photo mask.

2.2.5 Hydrogel swelling

The swelling property of the hybrid hydrogel sheet was characterized by using the swelling ratio which was measured gravimetrically after wiping off the excess water on the hydrogel's surface with a piece of Kimwipes in the temperature range from 22 to 36 ℃. The hybrid hydrogel sheet was incubated in a water bath for at least 48 h at each temperature. The swelling ratio was calculated by using the following formula[136]

$$\text{Swelling ratio} = W_s/W_d$$

where W_s is the weight of the swollen hydrogel at the particular temperature and W_d is the dry weight of the hydrogel.

2.2.6 Mechanical property

An AR2000 stress-controlled rheometer (TA Instruments) was used to study the mechanical properties of the hybrid hydrogel sheet. Rheological experiments were performed at 22 ℃ and 32 ℃, respectively by using cone-and-plate geometry (25 mm diameter and 2^o cone angle). A solvent trap was used to minimize drying of the sample during measurements. Dynamic stress-sweep experiments were first performed on the sample to identify its linear viscoelastic (LVE) region at different temperatures and dynamic frequency sweeps were then performed within the LVE region.

2.2.7 FTIR measurements

The compositions of the hydrogel sheet were analyzed by FTIR in the region of 650-4000 cm^{-1}. Before the measurement, the hydrogel samples were swollen for at least two days at room temperature and then were freeze-dried for 24 h. The dried hydrogel samples were directly put under the FTIR probe and the spectra were taken, which was shown in Figure 2.S3. From Figure 2.S3, it can be seen that the compositions of pure PNIPAM hydrogel, PEG-modified PNIPAM hydrogel and PEG-modified PNIPAM-AgNP hybrid hydrogel were the same. There exists a typical -C=O stretch band of PNIPAM at around 1644 cm^{-1} and a representative -N-H vibration band of PNIPAM at about 1538 cm^{-1}. In addition, there is no typical -C-O stretch band of PEG at around 1100 cm^{-1}. These findings indicated that the PEG only acted as a pore-

forming agent and did not react with the NIPAM monomer in the fabrication of PNIPAM hydrogel. The same conclusion was also reached in the previous report on PEG-modified PNIPAM hydrogel synthesized via a redox method.[136]

2.2.8 Optical property of hybrid hydrogel sheet

The optical property of the hybrid hydrogel sheet was characterized by measuring its absorbance using UV-Vis spectroscopy (Lambda 40 UV/VIS Spectrometer, PerkinElmer, USA). Briefly, swollen hybrid hydrogel sheet and PEG-modified PNIPAM hydrogel sheet of the same size were put onto a glass slide respectively. The excess water on the glass slide was removed by using Kimwipes to make sure the hydrogel sheet attached to the glass slide. Then the glass slides were put in the reference and sample light paths respectively. The hydrogel sheets were adjusted to be of the same position on the glass slides. The UV/VIS spectra were then taken in an absorption mode at a slit width of 1 nm, scanning speed of 480 nm/min and data interval of 1 nm.

2.2.9 Surface morphology of hydrogel sheet

The surface morphologies of the PEG-modified PNIPAM hydrogel and hybrid hydrogel sheet were studied by using scanning electron microscopy (XL Series-30, Philips, USA) (Figure 2.S4). Samples of the freeze-dried hydrogels were coated with either carbon (JFC-1200 Fine Coater, Japan) or gold prior to the SEM examination. From Figure 2.S4 a), it can be seen that the PEG-modified PNIPAM hydrogel sheet had a macroporous structure with pore sizes estimated to be in the range of 200 nm to 1 μm. After AgNPs were fabricated within the hydrogel, the pore size remained similar as that in the PEG-modfied PNIPAM hydrogel (see Figure 2.S4 b)). As Figure 2.S4 c)

showed, there was a sharp difference between the surface of the hybrid hydrogel sheet and its cross-section. We claim that the photothermal property of the hybrid hydrogel sheet under the 808 nm light was mainly due to the absorbance of the AgNPs from the hydrogel surface.

2.2.10 Photothermal property of hybrid hydrogel Sheet

The photothermal property of the hybrid hydrogel sheet was studied by photothermal imaging technique. Briefly, the hybrid hydrogel sheet was immersed in 100 mL water in a glass petri dish and was irradiated with an 808 nm laser at a power of 5W for 2 min and then the laser was shut off for another 3 min. During the irradiation, the laser spot that reached the hydrogel sheet took on a stripe shape due to the photomask used. The surface temperature of the hybrid hydrogel sheet was monitored by using a FLIR SC300 infrared camera (FLIR, Arlington, VA). Real-time thermal images were captured with frame rate at 60 Hz, and analyzed by FLIR Examiner software. We found that the hybrid hydrogel sheet started to bend while its surface temperature increased from 21 ℃ to 32 ℃ during the irradiation process and it went back to its original shape when it cooled down. We point out here that the surface temperature of the hybrid hydrogel sheet can increase to 40 ℃ by reducing the distance between the laser and the hydrogel surface (data not shown).

2.2.11 Free energy model of temperature-responsive hydrogel

In our PNIPAM hydrogel, the interacting aggregation of cross-linked polymer chain network and solvent molecules constitutes a thermodynamic system of which the macroscopic behaviors are governed by its thermodynamic energetics. The

deformation of PNIPAM hydrogel in balance with mechanical loads and a solvent reservoir can be modeled by the framework developed by Cai and Suo[137]. By thermodynamics consideration, the Helmholtz free energy of a swelling hydrogel arises from two origins: i) the stretching of the polymer network and ii) the mixing of the two species of molecules. Hence the free energy density function takes the form:

$$W = \frac{1}{2}NkT[\mathbf{F}:\mathbf{F} - 3 - 2\log(J)] + kT\left[c\log\left(\frac{vc}{1+vc}\right) + \frac{(A_0 + B_0T)c}{1+vc} + \frac{(A_1 + B_1T)c}{(1+vc)^2}\right] \quad (1)$$

where W is the free energy per unit volume in the dry state, N is the number of polymer chains per unit volume in the dry state, k is Boltzmann constant, T is the current temperature at the material point, **F** is the deformation gradient tensor which takes the original dry state as reference frame, J is the Jacobian of deformation gradient tensor, i.e., J=det(**F**), v is the molecular volume of water, c is the relative concentration of solvent molecules in the hydrogel-solvent aggregation, and A_0, B_0, A_1 and B_1 are parameters related to the enthalpy of mixing. The first term in Equation (1) denotes that the stretching of polymer chain network obeys a neo-Hookean hyperelastic material law, and the second term implies that the mixing of PNIPAM polymer and water molecules follows the Flory-Huggins theory of solution[138]. A_0, B_0, A_1 and B_1 in Equation (1) are to be fitted to the experimental data for different temperature-responsive hydrogels, as we will identify in the immediate section for our PNIPAM-AgNPs hybrid hydrogel.

Equation (1) specifies the explicit expression of the free energy density function which takes the extensive variables **F**, c as well as the intensive variable T as its

arguments. In such cases that the hydrogel is put in contact with a stable aqueous reservoir, the chemical potential of solvent molecule μ is constant; then upon Legendre transformation, the free energy density W is carried to its corresponding thermodynamic potential:

$$\widehat{W}(\mathbf{F}, \mu, T|N, A_0, B_0, A_1, B_1) = W(\mathbf{F}, c, T|N, A_0, B_0, A_1, B_1) - \mu c \qquad (2)$$

thus $\hat{W}$ is a natural function of $\mathbf{F}$, μ and T.

When the stress level is adequately low so that no new void or pore is generated in the hydrogel, the volumetric change of the material solely results from the migration of solvent molecules; hence the deformation $\mathbf{F}$ and solvent concentration c are correlated by[139]:

$$J = 1 + vc \qquad (3)$$

Substitute Equations (1) and (3) into Equation (2), one arrives at the explicit form of $\hat{W}$:

$$\begin{aligned}\widehat{W}(\mathbf{F}, \mu, T|N, A_0, B_0, A_1, B_1) &= \frac{1}{2}NkT[\mathbf{F}:\mathbf{F} - 3 - 2\log(J)] \\ &+ \frac{kT}{v}(J-1)\left[\log\left(\frac{J-1}{J}\right) + \frac{(A_0 + B_0 T)}{J}\right. \\ &\left. + \frac{(A_1 + B_1 T)}{J^2}\right] - \frac{\mu}{v}(J-1)\end{aligned} \qquad (4)$$

2.2.12 Free swelling of PNIPAM hydrogel in water and determination of parameters

When submerged in an aqueous environment with homogeneous temperature field, a piece of free standing PNIPAM hydrogel, in the absence of pre-introduced stress, will swell (or contract) freely in response to the uniformly varying temperature field. The free swelling case satisfies the condition that the hydrogel deforms uniformly in any three orthogonal directions and that the hydrogel retains its stress-free state since neither deformation mismatch nor mechanical constraint exists. For such a homogeneous deformation the principal stretch ratios have identical value, and the deformation gradient tensor becomes

$$\mathbf{F} = \begin{bmatrix} \lambda & 0 & 0 \\ 0 & \lambda & 0 \\ 0 & 0 & \lambda \end{bmatrix} \tag{5}$$

where λ is the uniform stretch ratio. And in this case the volumetric ratio $J=V/V_0= \lambda^3$, where V is the volume of the hydrogel piece in the deformed state and V_0 is the volume in the reference (dry) state.

As discussed above the stress tensor vanishes:

$$S_{ik}(\mathbf{F}, \mu, T|N, A_0, B_0, A_1, B_1) = \frac{\partial \widehat{W}}{\partial F_{ik}} = 0 \tag{6}$$

Equation (6) yields the relation between stretch ratio λ and temperature T in the free swelling case. In addition, if the chemical potential of water is known and set to zero, then T can be readily expressed by the following equation:

$$T = -\frac{Nv(\lambda^5 - \lambda^3) + \lambda^6 \log(1 - \lambda^{-3}) + \lambda^3 + (A_0 + A_1\lambda^{-3})}{B_0 + \lambda^{-3}B_1} \tag{7}$$

The equation above dictates the temperature required by the principle of minimum free energy, in free swelling cases, for the temperature-sensitive hydrogel to maintain certain amount of deformation. In other words it also depicts how the hydrogel deforms in response to the change of the homogeneous temperature field.

By fitting the function $T(\lambda|\mathbf{S}=0, \mu=0)$ to the experimentally obtained $T\sim J$ relation, we determined the parameters Nv, A_0, B_0, A_1 and B_1. Figure 2.S5 shows the fitted curve of volumetric ratio $V/V_0= \lambda^3$ as a function of temperature T, with the specified parameters: Nv=0.03317, A_0=-2.5418, B_0=0.01081, A_1=0.57099, B_1=-0.000418. We will use this set of parameters for our PNIPAM hydrogel in the following calculations.

2.2.13 Heat transfer model

When the top surface is exposed to NIR laser, the AgNPs embedded in PNIPAM absorb the photons and convert the light energy into heat, the surrounding hydrogel matrix is thus heated. In order to benchmark the thermal properties of our PNIPAM hydrogel, we setup the transient heat transfer model for a hydrogel piece with length L_d=1.7cm, width w_d=0.85cm and thickness t_d=0.5mm (same dimensions as the hydrogel piece in the NIR light irradiation experiment). The initial temperature of the entire body is the same as ambience temperature T_0=295K. Then the top surface of the hydrogel piece is brought to exposure to two adjacent laser stripes with width w_l=0.2cm and heat flux intensity H=1.2 $J\cdot cm^{-2}\cdot s^{-1}$, and the bottom surface away from the laser irradiation is set to the constant ambience temperature. Laser is switched on for 120 seconds and is shut down thereafter to let the hydrogel cool down through heat dissipation into the environment. Keeping track of the temporal evolution of the highest

temperature on the top surface, we are allowed to compare the temperature response curve with the experimental data and determined the thermal diffusivity of PNIPAM hydrogel $\alpha=K/\rho C_p=2.36\times10^{-5}$ cm^2/s, where K, ρ and C_p denote the thermal conductivity, density, and specific heat of the material respectively.

2.2.14 Deformation of PNIPAM hydrogel in inhomogeneous temperature field

The deformation behavior of a temperature-sensitive hydrogel is governed by a thermodynamic free energy thus resembling a hyperelastic material[137, 139]. Each thermodynamic equilibrium state of temperature-sensitive hydrogel is a local minimum of the system free energy which can be fully defined by the stretch ratios λ and a dependent solvent molecule concentration c as discussed above. Furthermore, the thermodynamic equilibrium is to be altered upon the change of environment variables. Therefore besides of being able to respond to the conventional mechanical loads, such materials as PNIPAM hydrogels are also able to deform in accordance with the change in temperature and chemical potential.

Solving for the equilibrium states is a boundary value problem (BVP). For simpler cases, e.g., free swelling hydrogel with homogeneous temperature, analytical solution can be obtained, whereas for more complicated case, e.g., hydrogel swelling in an inhomogeneous temperature field, the BVP can be solved numerically by FEM. We adopted the FEM framework established by Ding *et al*. for the temperature-responsive hydrogel[140], and prescribed the material properties determined above to the PNIPAM hydrogel used in this study. At this stage we assume that the deformation of PNIPAM hydrogel will not affect the heat transfer processes. A fully coupled thermomechanical

algorithm is implemented in the commercial FEM package ABAQUS by making use of its temperature-displacement elements.

We investigated the impact of the heat flux intensity H and the laser stripe width w_l on the deformation of the PNIPAM hydrogel piece. A 2-D plane strain model of 1.7cm×0.5mm hydrogel is exposed to a stripe-shaped laser irradiation with heat flux intensity H and width w_l. The heat transfer process from the top surface towards the bottom side creates temperature gradient within the hydrogel body. Dictated by the minimization of free energy the hotter part of the PNIPAM hydrogel tends to shrink more than the cooler part, whereas the deformation of one material particle has to be constrained by its neighbors to achieve thermodynamic equilibrium. Therefore this deformation mismatch causes the hydrogel piece to bend towards the side of elevated temperature.

We plotted the dimensionless curvature (κt_d) at the geometric center as the indicator of localized deformation and the dimensionless transverse deflection (h/t_d) as the measurement of overall deformation. Higher heat flux intensity leads to a higher temperature on the top surface thus results in an increased temperature gradient in the thickness direction of the hydrogel piece, which in turn promotes the localized deformation at the deformation tip. If the light stripe is wider, the temperature at heat transfer equilibrium will also be higher. Moreover the wider laser stripe makes a larger portion of hydrogel to contribute to the total deformation and as a result the deflection is larger. The curvature at the tip and the deflection in lateral direction both increases as H and w_l increase.

Additionally, if a PNIPAM hydrogel piece is brought to exposure to a fixed power laser source, i.e., the total quantity of energy absorbed by the hydrogel is fixed at certain amount ($P=Hw_l=const$), there exists an optimal combination of H and w_l which yields the largest deflection. As shown in Figure 2.S6, the wider laser stripe comes with a lower intensity and a narrower one comes with a higher intensity if the laser source power is fixed at $P=Hw_l$=3.6 J/s. Figure 2.S6(a) also shows the temperature field in the reference state and the stress field in the deformed state. The stress scale is normalized by $kT_0/v\lambda_0^3$, where the Boltzmann constant k=1.3806×10^{-23} m^{2}kg·s^{-2}K^{-1}, the initial temperature T_0=295K, the initial stretch ratio λ_0=1.5489 (at T_0=295K and relative to the dry state), and the molecular volume of water v=2.9922×10^{-29} m^3. Upon the increasing w_l, the intensity H decreases and the resulting localized deformation is deduced (Figure 2.S6(b)). However, the deflection of the hydrogel piece has a maximum at w_l=0.2cm, this is because the deflection indicates the level of the total deformation of the entire piece. The increasing w_l brings a larger part of hydrogel into irradiation, while the amount of heat which per unit area of top surface receives is reduced. The tradeoff between the increasing number of contributors and decreasing amount of the contribution per share allows the existence of the maximum deflection.

2.2.15 Effects of finite convection on heat transfer

The light responsive deformation behavior of the hybrid hydrogel depends on the heat transfer process inside the hydrogel which establishes an asymmetric temperature field triggering the directional bending towards the laser source side . The heat transfer process is determined by two main factors, namely the energy flux input from the laser

and the heat dissipation through convection into the ambience . In the model presented in section 2.2.13, we fixed the temperature on the back surface of the hydrogel at the ambience temperature. This case corresponds to the maximum convection condition on the back surface, i.e., the convection coefficient is infinite so that the energy dissipates at the highest rate. As a result, the back surface temperature of the hybrid hydrogel sheet equals the temperature of its surrounding water. Such a treatment is valid only if approach such as forced convection is implemented.

To investigate the effect of finite convection on the evolution of temperature and deformation, we prescribed finite convection boundary condition on the hydrogel surface, in addition to the heat flux over the central section of the top surface. Because the water molecules inside the hydrogel network still retained mobility of migrating back and forth between the network and the ambience, the convection coefficient was set at a moderate value 700 $Wm^{-2}K^{-1}$, and the ambience temperature was set at the room temperature 295K.

We used the angle change α to quantify the bending deformation. Figure 2.S7 showed the temporal evolution of α for different heat flux inputs. When heat flux was comparatively small (e.g., H=3 and 3.5W/cm^2), α increased monotonically with time and converged to an equilibrium state value of 29.5 °at ~6s. In all the other cases where H>3.5W/cm^2, the angle reached a maximum value and started to decay. For example, when H=3.5W/cm^2, α reached a peak value 35.2° at 1s, then gradually reduced to a steady state value at 21.6^o. Compared to the fixed temperature boundary condition, the heat dissipation was smaller for the finite convection case, thus temperature field was established at a higher rate, which resulted in a fast deformation response: at the

maximum bending angle, the highest temperature in the center of the top surface was 315K, and the back surface was heated up to 301K. A temperature difference of 14K was developed in ~1s. In addition, with finite convection both the top and back surfaces were heated to a higher temperature. The elevated temperature on the back surface leaded to a reduction of the bending angle. As shown in Figure 2.S8 a, the globule/coil phase transition of PNIPAM was accomplished at ~305K, and the volumetric deformation in the top layers reached its saturation. Therefore, any further temperature increase only resulted in the shrinkage in the back layers, pulling the hydrogel piece away from its initial deformation, which in turn reduced the bending angle. As indicated by the temperature profiles at the equilibrium state in Figure 2.S7, even though the temperature difference between the top/back surfaces at the maximum deformation state (14K) was slightly smaller than that at the final state (15K), the bending angle was 13.6 ° larger. This was because the increase of the top surface temperature from 315K to 327K was not accompanied with any further shrinkage, whereas the volume of the back-layer reduced as the temperature increased from 301K to 312 K. This resulted in the reduction of bending angle from the maximum bending state.

To compare the deformation capability of the hydrogel piece under finite and infinite convection boundary conditions, the bending angle was plotted in Figure 2.S9 against the top/back surface temperature difference. At first, the hydrogel with finite convection deformed more. This was because 1) the top surface temperature was higher with finite convection, and 2) the heat-affected zone was larger near the top. When $\Delta T>15K$, these two factors were overcome by increased temperature in the back-layer

and the deformation was larger for the infinite convection case. The dashed line showed the bending angle in the equilibrium state.

2.2.16 Effects of ambience temperature on heat transfer

In all the aforementioned calculations, we set the ambience temperature at 295K. Upon further illumination, the local temperature of water near the hydrogel piece will also increase due to its weak absorption of NIR light. To understand the effect of the increased ambience temperature, we set the ambience temperature at 300K over the 3.5mm section in the center of the back surface, and left the ambience temperature around all the other surfaces at 295K. The applied $5W/cm^2$ heat flux remained the same as the baseline case. The bending angle declined to $12.7°$ from $23.2°$ (Figure 2.S10). This further reduction of deformation corresponded to the dome collapse which was observed in the experiment for the thinner sheet (Figure 2.S11c). We pointed out our hybrid sheet system was very dynamic under light irradiation and its deformation was a result of a fine interplay between the heat transfer in the hydrogel and the dissipation into the environment.

2.3 Results and discussion

2.3.1 Fabrication of PNIPAM-AgNP hybrid hydrogel sheet

The PNIPAM-AgNP hybrid hydrogel sheet was fabricated by reducing $AgNO_3$ pre-soaked in PNIPAM hydrogel. The as-synthesized AgNPs in the hydrogel sheet showed a roughly spherical shape and a broad size distribution (Figure 2.S12). Under the current experimental conditions, the AgNPs-loaded hydrogel showed a fairly strong

absorption at 808 nm wavelength, though its absorption peak located at around 595 nm (see Figure 2.2a). The red-shift of absorption peak from around 400 nm of spherical AgNPs can be attributed to the dense packing of AgNPs in the hydrogel, as indicated by the dark, shining and non-transparent appearance of the gel (Figure 2.S13). The hybrid hydrogel sheet exhibited a macroporous structure with pore size ranging from 200nm to 1μm (Figure 2.2b).

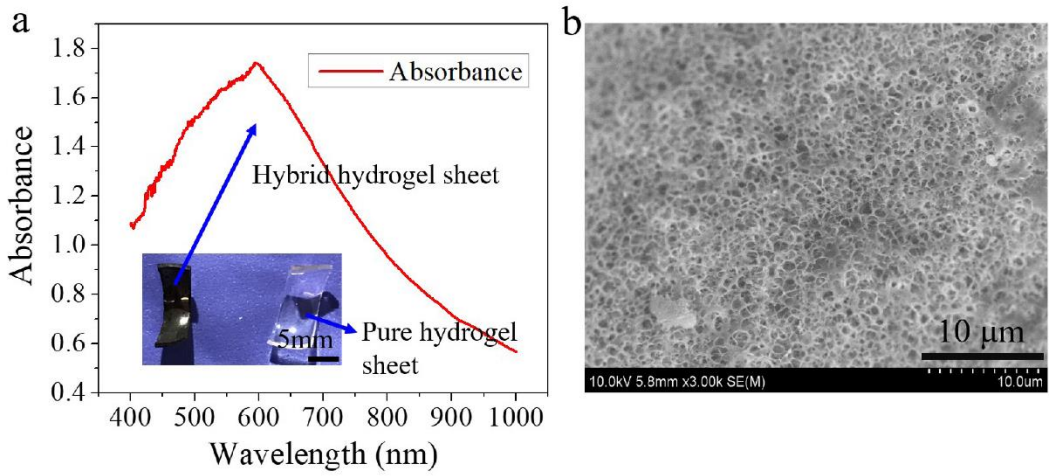

Figure 2.2 a) UV-Vis absorption of the hybrid hydrogel sheet. The hybrid sheet had a sufficient absorption at 808 nm wavelength-that matches the wavelength of continuous-wave NIR laser-in order to produce sufficient thermal energy to trigger the shape transformations. Since a pristine macroporous gel without Ag nanoparticles was used as the reference, the UV-vis spectrum of the hybrid hydrogel reflected the plasmonic absorption of Ag nanoparticles rather than the scattering of the gel. b) Macroporous structure of hybrid hydrogel sheet.

2.3.2 Bending deformation of hybrid hydrogel sheet under laser irradiation

Our self-shaping hybrid hydrogel sheet represents a non-equilibrium dynamic system: it requires continuous energy supply (light energy) and energy dissipation (heat dissipation) to sustain its shape. The competition between the supply and dissipation of energy determines the behavior of the sheet's shape transformation. To study this, we used a striped light pattern to trigger the bending of the sheet ((length: 20mm, width: 9mm, thickness: 0.5mm)) (Figure 2.3). It was found that either the NIR laser power density (PD) or the irradiation stripe width should reach a certain threshold for the hybrid hydrogel sheet to bend (Figure 2.3a). If supplied light energy was low (small laser PD or small irradiation stripe width), the fast heat dissipation diminished the thermal gradient and disabled the bending of the sheet. The FEM study confirmed a positive correlation between the bending and the laser PD as well as the irradiation stripe width (Figure 2.3c, Figure 2.3d and Figure 2.S14). It indicates that the bending increased with the increase of either the laser PD or the irradiation stripe width. Increasing the laser PD enhanced the heat generation. A larger thermal gradient was hence established in the sheet resulting in an increased bending. By increasing the irradiation stripe width, thermal gradient was generated in a larger lateral area, which contributed to the increased bending.

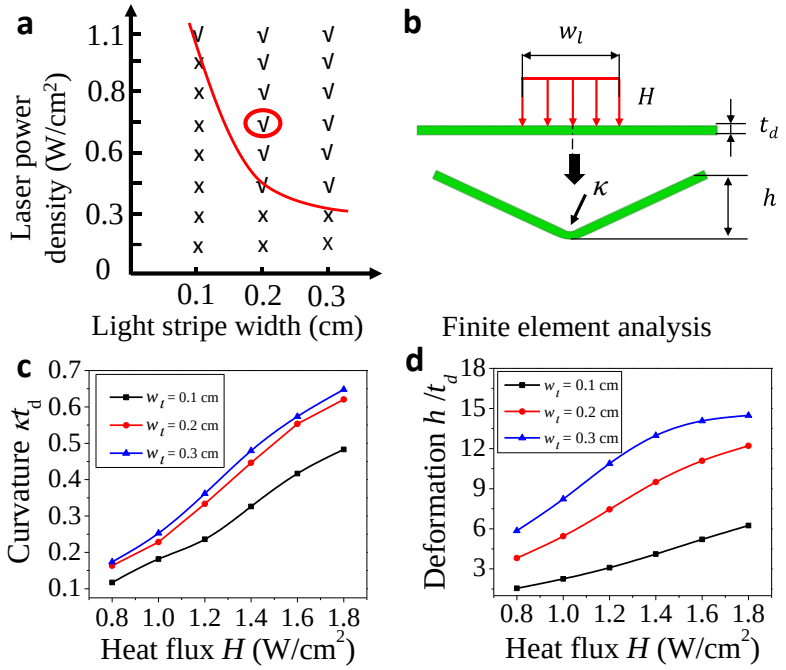

Figure 2.3 a) Experimental study on the bending of the hybrid hydrogel sheet as a function of laser power density and irradiation stripe width. The width of the rectangular irradiation stripe was varied while its length was kept as 0.9 cm. The red circle indicated the irradiation condition used in the current experiment. √: the sheet bent at the applied irradiation. x: the sheet exhibited no visible bending under the applied irradiation. b, c, d) FEM analysis of the sheet's deflection (h/t_d) and bending curvature (κt_d) with respect to laser power density and irradiation stripe width. The FEM results indicated that the deflection and bending curvature increased with the increase of either laser power density or irradiation stripe width.

When bending occurred, the bending angle increased with the increase of irradiation time and finally reached a stable bending state (Figure 2.4). The bending rate and time to reach a maximum bending angle were strongly dependent on the laser

PD. At higher laser PD, the hybrid sheet bent faster as indicated by the larger slope in the red curve (laser PD: 0.94 W/cm^2) as compared with the slope in the blue curve (laser PD: 0.57 W/cm^2) (Figure 2.4a). Also at a higher laser PD, the hybrid hydrogel sheet reached its maximum bending in a shorter time. It took about 20 seconds for the sheet to bend to maximum at a laser PD of 0.94 W/cm^2 (Figure 2.4a, red curve), while it took about 50 seconds at a laser PD of 0.57 W/cm^2 (Figure 2.4a, blue curve). The bending angle increased with increase of laser power density and decreased gradually to its original state as a function of time after the laser was switched off (Figure 2.4b). The bending/debending could be repeated for many times without appreciable change in bending deflection, demonstrating high reversibility of bending deformation (Figure 2.5).

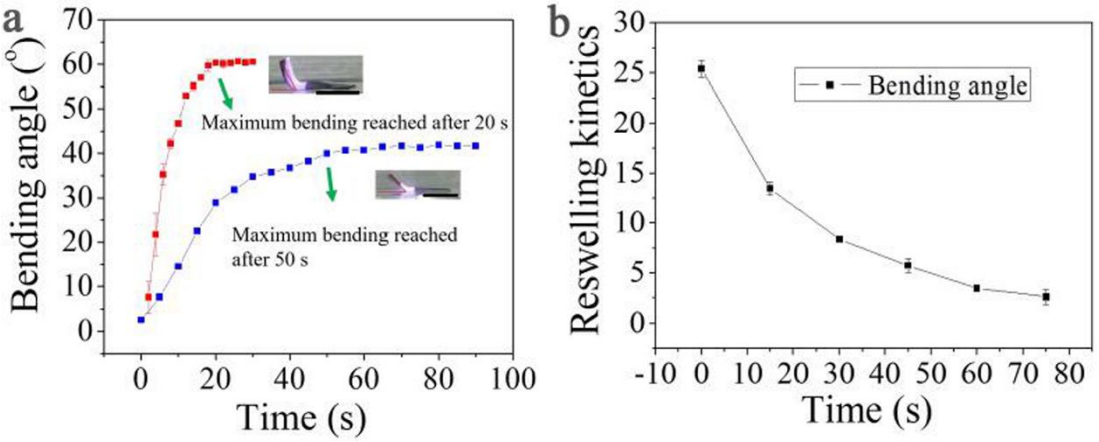

Figure 2.4. a) Bending angle of the composite sheet as a function of irradiation time at different laser power densities. The data points were obtained by averaging the bending angles from three separate cycles. The composite sheet was irradiated at the same position with a rectangular light stripe (width: 0.3cm) in all the cycles. b) Re-swelling kinetics of the composite sheet by measuring the

time-dependent decrease of bending angle after switching off the laser. The hybrid sheet was irradiated for 5 seconds at laser power density of 0.94 W/cm^2. Then the laser was switched off (corresponding to the data point at 0 second in the graph) and the bending angle was monitored as a function of time.

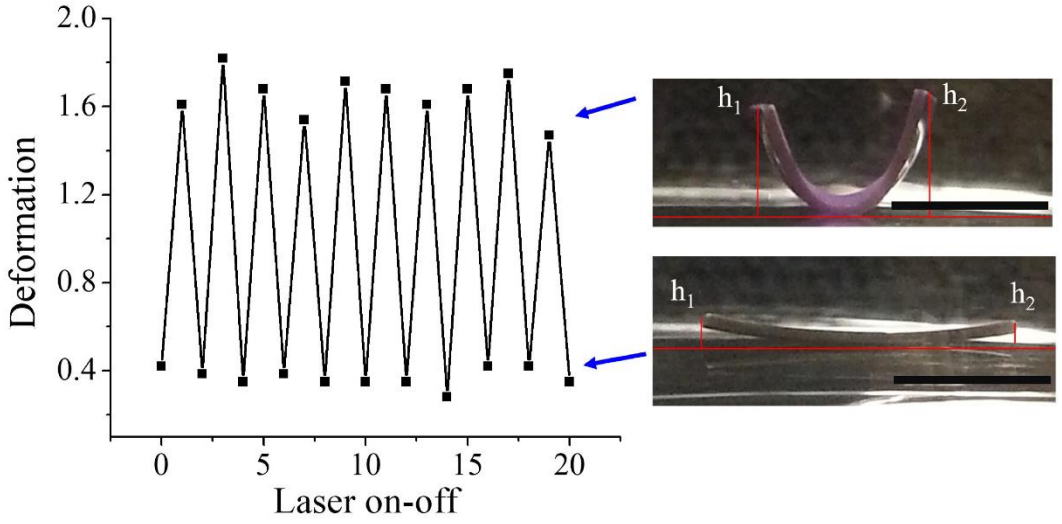

Figure 2.5 Reversibility of shape transformations of hybrid hydrogel sheet in response to light. The deformation of the hoof-like structure was monitored in each laser on-off cycle. In each cycle, the hydrogel sheet reached its maximum deformation within 5 seconds and recovered its original shape within 5 minutes. The deformation was calculated as $(h_1+h_2)/(2t_d)$, where t_d is the thickness of the hybrid sheet which was 0.5 mm. The scale bar represents 0.85cm.

2.3.3 Multiple shape transformations of hybrid hydrogel sheet under laser irradiation

By changing the NIR light irradiation pattern on the same hydrogel sheet using photo masks, various well-defined shape transformations were achieved from the same

hydrogel sheet, such as boat-like, helical, hoof-like, saddle-like structures (see Figure 2.6a). The shape transformations were further verified by finite element modeling (see Figure 2.6b).

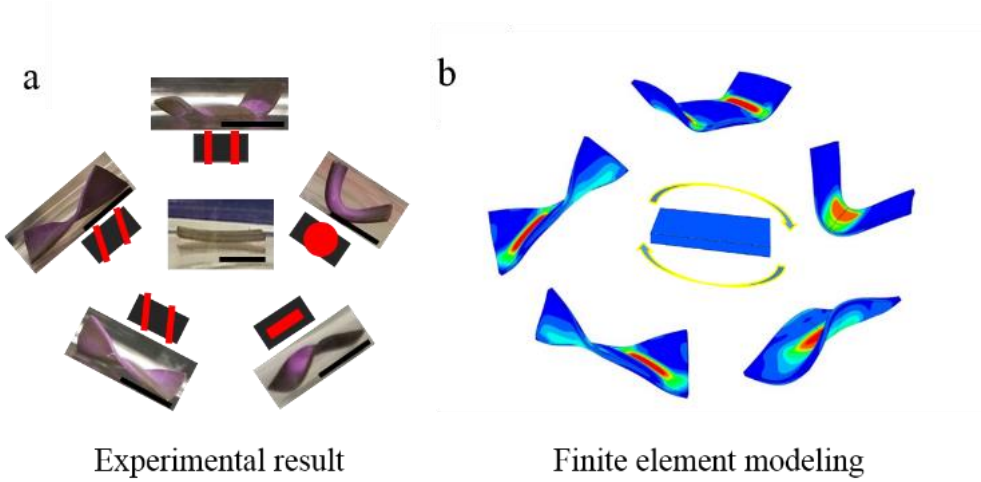

Figure 2.6 Experimental (a) and finite element modelling (FEM) (b) results of shape transformations of the same hybrid hydrogel sheet into five different shapes upon NIR light irradiation: boat-like, hoof-like, saddle-like, right-helical and left-helical shape (from top along clockwise direction). The red stripes in (a) indicated the shape of NIR light spot. Scale bar: 0.85cm. b) FEM analyses showed that a unique localized stress field was established within the hybrid sheet upon each irradiation, resulting in a specific shape transformation. The red and blue colors in (b) represent high and low stress within hydrogel, respectively.

In addition to use patterned light to transform the same hydrogel sheet into various 3-D geometries, the same hydrogel sheet can also be sequentially irradiated by un-patterned laser but without having macroscopic transformations during irradiation. Basically, the hydrogel sheet was put on a glass slide in air and then it was irradiated

by laser. After irradiation, the hydrogel sheet was immersed in water and macroscopic shape transformation occured by releasing the stored energy during irradiation process (the irradiated regions shrunk during irradiation but did not cause macroscopic deformation due to restriction of underlying glass slide) (Figure 2.7). In this case, the same hydrogel sheet can be pre-written with a wide range of patterns by using laser. After immersing the irradiated hydrogel sheet in water, it transformed to a large array of different 3-D geometries (Figure 2.7).

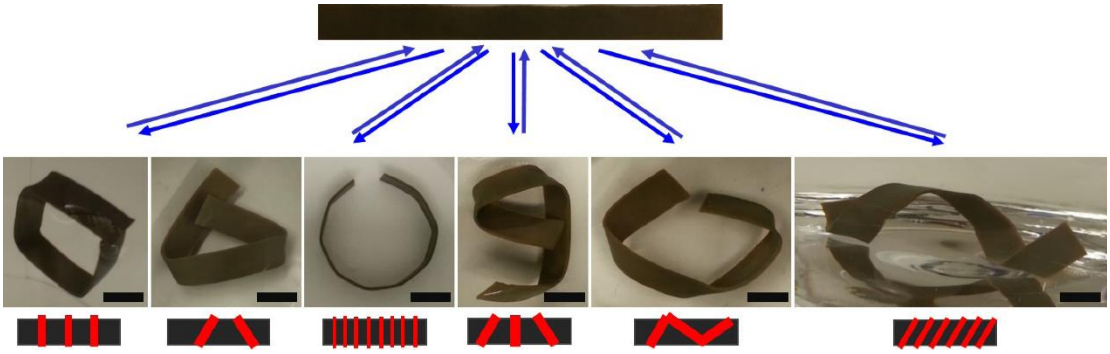

Figure 2.7 Various complex shape transformations from the same long rectangular hybrid sheet by pre-integrating stress within it. The swollen hybrid sheet was put onto a glass slide, which was then subject to step-by-step NIR light irradiation as indicated by the red stripes. The sheet shrunk in those areas that were irradiated. The sheet kept the shrinkage state in the previously irradiated areas when the laser was moved to the next area. In this way stress was integrated within the sheet in a specific pattern. After detaching the hybrid sheet from the glass slide and transferring it into water, the sheet transformed to various complex shapes to release the previously integrated stress. Scale bar: 4mm.

2.3.4 Mechanism of shape transformations of hybrid hydrogel sheet under laser irradiation

The underlying mechanism of the shape-transformation of the macroporous composited hydrogel sheets can be understood as following. The thermo-responsive polymer, PNIPAM, undergoes a coil-to-globule transition in its aqueous solution when the temperature is above its lower critical solution temperature (LCST) (~32 ℃).[141] This transition will result in a volumetric contraction in its hydrogel form due to the expelling of water molecules and aggregation of polymer chains.[142] When the hybrid PNIPAM hydrogel was regionally exposed to NIR laser irradiation, the temperature of irradiated region of the hydrogel increased, while the off-exposure areas remained a lower temperature. In other words, a non-uniform temperature field was established in the hydrogel under localized light irradiation. As shown in the thermogram (Figure 2.8), a remarkable thermal gradient (ranging from 22 ℃ to 32 ℃) was created along the sheet's surface when the sheet was locally irradiated with NIR light (Figure 2.8a). During the irradiation, the thermal gradient on the sheet's surface gradually propagated with the increase of the irradiation time (Figure 2.8a). In addition, the heat propagation occurred also along the thickness direction due to the heat flux input on the laser-exposed area and the convectional dissipation over the other surfaces. This phenomenon was confirmed by the presence of a z-direction thermal gradient in the cross-section temperature profile from the simulation (Figure 2.8b).

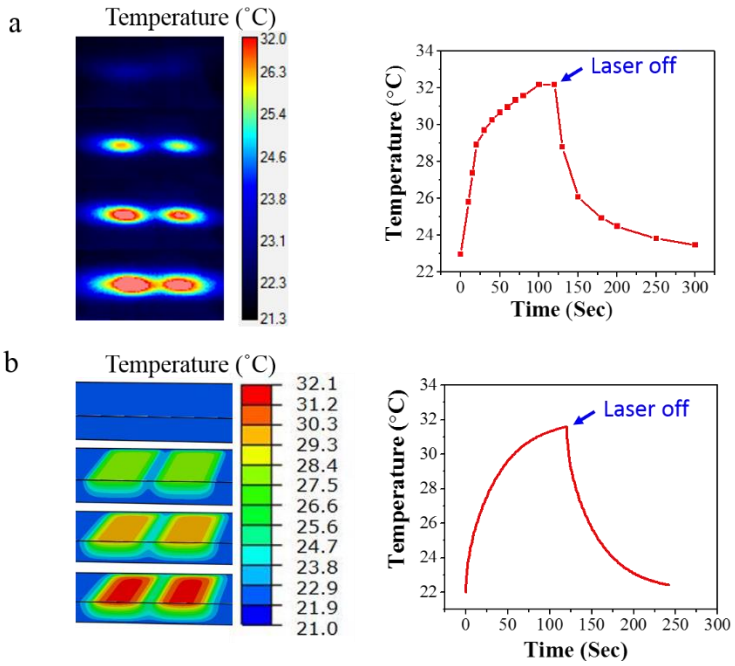

Figure 2.8 Experimental study (a) and finite element analysis (b) of the generation of thermal gradient within hydrogel sheet upon NIR laser irradiation. The hybrid sheet was irradiated for 120 seconds and then the laser was switched off. The temperature was measured for an interval of 30 seconds. As can be seen from a), a stable thermal gradient ranging from 21 to 32 °C was established on the sheet's top surface under light irradiation, which was confirmed by FEM analysis. We used infinite convection boundary condition in the heat transfer model to calculate the temperature profile in the sheet under light irradiation.

The main concept developed in this Chapter is that by using structured light to irradiate the composite hydogel sheet, the deformaton can be localized and erased by simply switching off the laser light. A different deformation can be achieved by simply switching on laser light which is structured with a different pattern.

2.3.5 Discussion

As discussed in section 2.3.4, there exist two types of temperature gradients in the hybrid sheet under localized light irradiation: the in-plane thermal gradient and z-direction thermal gradient (Figure 2.9a). These temperature gradients lead to swelling and modulus differences inside the hydrogel: the regions with higher temperature shrink more and become stiffer (Figure 2.S8). For the bending transformation, the in-plane temperature gradient determines the position of the localized deformation, as the bending tip resides at the center of the in-plane gradient. In contrast, the z-direction thermal gradient causes a larger volumetric change closer to the top-surface, thus breaking the deformation symmetry along the direction of hydrogel thickness and determining the bending direction. For more complicated shape transformations (saddle, helix, and boat in Figure 2.6), each NIR light illumination generates a signature temperature field inside the hydrogel body, and the interplay of the in-plane and z-direction thermal gradient contributes to a unique shape transformation. A real-time temperature evolution and the corresponding shape transformation was shown in the published article. During the establishment of the thermal gradient, the hybrid sheet gradually reached its bending maximum. The maximum bending transformation and the stable surface thermal gradient were achieved at a very similar time scale.

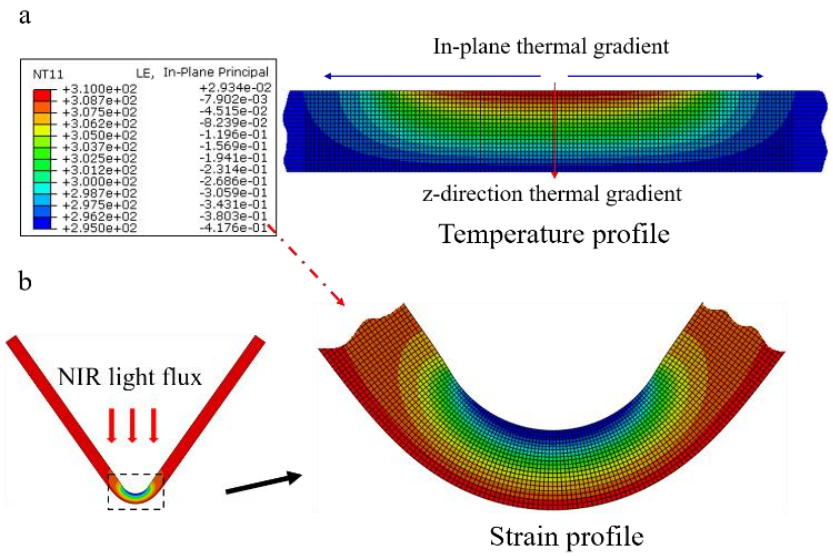

Figure 2.9 a) FEM analysis of temperature distribution within the hybrid sheet upon light irradiation. An infinite convection boundary condition was used in the calculation of the temperature profile. b) FEM analysis revealed that an asymmetric strain distribution was established within the sheet upon localized light exposure, which essentially actuated the sheet's bending.

As can be seen from the above discussions, our hybrid hydrogel sheet system is very dynamic under light irradiation. It coupled together heat transfer, mass (water) transport and macroscopic mechanical deformation. To provide deeper insights and more fundamental understanding of our system, we conducted a coupled thermo-mechanical analysis using the thermodynamics of PNIPAM hydrogel. The swelling behaviour of PNIPAM hydrogel stemming from this microscopic mechanism can be captured by its thermodynamics:[143] the coil-to-globule transition is associated with change in a macroscopic Helmholtz free energy. Moreover, the non-uniform swelling field in the hydrogel body is accompanied by interior stresses, as a result of the swelling

difference between the hydrogel and its neighboring material. In such case, the free energy of the hydrogel includes the strain energy in addition to the free energy due to the mixing of PNIPAM network and water molecules. At the presence of a temperature gradient, the equilibrium responses of PNIPAM hydrogel to the inhomogeneous temperature field are governed by a mechanical model which determines the steady states of PNIPAM hydrogel as the Helmholtz free energy minima of the entire system (See supporting information for details). The PNIPAM constitutive model is implemented in ABAQUS user subroutine and the deformation is computed using the directly coupled thermo-mechanical analysis. Without missing the nature of the deformation, the exterior surfaces of the hydrogel sheet are set to be at infinite convection thermal exchange with the ambience in the heat transfer model. Here it was found that a localized stress field was established within the hybrid hydrogel sheet upon light irradiation (Figure 2.9b). The hydrogel material in the exposed area underwent a gradual compression-to-stretch change due to the established thermal gradient, while the areas off exposure remain a stress-free state (Figure 2.9b). The asymmetry in the stress state in the hydrogel material actuated its bending. Further modelling studies show that the shape transformation of the hybrid hydrogel is robust for various boundary conditions and material properties (e.g., finite convection and ambient temperature) (See Figure 2.S7, S9-10 for details).

2.4 Conclusions

In conclusion, we reported a simple and effective design of a 2-D macroporous hybrid hydrogel sheet that can transform into at least five different shapes (unlimited number in theory) under NIR light irradiation. Representative shapes achieved from the same 2-D hybrid sheet include helical, boat-like, hoof-like and saddle-like shapes. The transformation is highly reversible and ultrafast (on the order of seconds, while previous nonporous hydrogels of similar thickness transforms on the order of minutes or even hours). The hybrid sheet is composed of a thermo-responsive polymer, PNIPAM and silver nanoparticles (AgNPs). Each shape transformation relies on the unique swelling pattern generated by the specific thermal gradient established upon light irradiation. The thermal gradient is created through a delicate balance between the continuous localized heating by the plasmonic AgNPs under NIR irradiation and the heat dissipation to the aqueous environment. We point out that accessible shape transformations of the hybrid hydrogel sheet rely on several factors, including: i) size (aspect ratio; thickness, see Figure 2.S15) and shape of the original hydrogel sheet (see Figure 2.S16); ii) laser irradiation pattern and its intensity; iii) photothermal efficiency of the inorganic nanoparticles; iv) mass and heat transport. We also highly expect that sequentially folding the same 2-D hydrogel material will further greatly enrich the potential of its shape transformations.[69] In the sequential folding, a shape transformation is fixed before next transformation is initiated. After the target shape is achieved, the hydrogel sheet can be restored to its original flat shape. Then new type of transformations can be implemented to obtain a different shape. This sequential folding can potentially lead to a large array of on-demand shapes by reprogrammable

origami of the same 2-D hydrogel material. The ultra-fast, reprogrammable and NIR-light-responsive macroporous hybrid hydrogel sheet reported here represents an important step towards designing novel soft materials that can transform to adapt in an on-demand manner. The macroporous hybrid hydrogel sheet may find applications in artificial muscles, soft robotics, microfluidics, actuators, and biomedicine, etc. As an example, the composited hydrogel sheet can potentially serve as dynamic scaffolds for the generation of three-dimensional tissue-like structures. After the seeding and growth of arrays of single or multiple cells on the sheet, controlled exposure of the sheet to patterned NIR light drives the shape transformation of the cell arrays into tissues-like structures with defined geometries such as vascularized nerve tubes.[144] Moreover, such shape-transforming materials can be used as smart sensing wrapper. The sheet patterned with arrays of sensors can be triggered remotely to transform and conformably contact the lesion tissues with arbitrary shapes. The conformal contact between the tissue surface and sensors allows for sensing and mapping the local environment or disease biomarkers. The use of NIR light is beneficial for in vivo application, owing to its large penetration depth and minimal damage to the soft tissues.

Chapter 3: Fabrication of composite hydrogel sheet with spatially patterned nanoparticles via contact printing

Chapter overview

In Chapter 2, a reprogrammable hybrid hydrogel sheet that transformed to various distinct geometries by using light with different irradiation patterns was developed. One technical challenge associated with this approach may arise when there is a need to use complicated exposure patterns to generate complex geometries. Another limitation of using structured light is that undesired shape transformation may originate from variation in the irradiation area upon the deformation of materials. Instead of using irradiation patterns, we can pattern the hydrogel instead and simply use un-patterned light to trigger deformation of the patterned hydrogel. While patterning polymer/elastomer films with molecules or nanoparticles has several mature techniques such as micro-contact printing, lithography, etc. The patterning approach reported in this Chapter allows us to pattern nanoparticles in both z-direction and xy-direction in the hydrogel.

3.1 Introduction

Recently, patterning nanoparticle in material was developed as a new route to guide material's shape transformation.[145] In this case, the presence of nanoparticle pattern in the material introduced swelling and modulus anisotropy in the material upon stimuli, thus directing material's shape-changing behavior. However, it remains challenging to introduce nanoparticle pattern with a gradient structure simultaneously

in lateral and thickness-direction of the material, which is expected to bring in new shape-transforming modes for the hybrid material.

Herein we reported a simple and efficient approach to pattern various types of nanoparticle with gradient structures in hydrogel material. For simplicity, we used gold nanoparticle pattern to illustrate the patterning process (see Figure 3.1). This diffusion-controlled patterning approach allows us to pattern nanoparticle in both z-direction and lateral direction of the hydrogel material simultaneously, which cannot be readily achieved by other approaches, such as microcontact printing[146] and photo-lithography.[147]

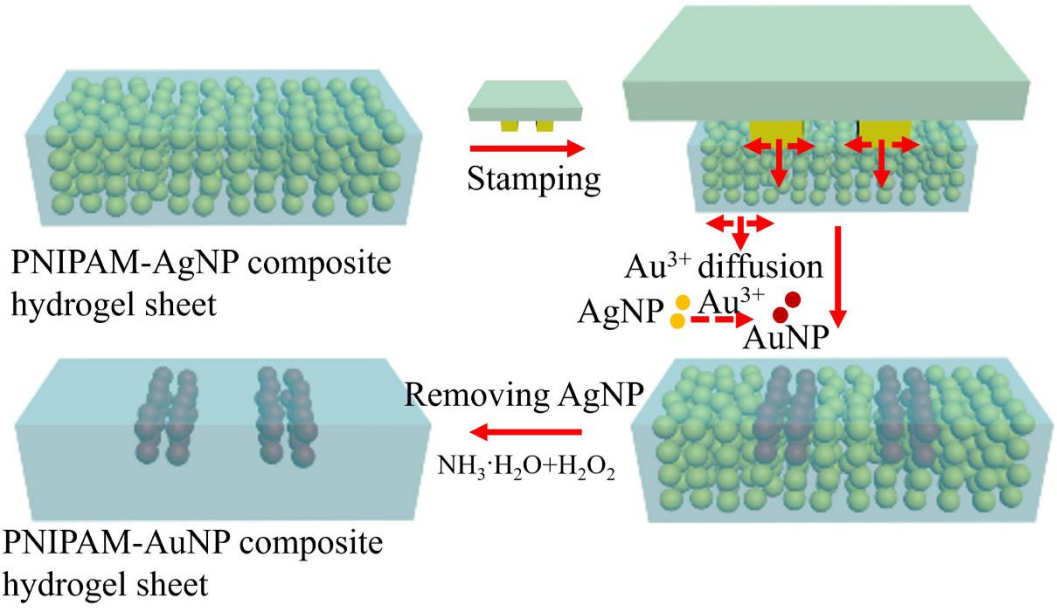

Figure 3.1 Schematic illustration of patterning plasmonic AuNPs in both lateral and z-direction of the thermo-responsive hydrogel matrix via galvanic replacement reaction between AgNP and gold ion.

3.2 Experiments

3.2.1 Materials

All chemicals were purchased from Sigma-Aldrich unless otherwise noted and the chemicals were used without further treatment. Chemicals used were as follows: N-Isopropylacrylamide (NIPAM, monomer), N,N'-Methylenebis(acrylamide) (BIS, cross-linker,), Ammonium persulfate (APS, initiator), N,N,N',N'-Tetramethylethylenediamine (TEMED, catalyst), Silver nitrate ($AgNO_3$), Polyvinylpyrrolidone (PVP, MW 55000), Gold(III) chloride trihydrate ($HAuCl_4$), Anhydrous ethanol, Ethylene glycol (EG), Ammonium hydroxide (25.0%-28.0%), Hydrogen peroxide (30%), Palladium (II) chloride, Chloroplatinic acid hexahydrate , iron (III) chloride, iron (II) chloride, Potassium iodide, Iodine. Agarose powder was purchased from EZ BioResearch. Polydimethylsiloxane (PDMS) elastomer kit (Sylgard 184) was bought from Dow Corning. Deionized water was used throughout the experiments.

3.2.2 Synthesis of silver nanoparticle (AgNP)

Silver nanoparticle was synthesized according to published literature (Synthesis of Ag Seeds section).[148]

3.2.3 Synthesis of AgNP-loaded hydrogel

AgNP-loaded hydrogel was fabricated by a redox method. Typically, 0.113g NIPAM monomer and 0.008g BIS cross-linker were dissolved in 500 μL AgNP aqueous solution. After adding 10 μL 10 wt% APS aqueous solution, this monomer

solution was purged with argon for 5 minutes on an ice-bed. Thereafter, 0.1 μL TEMED was added and mixed with the monomer solution. After mixing, the monomer solution was injected into a pre-made mold made of two cover slides and a spacer. The gelation took place at room temperature in a few minutes and was allowed to proceed for 1 hour. The glass mold was then immersed in water and was open to release the AgNP-loaded hydrogel. The AgNP-loaded PNIPAM hydrogel was kept in a large amount of water for one day to leak out unreacted chemicals.

3.2.4 Fabrication of agarose stamp

The agarose stamp was made by gelating agarose aqueous solution on a PDMS mold. Typically, a poly(lactic acid) (PLA) plastic mold with bas-relief features was first printed out by using 3D printer (Original Prusa i3 MK2S). Then PDMS was cured on this mold at 80 ^{o}C for 2 hours. The cured PDMS with opposite features was peeled off from PLA mold. After that, the surface of PDMS mold was made hydrophilic by subjecting it to air plasma for three minutes. Then 4 wt% hot agarose aqueous solution (pre-heated to dissolve agarose in water) was casted onto PDMS mold and cooled at room temperature to gelate. After gelation and keeping the mold in water for 4 hours, the agarose gel with bas-relief features was peeled off from the PDMS mold. This agarose gel was then used in wet stamping process.

3.2.5 Fabrication of flexible hydrogel stamp

The flexible hydrogel has a double-network structure composed of agarose hydrogel network and poly(acrylamide) hydrogel network. The hydrogel precursor was formulated according to published literature without change.[149] The hydrogel precursor

was casted onto PDMS mold fabricated according to section 3.2.4 and was subjected to UV irradiation (wavelength: 365nm) for 30 minutes. Then the hydrogel was removed from PDMS mold and was used as flexible stamp in the wet-stamping process.

3.2.6 Wet stamping

In a typical process, the agarose stamp with designed features was covered by a layer of metal ion aqueous solution for 2 minutes. During this process, metal ion diffused into agarose stamp. The remaining metal ion solution on the stamp was later removed by using Kimwipe. The agarose stamp containing metal ion was then brought in contact with AgNP-loaded hydrogel and metal ion diffused into AgNP-loaded hydrogel from the stamp. The metal ion precursor used in this study includes H_2PtCl_6, H_2PdCl_4 and $HAuCl_4$. The reason for choosing these metal ions is because they can react with AgNP (galvanic replacement reaction) which then generates platinum nanoparticle (PtNP), palladium nanoparticle (PdNP) and gold nanoparticle (AuNP), respectively.[150] The metal-ion-containing agarose stamp was kept in contact with AgNP-loaded hydrogel for certain time to control metal ion diffusion distance (hence metal nanoparticle domain size) in both lateral and z-direction of the hydrogel. Then the stamp was removed and the hydrogel was immersed in an aqueous solution of ammonium hydroxide and hydrogen peroxide (6:1 in volume ratio) to remove AgNPs. After removal of AgNPs, PtNP, PdNP or AuNP was retained in the hydrogel. By designing features in the stamp, various nanoparticle patterns can be generated in the hydrogel with controllable size and position in both hydrogel's lateral and thickness-

direction. Without notification, we used hybrid hydrogel to represent AuNP-containing hydrogel.

For patterning nanoparticle in non-planar hydrogel material, the flexible hydrogel stamp was used. After inking the flexible hydrogel stamp with metal ions, the stamp was wrapped on non-planar hydrogel with either concave or convex curvature to generate nanoparticle patterns in the non-planar hydrogel.

3.2.7 Diffusion study

The agarose stamp was brought in contact with the AgNP-loaded hydrogel for different amount of time. Then the AgNP was etched away. The size of the generated AuNP nanoparticle domain in both xy- and z-direction of the hydrogel was then analyzed by using optical microscope. The propagated distance of nanoparticle domain was obtained and was plotted with respect to stamping time.

3.2.8 Characterizations

The optical property of the hybrid hydrogel was characterized by measuring its light extinction using UV-VIS spectroscopy (Lambda 40 UV/VIS Spectrometer, PerkinElmer, USA). The UV-VIS-NIR spectra were taken at a slit width of 1 nm, scanning speed of 480 nm/min and data interval of 1 nm. The morphology of silver nanoparticle and the hybrid hydrogel sheet were characterized by using scanning electron microscopy (SEM) (XL Series-30, Philips, USA). For silver nanoparticle (AgNP) characterization, a drop of AgNP aqueous solution was dried on silicon wafer and the dried sample was imaged by using SEM. For hybrid hydrogel characterization,

the hybrid hydrogel was first freeze-dried and then coated with carbon (JFC-1200 Fine Coater, Japan). Following that, SEM was used to characterize AuNP in the hydrogel.

3.3 Results and discussion

3.3.1 Nanoparticle pattern generated by site-selective galvanic replacement reaction

By using agarose stamp with different bas-relief features, we obtained various nanoparticle patterns in the composite hydrogel via site-selective galvanic replacement reaction. For simplicity, we used gold nanoparticle patterns to illustrate the feature of the stamping approach developed in this Chapter.

In the stamping process, gold ion diffused from agarose matrix to PNIPAM-AgNP composite hydrogel matrix due to the presence of gold ion concentration gradient between the two hydrogel matrixes. When gold ion contacted with AgNP in the composite hydrogel, galvanic replacement reaction between gold ion and AgNP occurred, which generated gold nanoparticles. The gold nanoparticle pattern generated has desired feature size (~500 micron) and spacing (~1mm) with further potential of increasing its resolution (see Figure 3.2a-d). The high edge resolution of the patterns is evidenced by the sharp light intensity transitions between AuNP-containing and AuNP-free regions in the hydrogel (see inset graphs in Figure 3.2a-d). This approach could be readily scaled up. A 2cm by 2cm array of AuNP dots was patterned in the hydrogel to demonstrate the scale-up potential of this approach (see Figure 3.S1). After stamping, the AuNP-containing composite hydrogel showed broad light absorption in the NIR range (Figure 3.2f), presumably due to varied morphologies of resulting porous hollow

AuNPs in the gel (Figure 3.2e). In contrast, the original AgNP-loaded gel exhibited a lower absorption in the NIR range due to the solid spherical morphology of AgNPs (Figure 3.2f, Figure 3.S2).

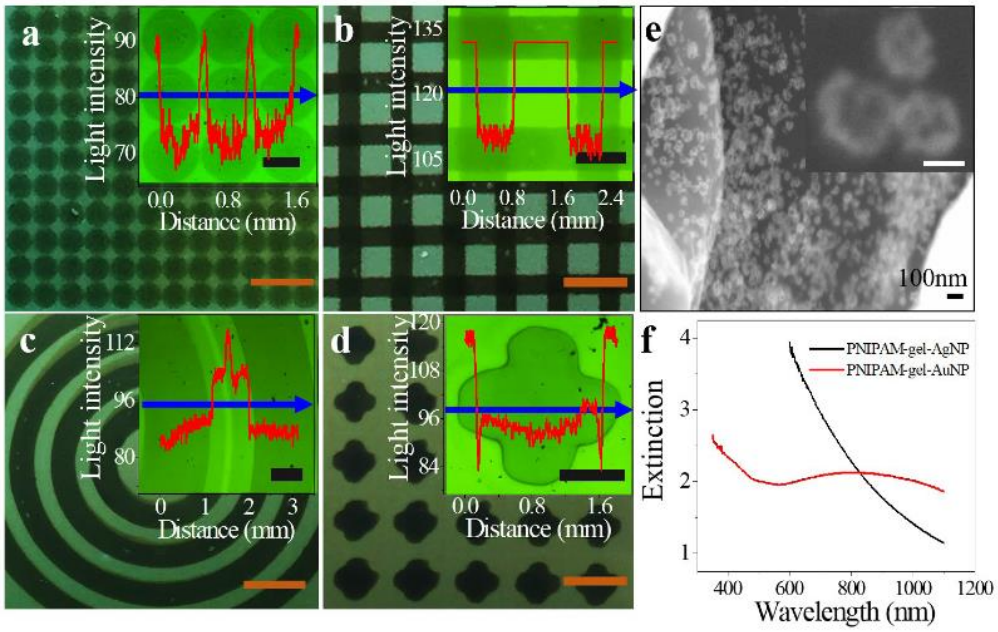

Figure 3.2 a-d) Composite hydrogel sheet patterned with plasmonic AuNP regions of different shapes by stamping approach. Insets are optical microscopic images of the patterns and light intensity profiles of the patterned domains along direction as indicated by blue arrow. e) SEM image of generated AuNPs with porous hollow feature. f) UV-Vis spectra of hydrogel hybrid before (black curve) and after stamping (red curve). Scale bars are 2mm in (a-d) and 0.5mm in insets of (a-d), and 40nm in inset of (e).

By modulating ion diffusion via varying stamping time or concentration of gold ion in the stamp, the pattern depth and width of gold nanoparticle can be controlled (Figure 3.3). Figure 3.3a-c clearly indicated the variation of AuNP domain size with

respect to $HAuCl_4$ concentration in both lateral and z-direction of the hydrogel, demonstrating the excellent control over the spatial distribution of AuNP domains in hydrogel. Figure 3.3d,e presented time-dependent growth of AuNP domain size in z-direction (Figure 3.3d) and lateral direction (Figure 3.3e) of the hydrogel, respectively. The depth and width of AuNP domains increased from 660 μm to 880 μm (Figure 3.3d) and increased from 260 μm to 360 μm (Figure 3.3e), respectively, with increase of stamping time from 1 minute to 2 minutes at a $HAuCl_4$ concentration of 10mM. Such fine control over AuNP domain size in the z-direction of material by using the diffusion-controlled method cannot be readily achieved by other approaches such as microcontact printing[146] and photon lithography.[147]

The pattern depth and width of Pd or Pt nanoparticle can be controlled by modulating ion (palladium or platinum ion) diffusion as well (Figure 3.4). They increased with increase of stamping time and ion precursor concentration (Figure 3.4).

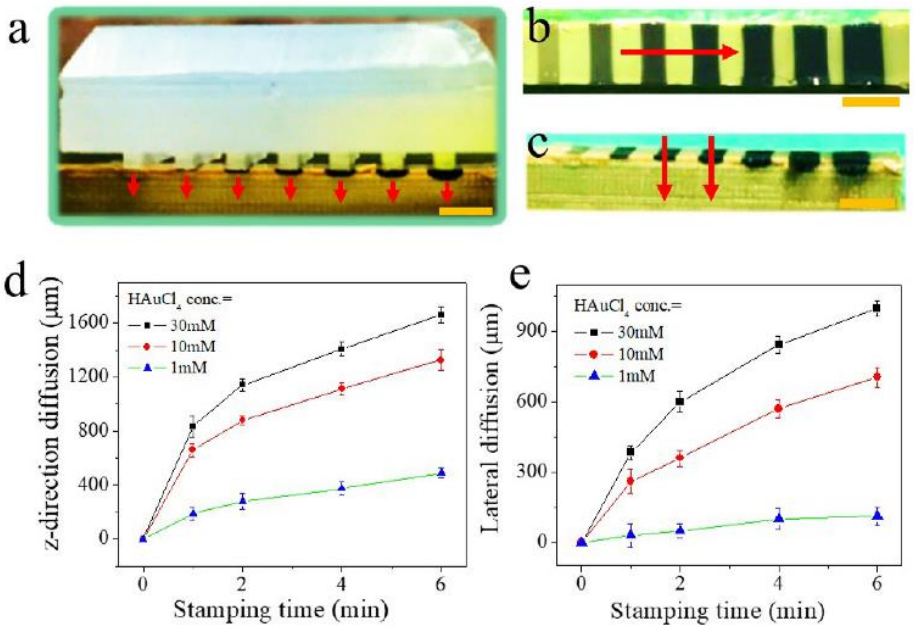

Figure 3.3 Analysis of diffusion-reaction process during stamping. a) The contact printing of stamp soaked with gold ion solutions of different concentrations (increasing from left to right) on hydrogel sheet. The red arrows indicate the propagation direction of AuNP domain along thickness direction of sheet. b,c) Top view (b) and side view (c) of the hydrogel after stamping. Arrows indicate the direction of increasing density or size of Au NP domains generated in the hydrogel; d, e) Time-dependent variation of AuNP domain size in z-direction and lateral direction of the hydrogel. Scale bars: 2mm.

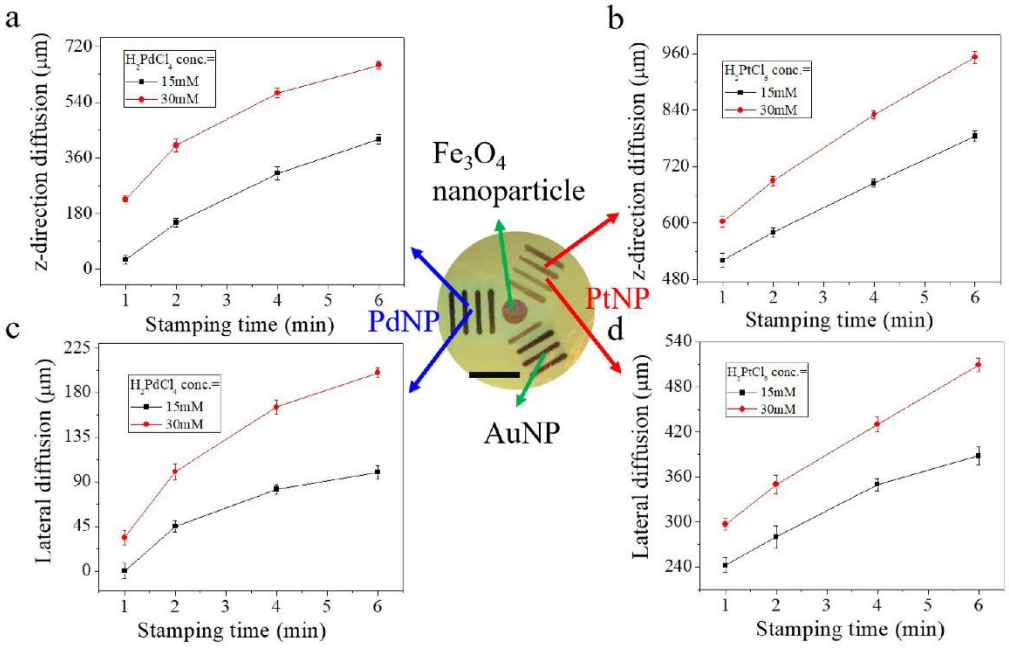

Figure 3.4 Variation of PdNP (a,c) and PtNP (b,d) domain size in z-direction and lateral direction of PNIPAM hydrogel material as a function of stamping time and concentration of metal ion precursor in the stamp

3.3.2 Nanoparticle pattern generated by site-selective shape-modification of pre-embedded nanoparticle

Plasmonic nanoparticle is known to have shape-dependent optical property, such as shape-dependent light absorption.[151] Instead of converting pre-embedded nanoparticle in the composite hydrogel to a different one by using the approach developed in section 3.3.1, here we modified shape of the nanoparticle to develop dual-light responsive composite hydrogel material.

Here triangular silver nanoplate (AgNPr) was integrated into PNIPAM hydrogel by polymerizing PNIPAM hydrogel precursor in the presence of silver nanoprism. The silver nanoprism was synthesized according to published literature.[152] The agarose hydrogel stamp pre-soaked in $NH_2OH{\cdot}HCl$ aqueous solution was brought in contact with silver nanoprism-loaded PNIPAM hydrogel. Interestingly, during diffusion of $NH_2OH{\cdot}HCl$ into PNIPAM hydrogel, silver nanoprisms were turned into silver nanodiscs, which shifted the light absorption peak of the composite hydrogel from ~820nm to ~425nm. By spatially controlling diffusion of $NH_2OH{\cdot}HCl$ in the composite hydrogel, dual-light responsive hydrogel material was developed (see Figure 3.5). As seen from inset image in Figure 3.5, distinct domains of silver nanoprism (dark color) and silver nanodisc (light color) were patterned in the hydrogel. The sharp difference in the shape of nanoparticle enabled the hydrogel to absorb two different light wavelengths with little overlap in the absorption spectra (Figure 3.5). It is expected that the bending deformation of the composite hydrogel sheet can be orthogonally tuned by using two light wavelengths, bringing in new shape transformation mode.[153]

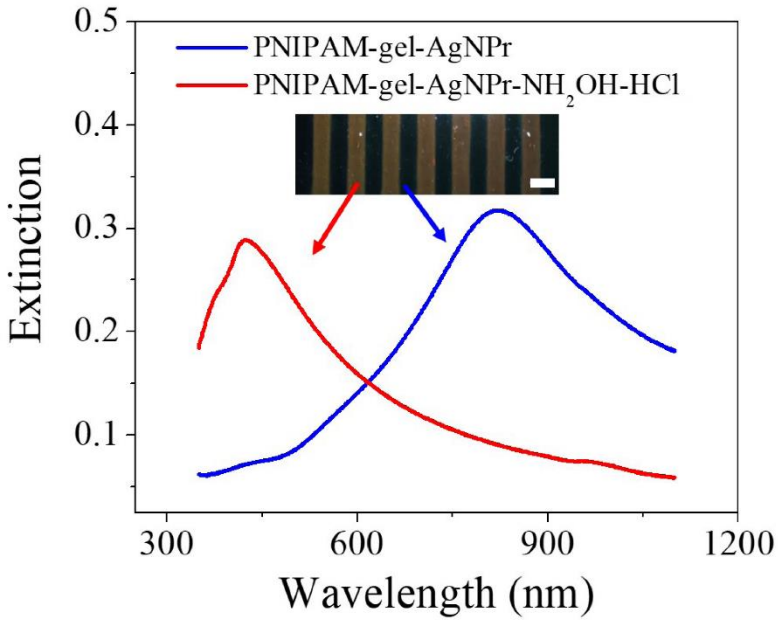

Figure 3.5 UV-Vis extinction spectra of PNIPAM-AgNPr hydrogel before (blue curve) and after $NH_2OH{\cdot}HCl$ treatment (red curve). As clearly seen, after stamping $NH_2OH{\cdot}HCl$ into PNIPAM-AgNPr composite hydrogel, the hydrogel has nanoparticle-containing domains that have distinct light extinction property. Scale bar: 2mm.

3.3.3 Nanoparticle pattern generated by site-selective removal of pre-embedded nanoparticle

Nanoparticle pattern can also be generated by selectively removing nanoparticles pre-loaded in the material. Here gold nanorod was pre-loaded in the PNIPAM hydrogel during hydrogel fabrication by polymerizing PNIPAM hydrogel precursor in the presence of gold nanorod. The gold nanorod was synthesized via seed-mediated approach developed in our group.[154] Its surface was modified by thiol-terminated polyethylene glycol via ligand exchange method,[155] which made the gold nanorod well-dispersed in hydrogel precursor. The agarose hydrogel stamp was pre-soaked in an aqueous solution of gold etchant composed of potassium iodide (KI) and iodine (I_2)

and was brought in contact with gold nanorod-loaded PNIPAM hydrogel. During diffusion of KI and I_2 into PNIPAM hydrogel, gold nanorod was etched away.[156] By spatially controlling diffusion of KI and I_2 in the composite hydrogel, PNIPAM hydrogel with spatially patterned gold nanorod was developed (see Figure 3.6). In this example (Figure 3.6), a ring-shaped domain in the circular hydrogel sheet (middle image in Figure 3.6) was depleted of gold nanorod through etching. The patterned circular hydrogel sheet deformed to a saddle-type geometry under near-infrared laser. Though gold nanorod was used in this demonstration, other gold material with different shapes and surface ligands can be integrated in the hydrogel as well, making the composite hydrogel sheet respond to different light wavelengths.[157]

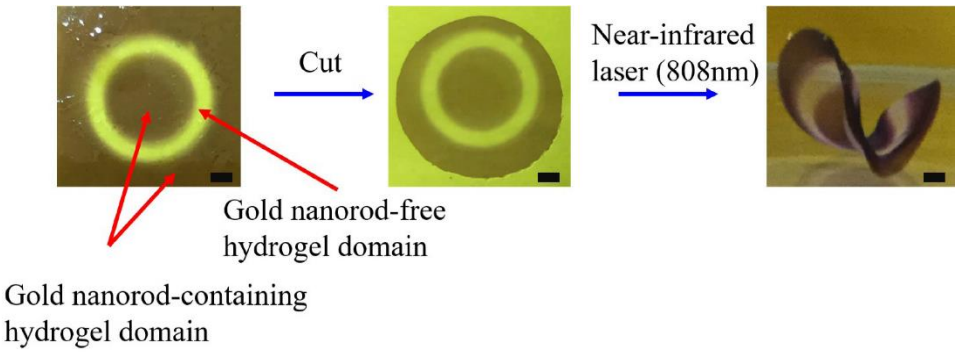

Figure 3.6 Composite hydrogel sheet patterned with gold nanorod and its shape transformation under laser irradiation. Scale bar: 2mm.

3.3.4 Nanoparticle pattern generated by site-selective generation of nanoparticle from its ion precursor

Instead of loading pre-synthesized nanoparticle in hydrogel material during its fabrication and patterning nanoparticle thereafter as described in previous sections, here we pre-loaded metal ion precursor and later converted it to nanoparticle. In this example, the agarose hydrogel stamp pre-soaked in a mixture aqueous solution of iron

ions (Fe^{2+} and Fe^{3+}, molar ratio between Fe^{2+} and Fe^{3+} is 1:2), which was then brought in contact with PNIPAM hydrogel. During the contact, iron ions diffused into PNIPAM hydrogel matrix and the diffusion distance increased with increase of stamping time and iron ion concentration in the stamp (see Figure 3.S4). By subjecting the iron-ion-containing PNIPAM hydrogel to sodium hydroxide aqueous solution, iron oxide (Fe_3O_4) nanoparticle was generated in the hydrogel matrix through co-precipitation of iron ions.[158] By spatially modulating diffusion of Fe^{3+} and Fe^{2+} in the composite hydrogel, PNIPAM hydrogel with spatially patterned Fe_3O_4 nanoparticles was developed (see Figure 3.7). As evidenced by the inset graphs in Figure 3.7a-d, there is a concentration gradient of Fe_3O_4 nanoparticle in the patterned feature reflected by the relatively smooth light intensity transition between Fe_3O_4-containing and Fe_3O_4-free domains. The spacing between Fe_3O_4 domains can be as small as ~400 μm and Fe_3O_4 domain size is ~1mm, which can be further reduced by using agarose stamp with smaller bas-relief feature.

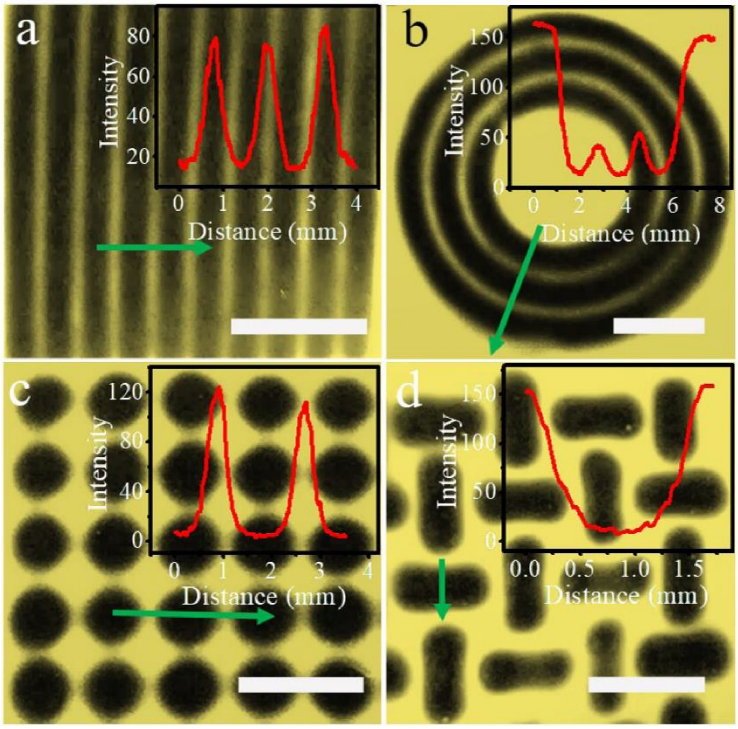

Figure 3.7 Various Fe_3O_4 NP patterns generated by the stamping approach. Inset graphs are light intensity profiles among Fe_3O_4-containing and Fe_3O_4-free domains along the direction as indicated by green arrows. Scale bar: 4mm.

3.3.5 Nanoparticle pattern generated in non-planar hydrogel material

By using flexible hydrogel stamp inked with gold ion, gold nanoparticle pattern was generated in non-planar AgNP-loaded hydrogel material with either concave or convex curvature as well (see Figure 3.8). In Figure 3.8a, the flexible hydrogel stamp with bas-relief feature conformed to the geometric curvature of the non-planar hydrogel, while in Figure 3.8b, the tubular AgNP-loaded hydrogel was rolled along the flexible hydrogel stamp with bas-relief feature. During the contact between flexible hydrogel stamp and AgNP-loaded hydrogel, gold ion diffused into the hydrogel and generated AuNP patterns.

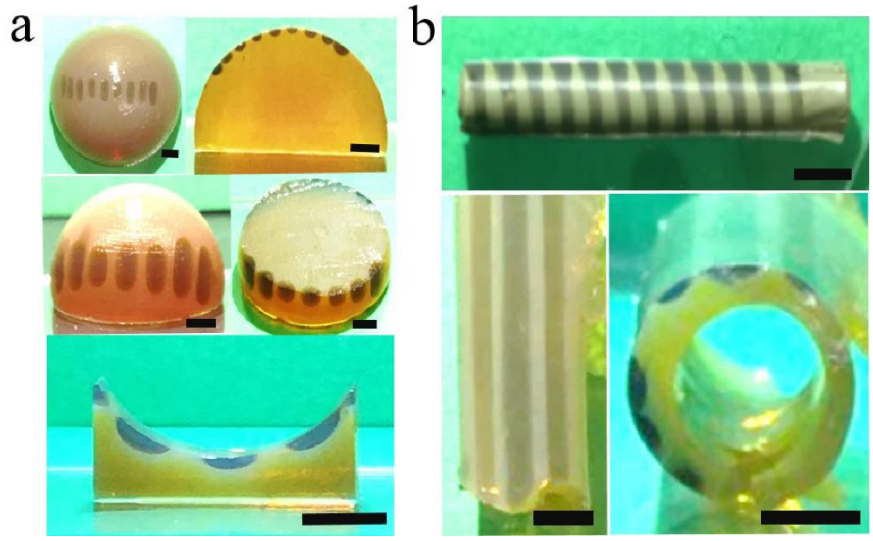

Figure 3.8 Gold nanoparticle pattern generated on hydrogel material with non-planar geometry (concave or convex surface). a) The flexible hydrogel stamp with bas-relief features conforms to the curvature of the non-planar hydrogel and gold ion diffused into hydrogel to generate AuNP patterns; b) the tubular AgNP-loaded hydrogel was rolled along the flexible hydrogel stamp and during this process gold ion diffused in the hydrogel to generate AuNP patterns. Scale bar: 2mm.

3.4 Conclusions

In conclusion, this Chapter developed a simple and efficient stamping approach to pattern nanoparticle in both lateral and z-direction of hydrogel material with desired feature size and spacing. The pattern depth and width of nanoparticle can be controlled by modulating ion diffusion during stamping process. This patterning technique is expected to greatly enrich shape transformation of thermo-responsive hydrogel material which will be explored in Chapters 4 and 5.

Chapter 4: Shape-shifting composite hydrogel sheet with spatially patterned plasmonic nanoparticles

Chapter overview

In Chapter 3, we developed a simple and effective stamping approach to pattern nanoparticle in both lateral and z-direction of hydrogel material. The pattern depth and width of nanoparticle can be controlled by modulating ion diffusion in the stamping process. This Chapter explored the shape transformation of composite hydrogel sheet patterned with gold nanoparticle under laser irradiation. It was found that the same composite hydrogel sheet can be designed to have distinct deformation behaviors, depending on laser irradiation and spatial distribution of gold nanoparticle, which has rarely been reported previously.

This chapter was adapted from the accepted manuscript as follows: Guo, H. Y., Liu, Y. J., Yang, Y., Wu, G. Y., Demella, K., Raghavan, S. R., and Nie, Z. H.*, Shape-shifting composite hydrogel sheet with spatially patterned plasmonic nanoparticles, *J. Mater. Chem. B*, **2018**, 10.1039/C8TB01959B.

4.1 Introduction

Shape-changing materials have attracted considerable attention in the past decades, owing to their potential applications in soft robot, artificial muscle, biomedicine and mechanical device.[9, 16, 45, 53-56, 159-160] Among these materials, hydrogel, a water-swollen network, is unique since its deformation usually relies on a differential swelling in the material, which mimics naturally occurring shape-changing objects, such as tendril, pine cone, Venus flytrap, etc..[53-55] Common strategies to generate differential swelling in hydrogels include layering materials that have varying swelling

capability or generating domains within hydrogel that have swelling extent different from their surrounding materials.[16, 53-54] Many environmental stimuli have been used to induce differential swelling in the hydrogel to trigger its deformation, such as temperature,[62-64] pH,[65] ionic strength,[66] enzyme,[67] DNA,[68] ions,[69] humidity,[70-71] light[28, 72-73] and external fields.[74-75] Among others, light is particularly attractive as it can be remotely delivered to material with desirable spatial and temporal resolution, which brings more controllability to the shape transformation of materials, such as liquid crystal polymer/elastomer,[161] shape memory film,[162-163] supramolecular assembly,[46-47] and hydrogel.[93, 118, 135, 164] For example, light can be used to drive the transformation of the same hydrogel sheet into multiple distinct shapes by modulating light irradiation patterns,[135, 164] which cannot be readily achieved by using chemical-responsive hydrogel.[96] Controllable motion of shape-changing hydrogel can be realized by region-selective exposure of materials to light to induce shape deformation.[93, 118] Despite the shape-transformation versatility enabled by local irradiation of light in these platforms, this strategy often requires a special set-up or is limited by undesired shape transformation originated from variation in the irradiation area upon the deformation of materials.[135]

Instead of modulating area of light exposure, one can structure the materials with light-responsive components and use un-patterned light to control the shape transformation of the material. This concept has been extensively used in the deformation of azobenzene-based materials in which azobenzene moiety is pre-patterned in the materials, thus enabling defined deformation under light.[46, 165] Another example is the shape transformation of pre-strained polystyrene film where the regions

patterned with colored inks serve as actuation hinges in response to light.[163] In this case, the spatial distribution of the light responsive components is crucial to the mode and complexity of the shape transformation of materials.[163] However, there remains challenge to readily control the distribution of light-responsive elements in materials simultaneously along both in-plane and axial direction, in order to achieve more complex shape transformation modes.

In Chapter 3, we developed a simple approach to pattern nanoparticle in lateral and z-direction of hydrogel material. Herein we explored shape transformation of patterned composite hydrogel sheet under laser irradiation. The composite hydrogel exhibits distinct deformation modes upon NIR light irradiation, depending on irradiation direction and spatial distribution of AuNP domain (see Figure 4.1). This shape-transforming scenario has rarely been reported previously.

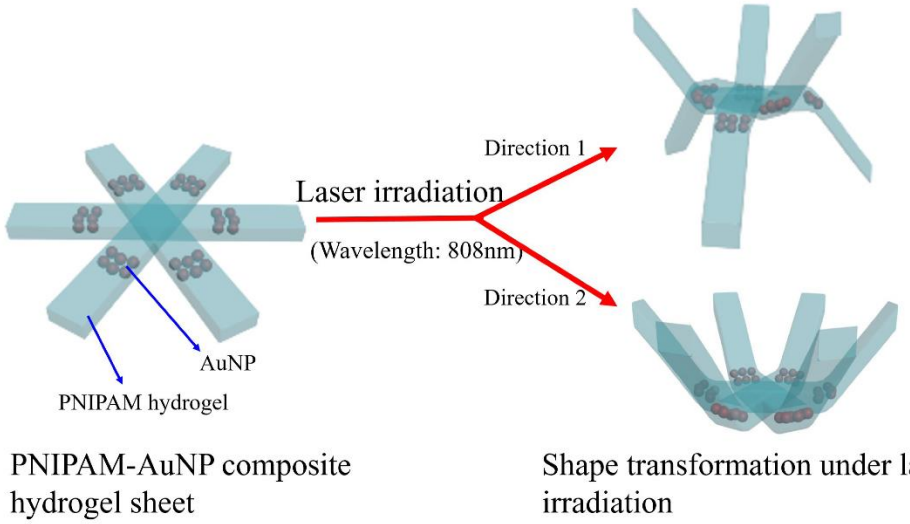

Figure 4.1 Schematic illustration of shape transformation of patterned composite hydrogel sheet under laser irradiation.

4.2 Experiments

Materials, AgNP synthesis, AgNP-loaded hydrogel synthesis, agarose stamp fabrication, wet stamping and diffusion study were presented in Section 3.2.1, 3.2.2, 3.2.3, 3.2.4, 3.2.6, 3.2.7 in Chapter 3, respectively. Characterization method for hybrid hydrogel was described in Section 3.2.8 in Chapter 3.

4.2.1 Light-triggered shape transformation

An 808 nm laser (MDL-N-808, Changchun New Industries Optoelectronics Technology Co., Ltd, China) with tunable output power (0-8W) was used as the laser source throughout the experiments. During the experiments, the hybrid hydrogel was immersed in 600 mL water in a glass petri dish.

4.2.2 Hydrogel swelling

The swelling property of the hydrogel was characterized by using the swelling ratio which was measured gravimetrically after wiping off the excess water on the hydrogel's surface with a piece of Kimwipe in the temperature range from 18 to 36 ℃. The hydrogel was incubated in a water bath for at least 24 h at each temperature. The swelling ratio was calculated by using the following formula,

$$\text{Swelling ratio} = W_s/W_d$$

where W_s was the weight of the swollen hydrogel at the particular temperature and W_d was the dry weight of the hydrogel.

4.2.3 Mechanical property

An AR2000 stress-controlled rheometer (TA Instruments) was used to study the mechanical properties of the hybrid hydrogel sheet. Rheological experiments were performed at 25 ℃, 28 ^{o}C and 35 ℃, respectively by using cone-and-plate geometry (20 mm diameter and 2^{o} cone angle). A solvent trap was used to minimize drying of the sample during measurements. Dynamic stress-sweep experiments were first performed on the sample to identify its linear viscoelastic (LVE) region at different temperatures and dynamic frequency sweeps were then performed within the LVE region.

4.2.4 Photothermal imaging of hybrid hydrogel

The photothermal property of the hybrid hydrogel was studied by photothermal imaging technique. Briefly, the hybrid hydrogel sheet was immersed in 3 mL water in a plastic petri dish and was irradiated with an 808 nm laser at a power density of 6.37 W/cm^2 for 1 min and then the laser was shut off. The surface temperature of the hybrid hydrogel was monitored by using a FLIR SC300 infrared camera (FLIR, Arlington, VA). Real-time thermal images were captured with frame rate at 60 Hz, and analyzed by FLIR Examiner software.

4.2.5 Jumping and load-lifting of composite hydrogel sheet

The composite hydrogel sheet (length: 20mm, width: 2.2mm, thickness: 0.25mm) was patterned with AuNP strip (width: 2mm, length: 3mm, thickness: 0.06mm). The patterned composite hydrogel sheet deformed and jumped towards laser after

irradiation for 20s by releasing the stored energy during its deformation. For load-lifting, the composite hydrogel sheet was patterned with two AuNP strips (width: 2.2mm, length: 1.5mm, thickness: 0.06mm) A gelatin bead (3 milligram) was glued onto the patterned composite hydrogel sheet (eighteen milligram) and it was irradiated by laser. The composite hydrogel sheet bent and raised the gelatin bead to 1cm high in 30 seconds under laser irradiation.

4.2.6 Estimation of minimum laser energy required for bending to occur

The composite hydrogel sheet ((length: 20mm, width: 2.2mm, thickness: 0.25mm)) was patterned with AuNP strip as the "hinge" in bending under irradiation. The width of AuNP was 2.2mm, while its length varied. We found that a larger laser power density was needed to initiate bending of composite sheet with a smaller hinge width in water. We estimated the minimum laser energy (*E*) required for bending to occur by using the following equation,

$$E = (I_o - I_o * 10^{-Abs})wlt$$

where I_o, *Abs*, *t*, *w*, *l* are the intensity of incoming laser, absorbance of hydrogel sheet, onset time of bending, hinge width and length, respectively. Using this equation, *E* was calculated to be 0.9 J for this hydrogel (see Table 4.S1).

4.3 Results and discussion

4.3.1 Bending analysis of patterned composite hydrogel sheet

Bending behavior of the patterned composite hydrogel sheet was studied by using a bilayer-type hydrogel sheet (Figure 4.2). Here the bilayer sheet consists of a hybrid gel layer (containing AuNP domain) with a thickness of h_{hybrid} and a pure gel layer (without AuNPs) with a thickness of h_{pure} (Figure 4.2a). The thickness of AuNP-containing domain (h_{hybrid}) was varied by modulating ion diffusion during stamping process as presented in Chapter 3. The experimental finding for bending deformation was presented in Figure 4.2b.

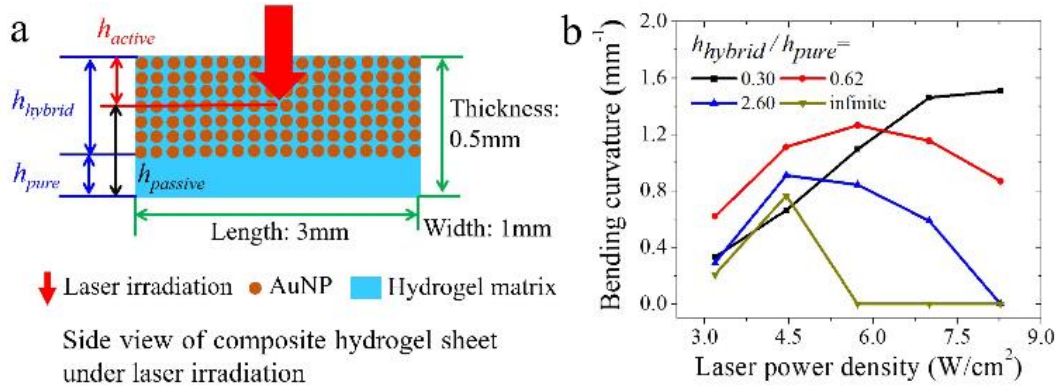

Figure 4.2 a) Schematic illustration of the cross-section of the composite hydrogel sheet under laser irradiation. b) Bending analysis of the composite hydrogel sheet as a function of laser power density.

As shown in Figure 4.2b, when h_{hybrid}/h_{pure}=0.3, the bending curvature of the composite hydrogel sheet increased with increase of PD. When $h_{hybrid}/h_{pure} \geq 0.6$, the bending curvature exhibited a peak as a function of laser PD. These bending behaviors can be explained by using the classical model developed for bending deformation of

bi-metal thermostats. The bending curvature of hydrogel sheet (κ) is described as, [166-167]

$$\kappa = 6\frac{eh(1+h)\Delta\xi}{h_{total}(1+4eh+6eh^2+4eh^3+e^2h^4)}$$

where h_{total}, e, h and $\Delta\xi$ are thickness of composite hydrogel sheet, ratio between Young's modulus of active and passive gel layer, ratio between thickness of active and passive gel layer and actuation force, respectively. Here the actuation force is the volumetric swelling ratio difference between active and passive gel layer. This model has been used previously to interpret bending of shape-changing hydrogel material[68, 86].

In the bending deformation of our composite sheet, the active gel layer is the layer that absorbs light and generates heat, while the passive gel layer is the layer that does not absorb laser energy (Figure 4.2a). Due to laser intensity decay (caused by strong absorption of AuNPs in the hydrogel sheet) along irradiation direction, thickness of active and passive gel layer (h_{active}, $h_{passive}$, Figure 4.2a) varied depending on thickness of hybrid gel layer and laser PD. When h_{hybrid}/h_{pure}=0.3, light can access all the hybrid gel layer. In this case, since $h=h_{active}/h_{passive}$ =0.3 ($h_{active}=h_{hybrid}$, $h_{passive}=h_{pure}$) is a constant, the increase in laser PD led to an increase in $\Delta\xi$ (see Figure 4.S1b) and hence increase in bending curvature. In contrast, at high h_{hybrid}/h_{pure}, light can only penetrate part of the hybrid layer due to strong light absorption by AuNPs and intensity decay along hydrogel's thickness direction. The light penetration depth increased with increase of laser PD, leading to an increase of $h=h_{active}/h_{passive}$. As a result, the dependency curve of bending curvature on laser PD exhibited a parabolic form[86]. The bending curvature was found to increase with decreasing gel thickness (see Figure 4.3,

Figure 4.S2). The result is in a good agreement with the model, since a smaller h_{total} of thinner gel gives rise to a larger κ when other parameters (h, e and $\Delta\xi$) are the same.

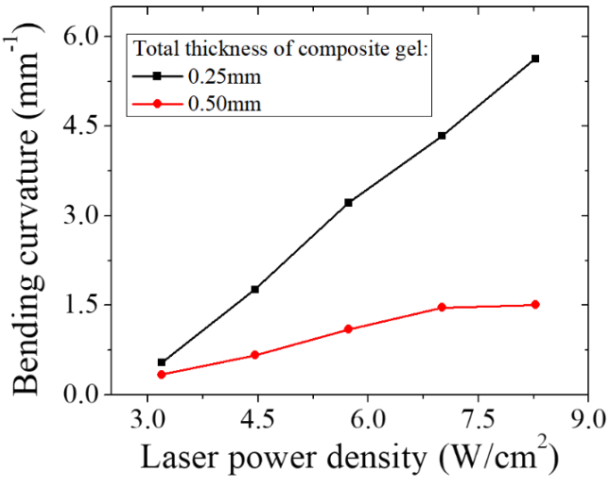

Figure 4.3 Quantitative analyses of bending curvature of composite hydrogel sheet with different thicknesses.

The deformed hydrogel returned to its original state in 2 minutes after removing the laser (see Figure 4.S3). The bending/recovering could be repeated for many times without appreciable change in bending angle, demonstrating high reversibility of the deformation (see Figure 4.4).

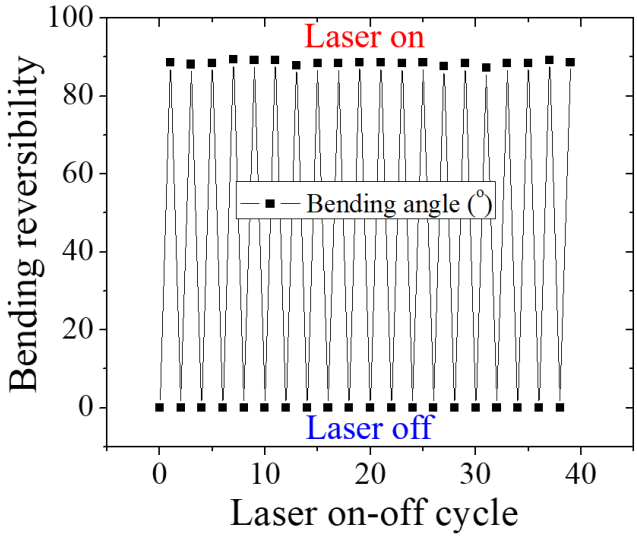

Figure 4.4 Bending reversibility of composite hydrogel during laser on-off cycle

As studied in Chapter 2, the bending deformation of hybrid hydrogel occurred after a certain amount of laser energy was delivered to the system. Here for the patterned composite hydrogel sheet, it was also found that a minimum laser power density was needed to initiate bending deformation at a certain nanoparticle stripe length (see Figure 4.5). For example, when nanoparticle stripe length is smaller, a larger laser power density is needed for bending to occur. The estimated minimum laser energy required for bending deformation to occur was 0.9J for the patterned hybrid hydrogel in water (see Table 4.S1).

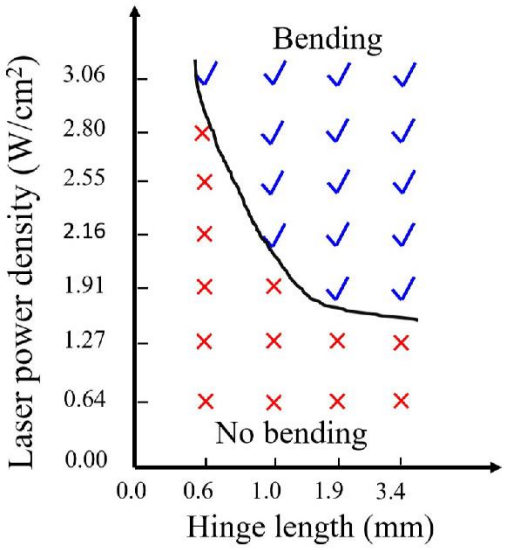

Figure 4.5 Bending analysis of composite hydrogel sheet patterned with AuNP strip as hinge in its bending under laser irradiation. Length, width and thickness of composite hydrogel sheet were 20mm, 2.2mm and 0.25mm, respectively. The width of AuNP strip was 2.2mm, while its length varied.

4.3.2 Shape transformation of patterned composite hydrogel sheet

The composite hydrogel sheet with varied AuNP patterns were fabricated. In these composite sheets, AuNPs were patterned throughout the hydrogel in certain region (colored black in illustrations in Figure 4.6) and partially into the hydrogel in other region (colored grey in illustrations in Figure 4.6) along hydrogel's thickness direction. For simplicity in discussion, we defined "front side" of the hydrogel as the side that has more AuNP domains and the "back side" as the side that has smaller number of AuNP domains. As an example, the "front side" of star-like composite sheet has six AuNP domains while its "back side" has three AuNP domains (Figure 4.6a).

We found that the patterned composite hydrogel sheet had distinct deformation behaviors, depending on which hydrogel side was irradiated (Figure 4.6). As an example, when "front side" of the patterned star-like hydrogel sheet was irradiated, all six petals bent to same direction; while they bent to opposite directions when its back side was irradiated (see Figure 4.6a). This is because when irradiated from "back side" of the star-like hydrogel sheet, the three petals with AuNP domains on this side bent towards laser while the other three petals bent away from laser since the AuNP domains were located on their "front side". The deformations of composite sheet with other AuNP patterns were affected by light exposure direction as well (Figure 4.6b-f). For example, when "front side" was irradiated, the square-shaped composite hydrogel sheet with AuNP patterned on its corner transformed to a saddle geometry; while it deformed to an incomplete tube-like structure when its "back side" was irradiated (Figure 4.6f). As far as we know, this deforming scenario has not been reported previously.

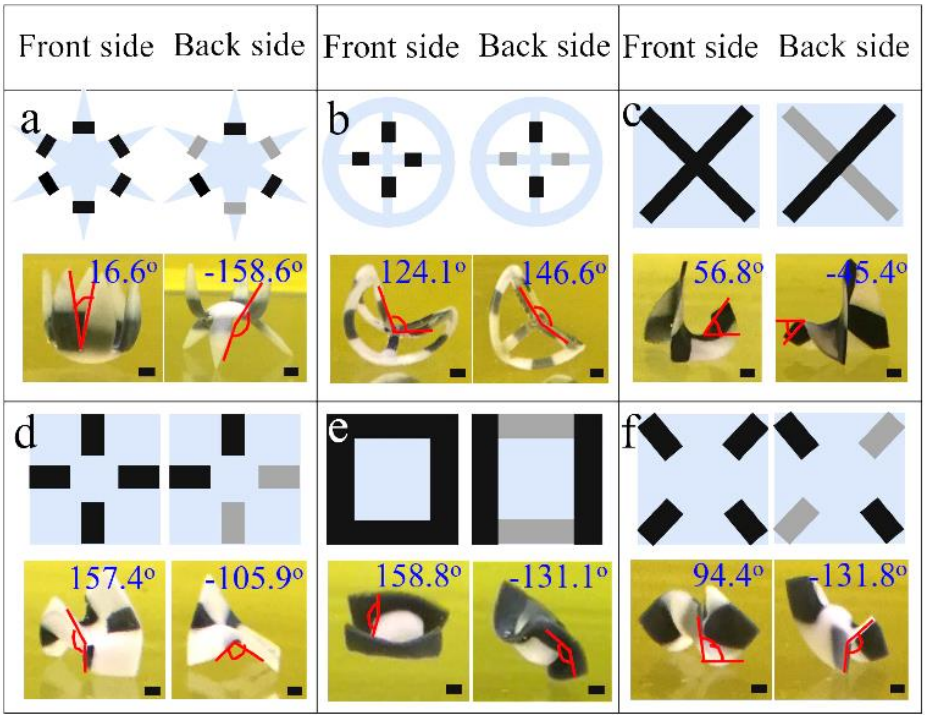

Figure 4.6 Shape deformation of patterned composite hydrogel sheet under a continuous laser irradiation (wavelength: 808nm). The black and grey regions represent areas with AuNPs patterned throughout the hydrogel and partially into the hydrogel along thickness direction, respectively. The negative bending angle indicates a bending direction was opposite when laser was irradiated onto the hybrid hydrogel from different sides (front side vs. back side). Scale bars are 1mm.

4.3.3 Jumping and load-lifting of patterned composite hydrogel sheet

With proper design, the patterned composite hydrogel sheet can deform and jump under laser irradiation by releasing stored energy during its deformation against the container. For example, the composite hydrogel sheet patterned with AuNP strip jumped to 1cm high after laser irradiation for 20 seconds (Figure 4.S4).

The patterned composite hydrogel sheet was also used to lift up load. A gelatin bead (3 milligram) was raised to 1cm high in 30 seconds by the patterned composite hydrogel sheet (18 milligrams) under laser irradiation (Figure 4.S5). The input energy was calculated to be 12.5J and the output work was 2×10^{-6}J (specific work: 0.1J/kg). The energy conversion efficiency was 0.000016% for the patterned composite hydrogel sheet.

4.3.4 Mechanism of shape transformation of patterned composite hydrogel sheet under laser irradiation

Shape transformation of composite hydrogel sheet patterned with gold nanoparticle is due to the combination of photo-thermal property of gold nanoparticle and thermo-responsiveness of hydrogel matrix (see Figure 4.S1). Under laser

irradiation, the surface temperature of the patterned composite hydrogel sheet was raised from 22°C to 29°C, causing shrinkage and modulus change of the composite hydrogel sheet and hence the bending deformation (see Figure 4.S1b,d). We note that the surface temperature of the patterned composite hydrogel (length: 3mm, width: 1mm, thickness: 0.5mm) under laser irradiation depends on the amount of water in which the composite hydrogel sheet is immersed. For example, when the hybrid hydrogel sheet was immersed in 600mL water, its surface temperature did not change due to prompt heat dissipation to the large heat sink (see Figure 4.S1c). However, when the same composite hydrogel sheet was immersed in a small amount of water (3mL), its surface temperature was raised from 22 °C to 29 °C in 1 minute under laser irradiation with same power density. Further when the composite hydrogel sheet was irradiated in air, its surface temperature was raised from 20°C to 136°C (data not shown). By introducing anisotropic swelling in the hydrogel sheet by patterning it with gold nanoparticle and subjecting it to laser irradiation, the composite hydrogel sheet transformed to a certain geometry depending on gold nanoparticle patterns.

4.3.5 Discussion

In the experiments conducted in this chapter, the hydrogel thickness was equal to or larger than 250 μm. Reducing the hydrogel thickness could potentially diminish the temperature difference in hydrogel's thickness-direction when being irradiated by laser light. In this circumstance, in-plane swelling difference due to localized irradiation may play an important role in the hydrogel's deformation. It was found that three problems needed to be solved for thin hydrogel (i.e. gel thickness: 25 μm). The first one is that

AgNP loading should be increased so that the thin hydrogel will have sufficient absorption at 808 nm at a certain laser power density. As seen from Figure 4.7, light absorption depended on concentration as well as on light path (gel thickness in this case). We noted that the light absorption of AgNP-gel was similar to AuNP-gel after patterning. The second one is that the thin hydrogel preferred to float on water surface instead of sinking in water. It also easily attached to other surface, such as plastic or metal spatula. The third one is that the mechanical property of the thin hydrogel was poor making it fragile. Solving these problems will be future work.

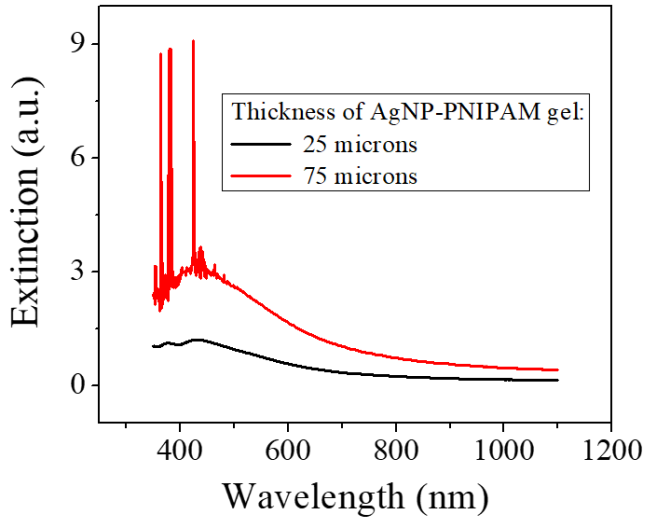

Figure 4.7 UV-Vis extinction spectra of the composite hydrogel sheet with different thicknesses

In addition to use nanoparticles as the filler which are loaded during hydrogel synthesis, it is also possible to attach a nanoparticle film onto the hydrogel surface, which serves as photo-thermal converting agent. Figure 4.8 was an example of this. A self-assembled gold nanorod film was successfully transferred onto PNIPAM hydrogel

surface. The hydrogen bonding between the carboxyl groups on gold nanorod surface and the amide groups in PNIPAM hydrogel made the interfacial adhesion strong. Under laser light irradiation (wavelength: 808nm), the layered hybrid hydrogel (gel thickness: 125μm) deformed (data not shown), although the photo-thermal conversion layer was only tens of nanometers (gold nanorod diameter was 30nm).

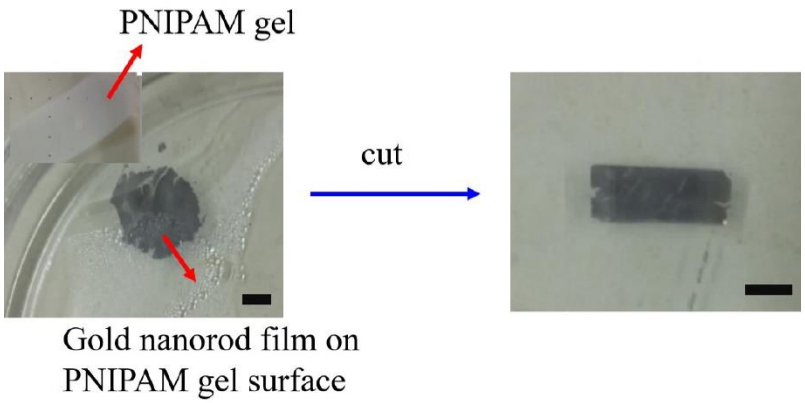

Figure 4.8 A self-assembled gold nanorod film was attached onto PNIPAM hydrogel via electrostatic interaction. The gold nanorod film was the photothermal converting agent in shape transformation (not shown) of the composite hydrogel sheet. Scale bar: 2mm.

4.4 Conclusions

In conclusion, this Chapter explored shape transformations of composite hydrogel sheet with varied AuNP patterns. The composite hydrogel sheet transformed to 3-D geometries under a continuous NIR laser irradiation by the combination of photo-thermal effect of AuNPs and thermo-responsive property of the hydrogel matrix. Due to the controllable distribution of AuNP patterns in both hydrogel's lateral and z-

direction, the same composite hydrogel sheet was designed to exhibit distinct transformation modes depending on laser irradiation direction, which has rarely been reported previously. We foresee that the patterning technique reported here is general and can be applied to other thermo-responsive hydrogel systems, while the patterned composite hydrogel may find applications in biomedicine and soft robotics.

Chapter 5: Shape-shifting composite hydrogel sheet with erasable and rewritable patterns of nanoparticle

Chapter overview

In Chapter 4, the hydrogel sheet was patterned with gold nanoparticles via a site-selective galvanic replacement reaction between gold ion and silver nanoparticles pre-embedded in the hydrogel sheet. The same hydrogel sheet was designed to exhibit distinct deformation modes depending on laser irradiation direction. One limitation with this approach is that gold nanoparticle pattern cannot be erased and rewritten in the same hydrogel sheet. This Chapter developed a simple approach to pattern iron oxide nanoparticle (photo-thermal converting agent) in the hydrogel. The iron oxide nanoparticle pattern can be readily erased and rewritten in the same hydrogel sheet. Therefore, the same hydrogel sheet can be reprogrammed to have distinct shape transformations under laser irradiation by altering iron oxide nanoparticle pattern.

A manuscript based on this Chapter is prepared for submission to *Advanced Functional Materials*.

5.1 Introduction

Shape-transforming material is often programmed to have one or several shape transformation under environmental stimuli. Recently, reprograming material's shape-transformation was proposed as a new concept in the field of shape-transforming material. Several approaches have been developed to achieve re-programmability in material's shape transformations. For example, Li *et al.* developed a shape memory polymer film doped with polydopamine (PDA) molecules which converted light to heat

to trigger film's shape recovery.[168] Though PDA can be erased and reintegrated in the polymer film to program new type of shape transformation, the polymer film needs to be re-stretched before programming which may limit its application in settings that require immediate transformation of the material. In another example, Gelebart *et al.* developed a photo-responsive liquid crystal polymer film. The polymer film can respond to dual light wavelengths after locally changing the molecular state of the photo-responsive unit in the material.[153] The pattern of dual light responsive domains can be re-designed after converting photo-responsive unit back to its initial state. However, the switching cycles (4 cycles) between two different molecular states of the photo-responsive units are limited which may be fundamentally due to the instability of organic molecules under cyclic treatment by harsh chemicals.

Herein we developed a simple and efficient approach to reprogram photo-guided shape transformation of composite hydrogel sheet. Photothermal converting agents- Fe_3O_4 nanoparticles were patterned in a thermo-responsive PNIPAM hydrogel sheet using method developed in section 3.3.4 in Chapter 3 (see Figure 5.1). Since Fe_3O_4 nanoparticle can be readily erased and rewritten in the hydrogel, reprogrammable shape transformations of the composite hydrogel sheet are readily achieved by changing Fe_3O_4 patterns.

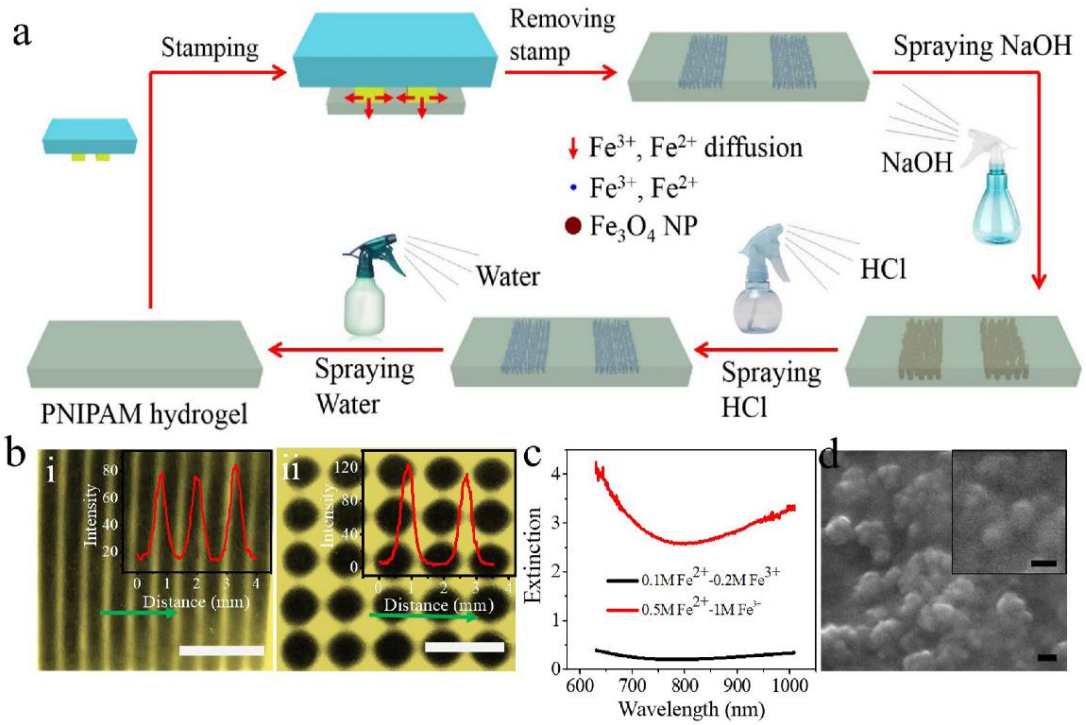

Figure 5.1 a) Schematic illustration of patterning, erasing and rewriting iron oxide (Fe_3O_4) nanoparticle in thermo-responsive PNIPAM hydrogel matrix; b) Fe_3O_4 nanoparticle patterns generated by stamping approach. Inset graphs are light intensity profiles of the composite hydrogel sheet along the direction indicated by green arrows; c) UV-Vis extinction spectra of composite hydrogel sheet; d) Morphology of Fe_3O_4 nanoparticle. Scale bar: 4mm in b), 100nm in d) 60nm in inset image of d).

5.2 Experiments

5.2.1 Materials

All chemicals were purchased from Sigma-Aldrich without special notification and were used without further treatment. Chemicals used were as follows: N-Isopropylacrylamide (NIPAM, monomer), N,N'-Methylenebis(acrylamide) (BIS,

cross-linker,), ammonium persulfate (APS, initiator), N,N,N',N'-Tetramethylethylenediamine (TEMED, catalyst), Ferric chloride ($FeCl_3$), Ferrous chloride ($FeCl_2$). Agarose powder was purchased from EZ BioResearch. Polydimethylsiloxane (PDMS) elastomer kit (Sylgard 184) was bought from Dow Corning. Deionized water was used throughout the experiments.

5.2.2 Fabrication of PNIPAM hydrogel

0.113g NIPAM monomer, 0.006g methylenebisacrylamide (cross-linker) and 10μL 10wt% APS (initiator) were dissolved in 1mL water. The solution was then purged with nitrogen on an ice-bed for 5 minutes. Following that, 5 μL TEMED (catalyst) was added into the solution. The solution was then injected to the hydrogel mold made by two cover slides separated by parafilm as the spacer. The polymerization was allowed to proceed for 2 hours at room temperature. After polymerization, the hydrogel mold was immersed in water and the hydrogel was removed from the mold.

5.2.3 Wet stamping

The agarose stamp was fabricated according to section 3.2.4 in Chapter 3. The stamping procedure was presented in section 3.3.4 in Chapter 3.

5.2.4 Erasing and rewriting iron oxide nanoparticle in hydrogel

Iron oxide-containing PNIPAM hydrogel was fabricated according to section 5.2.3. To erase iron oxide from the hydrogel, a concentrated hydrochloric acid (HCl, 37.5%) was sprayed onto the hydrogel, which dissolved iron oxide and generated Fe^{3+} and Fe^{2+} in the hydrogel. Then the hydrogel was immersed in water to remove Fe^{3+} and

Fe^{2+}. After that iron oxide nanoparticle was rewritten in the hydrogel by using the approach presented in section 5.2.3.

5.2.5 Photothermal property of hydrogel

In the experiment, a piece of pure PNIPAM hydrogel (length: 30mm, width: 12mm, thickness: 2mm) was put on a plastic petri dish (made of polystyrene) in air at room temperature (19.5^{o}C). The hydrogel was irradiated by laser at 6.38W/cm^2 for 1 minute. Then the laser was switched off and the surface temperature of the pure hydrogel was measured by using a digital thermometer. A piece of composite PNIPAM hydrogel (length: 30mm, width: 12mm, thickness: 2mm) was also irradiated in air at 6.38W/cm^2 for 1 minute and its surface temperature was measured in the same way as pure hydrogel. The composite hydrogel was prepared following method presented in preceding sections.

5.2.6 Hydrogel swelling

Swelling property of hydrogel was probed by measuring its size change as a function of temperature. A disk-shape hydrogel was immersed in a large amount of water whose temperature was controlled. The diameter of the disk-shape hydrogel was measured at each set temperature.

5.2.7 Mechanical property of hydrogel

An AR2000 stress-controlled rheometer (TA Instruments) was used to study the mechanical properties of the pure and composite hydrogel sheet. Rheological experiments were performed at 25 ℃ and 34 ℃, respectively by using cone-and-plate

geometry (20 mm diameter and 2^{o} cone angle). A solvent trap was used to minimize drying of the sample during measurements. Dynamic stress-sweep experiments were first performed on the sample to identify its linear viscoelastic (LVE) region at different temperatures and dynamic frequency sweeps were then performed within the LVE region.

5.2.8 UV-Vis measurement

The optical property of the composite hydrogel was characterized by measuring its light extinction using UV-VIS spectroscopy (Lambda 40 UV/VIS Spectrometer, PerkinElmer, USA). In the measurement, air was used as reference and a piece of hydrogel was then put on a glass slide. The UV-VIS spectra were then taken at a slit width of 1 nm, scanning speed of 480 nm/min and data interval of 1 nm.

5.2.9 Scanning electron microscopy (SEM)

For composite hydrogel characterization, the composite hydrogel was first freeze-dried and then coated with carbon (JFC-1200 Fine Coater, Japan). Following that, scanning electron microscopy (XL Series-30, Philips, USA) was used to characterize Fe_3O_4 nanoparticle in the hydrogel.

5.2.10 Diffusion study

The ion-inked agarose stamp was brought in contact with PNIPAM hydrogel for different amount of time, which was then immersed in 0.5M NaOH solution for 2 minutes to generate Fe_3O_4 nanoparticle. The size of the generated nanoparticle domain

in both xy- and z-direction of the hydrogel was then analyzed by using optical microscope. The nanoparticle domain size was plotted with respect to stamping time.

5.2.11 Characterization of bending behaviors of composite hydrogel sheet

A PNIPAM hydrogel sheet (length: 20mm, width: 4mm, thickness: 0.25mm) was patterned with iron oxide nanoparticle strip. The strip width was fixed as 4mm while its length varied. The patterned composite hydrogel sheet was subjected to laser irradiation at varied laser power density. The bending deformation was then monitored and analyzed.

5.2.12 Light-triggered shape transformation

An 808 nm laser (MDL-N-808, Changchun New Industries Optoelectronics Technology Co., Ltd, China) with tunable output power (0-8W) was used as the laser source throughout the experiments. During the experiments, the hybrid hydrogel was immersed in 600 mL water in a glass petri dish.

5.2.13 Regulation of chemical release by using composite hydrogel sheet

The composite hydrogel sheet was used as a “smart gate” to regulate chemical (Rhodamine B) release through its bending and unbending which was controlled by laser light. A hollow cavity with circular shape (diameter: 6mm) was made in the gelatin hydrogel and then a Rhodamine B aqueous solution (0.1mM) was added to the cavity. After that, the composite hydrogel sheet was partly glued using a cyanoacrylate-based adhesive onto the gelatin hydrogel, covering the Rhodamine B-

loaded region. Subsequently, the hydrogel device was immersed in 600mL water in a glass petri dish and the composite hydrogel sheet was exposed to laser at 6.38W/cm^2 to study release of Rhodamine B.

5.3 Results and discussion

5.3.1 Bending analysis of composite hydrogel sheet

Bending deformation of the composite sheet was studied by using a hydrogel sheet patterned with an iron oxide nanoparticle stripe, which acted as hinge along which the sheet bent during NIR laser irradiation. The bending deformation was due to combination of photothermal effect of Fe_3O_4 nanoparticle and temperature-dependent swelling state of the sheet (Figure 5.S1,2). It was interestingly found that the hydrogel sheet reached a bending angle of 180^o with increase of laser power density (PD) (Figure 5.2a), which has rarely been reported for light-responsive hydrogel-based shape-changing system. By varying hinge length and laser PD, a bending deformation diagram was constructed in which parameters (hinge length and laser PD) were identified for the sheet to have a 180^o bending angle (Figure 1b). It was found that a larger hinge length required a smaller laser PD to reach a bending angle of 180^o. We ascribed the 180^o bending angle achieved in current system to two factors: i) the presence of concentration gradient of iron oxide nanoparticle along hydrogel sheet's thickness direction; ii) the soft nature of the hydrogel sheet. The presence of iron oxide nanoparticle concentration gradient was reflected by the bending direction when different sides of composite hydrogel sheet were irradiated (Figure 5.S3). When side of the sheet that contacted stamp during ion patterning was exposed to laser, the sheet

bent towards laser (Figure 5.S3a); while when the opposite side of sheet was irradiated, the sheet bent away from laser (Figure 5.S3b), which suggested an iron oxide concentration gradient in hydrogel's thickness direction. Due to soft nature of the current hydrogel sheet, the hinge region deformed markedly during laser irradiation which brought the unexposed side over to laser sight, which increased the bending angle to 180^{o} with increasing exposure time (Figures 5.S4,5).

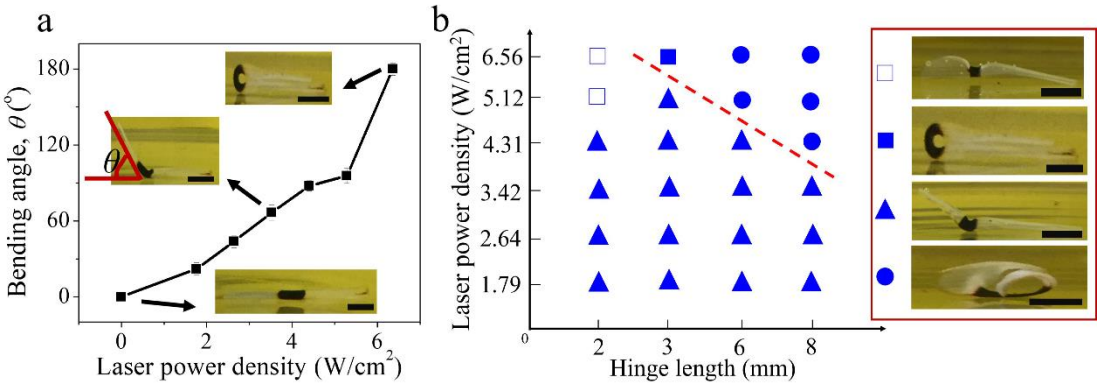

Figure 5.2 Bending analysis of composite hydrogel sheet with patterned Fe_3O_4 NP stripe/hinge (black area in the hydrogel). a) The composite hydrogel sheet reached a bending angle of 180^{o} with increasing laser power density (Fe_3O_4 NP stripe length: 3mm); b) Bending deformation of composite hydrogel sheet as a function of Fe_3O_4 NP stripe length and laser power density. Different symbols in the graph indicated different deformation types shown on right-hand side. Dashed red line was used to distinguish between deformations with bending angle of 180^{o} and those with bending angle less than 180^{o}. Scale bars are 3mm in a) and 4mm in b).

5.3.2 Reprogrammable shape transformation of composite hydrogel sheet with varied Fe_3O_4 nanoparticle patterns

The Fe_3O_4 nanoparticle patterns can be readily erased by spraying HCl onto the composite hydrogel sheet. After washing away excess HCl, new Fe_3O_4 nanoparticle pattern can be written in the sheet (Figure 5.1a). The erasing and rewriting took about 5 minutes. A multitude of distinct shape transformations achieved from a single sheet with varied nanoparticle patterns were shown to demonstrate the capability of this approach in reprogramming shape transformation of hydrogel sheet (Figure 5.3). Many more transformations were expected by writing in the sheet with new nanoparticle patterns (Figure 5.S6). After switching off laser, the deformed sheet recovered its original flat state within 15 minutes.

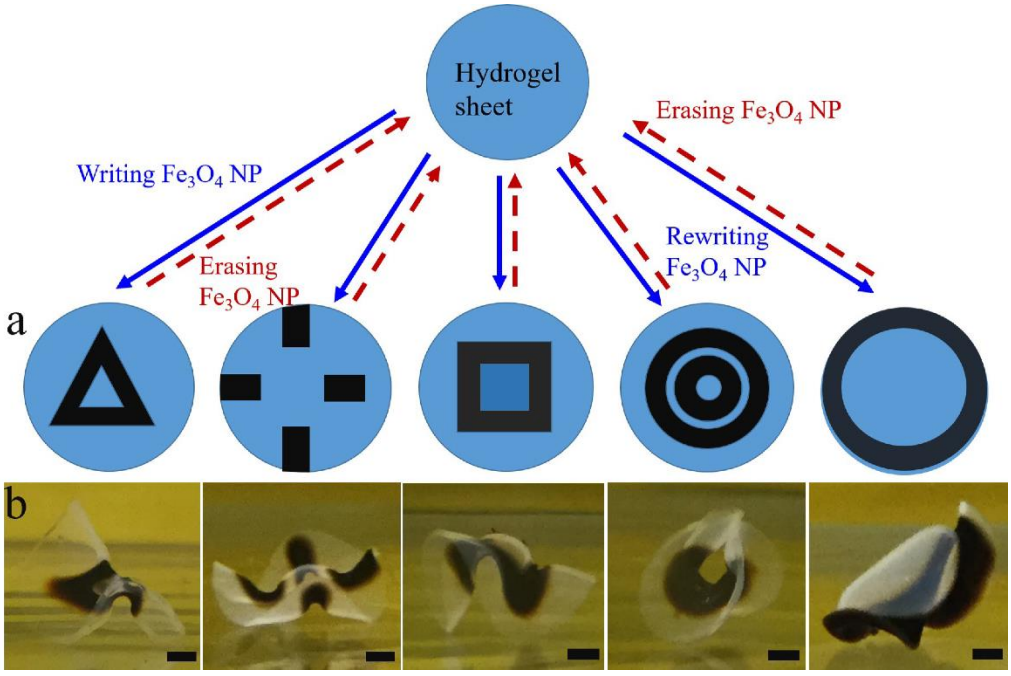

Figure 5.3 a) Schematic illustration of various Fe_3O_4 patterns (black domains) in the hydrogel; b) corresponding 3-D geometries transformed from 2-D composite hydrogel sheet under laser irradiation. Scale bar: 2mm.

5.3.3 Shape transformation of composite hydrogel tube with Fe_3O_4 nanoparticle pattern

The approach developed in this Chapter allows us to pattern Fe_3O_4 nanoparticle on non-planar composite hydrogel such as hydrogel tube as well. A piece of paper soaked with iron ions was wrapped around PNIPAM hydrogel tube for 10 minutes. Then the iron-ion-loaded PNIPAM hydrogel tube was immersed in 0.5M sodium hydroxide aqueous solution for 2 minutes to generate iron oxide (Fe_3O_4) nanoparticle in the hydrogel. Under laser irradiation, the tube patterned with iron oxide nanoparticle was necked in the Fe_3O_4-loaded region after being irradiated for 5 minutes (Figure 5.4).

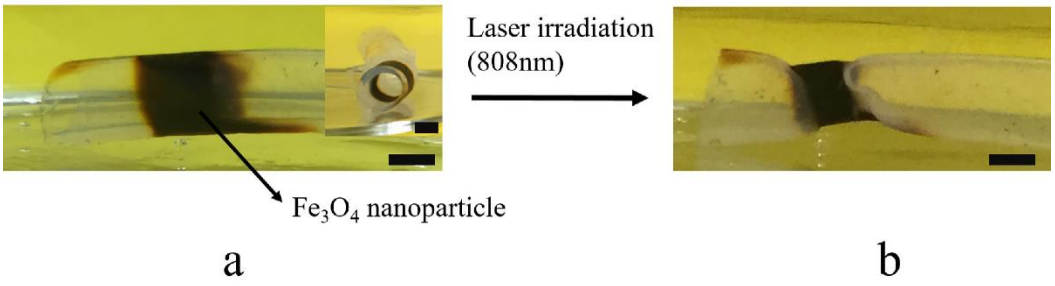

Figure 5.4 Shape transformation of hydrogel tube patterned with Fe_3O_4 nanoparticle under laser irradiation. Scale bar:3mm.

5.3.4 Mechanism of shape transformation of composite hydrogel sheet

Shape transformation of composite hydrogel sheet patterned with Fe_3O_4 nanoparticle can be attributed to the combination of photo-thermal property of Fe_3O_4 nanoparticle and thermo-responsiveness of hydrogel matrix (Figure 5.S3). Under laser irradiation, the temperature of the composite hydrogel sheet was raised from 19^oC to 61^oC in 1 minute as measured by the digital thermometer (Figure 5.S2). Simultaneously, the composite hydrogel sheet shrunk and water inside the hydrogel was squeezed out (Figure 5.S2). Therefore by introducing anisotropic swelling in the hydrogel sheet by patterning it with Fe_3O_4 nanoparticle, the composite hydrogel sheet transformed to a certain geometry depending on Fe_3O_4 nanoparticle patterns.

5.3.5 Regulation of chemical release by using composite hydrogel sheet as smart gate

Finally we used the composite hydrogel sheet as a "smart gate" in regulating chemical release through its opening and closing remotely controlled by laser light (Figure 5.5). For demonstration, Rhodamine B was loaded in the hollow cavity in gelatin hydrogel and then the composite hydrogel sheet was partly glued onto the gelatin hydrogel, covering the Rhodamine B-loaded region (Figure 5.5a,b). Thereafter, the hydrogel sheet gradually bent upwards the laser to open the "gate" upon laser irradiation (Figure 5.5c). With increase of irradiation time, Rhodamine B migrated from gelatin hydrogel cavity to water surrounding through the gate (Figure 5.5d). By switching off laser, the bent sheet gradually recovered its original flat state to close the

gate (Figure 5.5e,f). When necessary, more Rhodamine B can be added in the cavity of gelatin hydrogel by manually opening the closed gate.

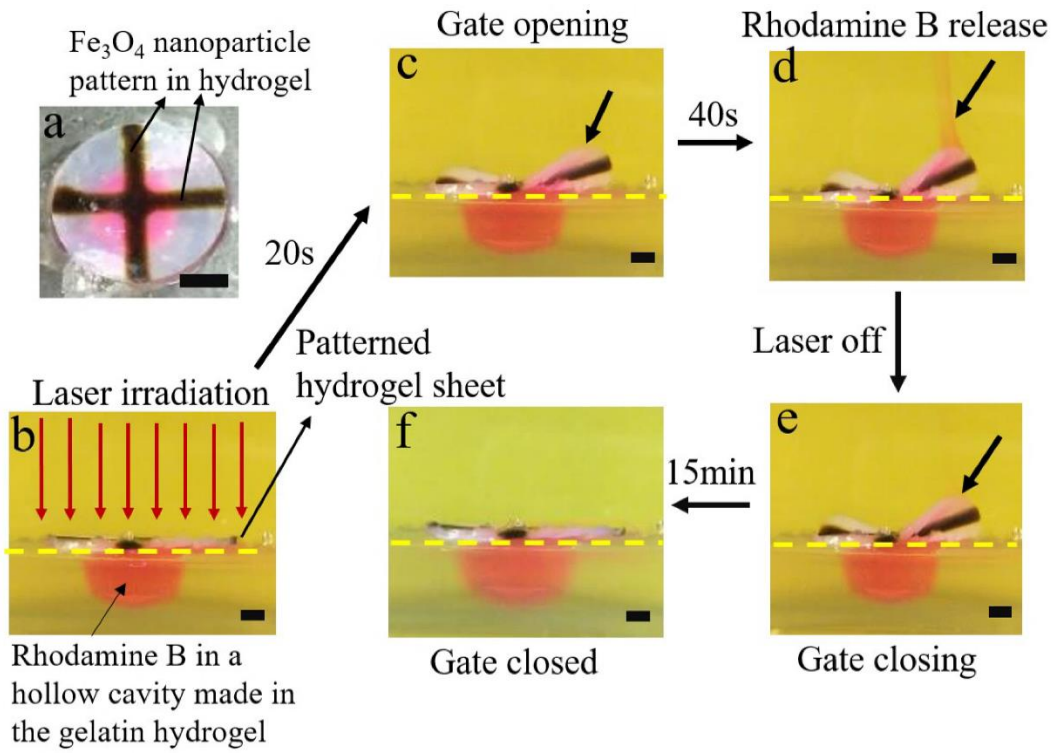

Figure 5.5 Regulation of chemical release by using composite hydrogel sheet as a smart gate. a) top view of composite hydrogel sheet with Fe_3O_4 nanoparticle pattern. The sheet covered Rhodamine B-loaded region in gelatin hydrogel shown in b) (detailed configuration was in Figure 5.S7); b) the composite hydrogel sheet was partly glued on gelatin hydrogel with Rhodamine B-loaded in its cavity; c) the composite sheet gradually bent towards laser under laser irradiation (gate opening); d) Rhodamine B migrated from gelatin hydrogel cavity to water surrounding with increase of irradiation time; e) by switching off laser, the bent sheet gradually recovered (gate closing); f) the bent hydrogel sheet fully recovered its original flat state (gate closed).

Scale bars are 3mm in a) and 1.5mm in b-f). Dashed yellow lines in b-f) are used to distinguish between gelatin hydrogel loaded with Rhodamine B and patterned hydrogel sheet.

5.4 Conclusions

In conclusion, we have presented a simple and robust strategy to reprogram shape transformation of thermo-responsive composite hydrogel sheet with erasable and rewritable iron oxide nanoparticle patterns by using an external near-infrared laser (808nm). The composite sheet patterned with nanoparticle stripe can reach a bending angle of 180^{o} which has rarely been reported previously for light-responsive shape-changing hydrogel system. The shape transformation is due to the combination of photo-thermal property of Fe_3O_4 nanoparticle and thermo-responsiveness of hydrogel matrix. Numerous distinct and reversible shape transformations were achieved from a single hydrogel sheet by writing in the sheet different nanoparticle patterns. The present strategy is simple, fast and efficient in reprogramming shape change of hydrogel material and it is expected this strategy can be extended to other thermo-responsive hydrogel system. The composite hydrogel sheet reported in this study may find applications in soft robotics and biomedicine.

The approach developed in this Chapter expands the current strategy to reprogram material's shape transformation. It is noted that by introducing acrylic acid to the hydrogel precursor, the lower critical solution temperature of the hydrogel can be increased to 45 ^{o}C. This hydrogel can also be patterned with iron oxide nanoparticle using the approach developed in this chapter. By subjecting the patterned hydrogel to

near-infrared laser irradiation at elevated temperature (37 ^{o}C), the patterned hydrogel deformed. This hydrogel may find application in bio-related field, such as in drug delivery and cell scaffold.

Chapter 6: Photo-guided shape-transforming magnetic composite hydrogel sheet

Chapter overview

This Chapter developed a simple one-step approach to fabricate multifunctional 3-D shape-transforming composite hydrogel material. The 3-D composite hydrogel material was generated from the 2-D composite hydrogel sheet by releasing stress in the 2-D sheet introduced in the fabrication process (photo-polymerization). The 3-D composite hydrogel material can be transported by magnetic field and can deform largely under 808nm laser irradiation. A self-rolled composite hydrogel tube was used to demonstrate its capability in loading, transporting and releasing cargo, which was manipulated by magnetic field and light.

A manuscript based on this Chapter is prepared for submission to *Soft Matter*.

6.1 Introduction

Shape-shifting hydrogel material represents a distinct category of dynamic materials, which changes shapes in the presence of environmental cues.[56] In contrast to other shape-changing materials, such as shape-memory polymer materials, hydrogel is unique in that its deformation usually relies on an asymmetric-swelling-driven mechanism, while deformation of shape-memory polymer material, for example, is usually caused by release of its internal stress.[159] The natural counterparts of self-shaping hydrogel material exist broadly, such as seed pod, pine cone, tendril, etc..[53, 55] Till now, plenty of approaches/techniques have been utilized to create asymmetric-

swelling difference within the hydrogel material to drive its deformation (folding, bending/rolling, twisting, etc.). Together with geometric design of the hydrogel material system, these approaches have generated a variety of complex shapes. These shape-changing hydrogel materials are finding applications in various fields, such as in biomedicine, microfluidics, soft robotics, sensors, etc.

Generally speaking, shape-shifting hydrogel usually has a layered structure or is programmed with in-plane swelling anisotropy. Though these structures are frequently utilized in designing shape-changing hydrogels, they suffer from some limitations. For example, delamination between layers is often a concern for self-shaping hydrogels with layered structures and multi-step fabrication is often needed to program in-plane swelling anisotropy in shape-changing hydrogels with complex deformations. Very recently Zhao et al reported a relatively simpler approach to fabricate origami structure from a polymer resin by releasing the internal stress built up during photopolymerization.[169] Though complex origami structures were generated by using this approach, the origami structure at the current stage did not respond to external stimulus, which limited its functionality.

Herein, we reported a simple design that integrated temperature-, magnetic- and light-responsiveness in a single hybrid shape-shifting hydrogel platform by using photopolymerization technique. The residual stress generated in the composite hydrogel during the one-step photopolymerization produced a variety of stable buckled 3D structures via releasing stress generated during fabrication (Figure 6.1). In addition, the hybrid hydrogel was readily transported by magnetic field and it was largely deformed by a near-infrared (NIR) light (wavelength: 808nm) via a photothermal effect

of the embedded magnetic nanorod (Figure 6.1). The easy fabrication, large- and tunable deformation, and multi-responsiveness of our shape-shifting hydrogel represents an important step towards advanced hydrogel machines. By using a self-rolled hybrid hydrogel tube, we demonstrated the capability of our multi-responsive self-shaping hydrogel platform in loading, transporting and releasing cargos.

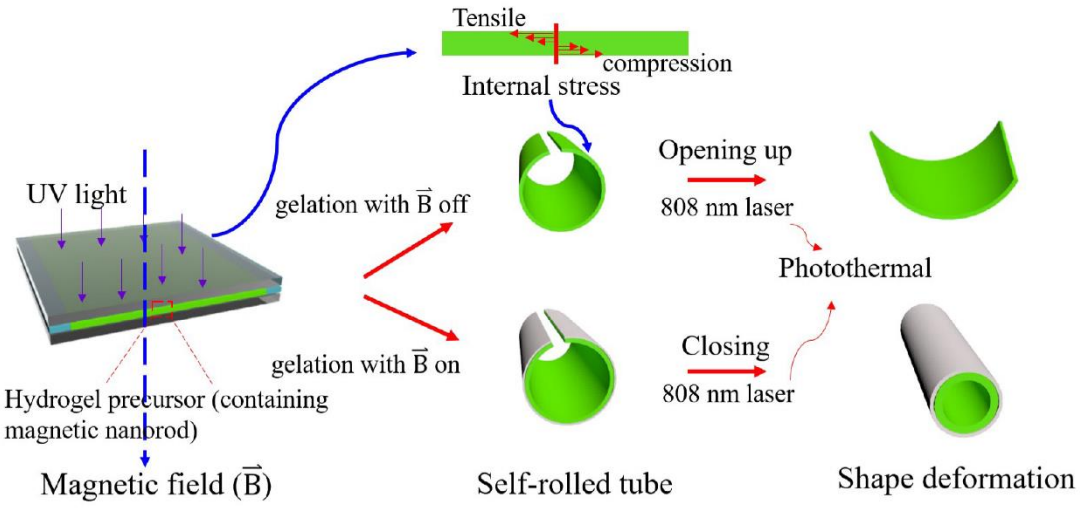

Figure 6.1 Schematic illustration of multifunctional shape-shifting composite hydrogel fabricated by one-step photopolymerization.

6.2 Experiments

6.2.1 Materials

All chemicals were purchased from Sigma-Aldrich and were used without further treatment. Chemicals used were as follows: N-Isopropylacrylamide (NIPAM, monomer), N,N'-Methylenebis(acrylamide) (BIS, cross-linker,), 2,2'-Azobis(2-methylpropionamidine) dihydrochloride (photo-initiator, V50). Polyvinylpyrrolidone (PVP, MW 29000), Tetraethyl orthosilicate (TEOS), Anhydrous ethanol, Ammonium hydroxide (25.0%-28.0%), Anhydrous ferric chloride ($FeCl_3$), Hydrochloric acid (HCl,

37.5%), Diethylene glycol (DEG). Deionized water was used throughout the experiments.

6.2.2 Synthesis of magnetic nanorod

The first step was to synthesize rod-like FeOOH. Typically, 50 μL hydrochloric acid was added to 80 mL water in a 100mL round bottom flask with a magnetic stirring bar. Following that, 7.776g anhydrous $FeCl_3$ was added and stirred to dissolve on an ice-bed. The solution was heated to 98 ^oC with a condenser attached. After 16 hours, the flask was cooled down in an ice bath. The solution was then centrifuged at 10000 rpm for 10 minutes and washed by using water for four times. Finally the rod-shaped FeOOH was dried under vacuum at room temperature. Next, PVP was coated onto FeOOH rod. 9.67g PVP was dissolved in 400 mL water in a round bottom flask. To which 200mg dried FeOOH rod was added. The solution was subject to sonication to disperse FeOOH rod. Finally the solution was mechanically stirred overnight for PVP coating. After PVP coating, the solution was centrifuged at 10000 rpm for 10 minutes and washed by using water for four times and then washed by using ethanol for two times. After washing, these PVP-coated FeOOH rods were re-dispersed in 350 mL ethanol. Under mechanical stirring, 31.5mL ammonium hydroxide was added, followed by addition of 833 μL TEOS. The solution was mechanically stirred for 20 hours to coat silica on FeOOH rod. After silica coating, the solution was centrifuged at 10000 rpm for 10 minutes and washed by using water for six times. The silica-coated FeOOH rod was then re-dispersed in 80 mL diethylene glycol (DEG). The DEG solution containing silica-coated-FeOOH rod was transferred to a 100 mL autoclave

vessel and was subject to 220 ºC for 24 hours in air in an oven. At this step, the silica-coated FeOOH rods were converted to silica-coated magnetic nanorods. After the conversion, DEG solution was diluted with ethanol and was subject to centrifugation at 10000 rpm for 10 minutes and washing using water for five times. Finally the silica-coated magnetic nanorod was dried under vacuum at room temperature for two days.

6.2.3 Synthesis of hybrid hydrogel

The hybrid hydrogel was fabricated by photopolymerization. Typically, 0.045g magnetic nanorod was dispersed in 1 mL water under sonication. Following that, 0.113 g NIPAM monomer, 0.008g BIS crosslinker, 0.002g photo initiator (V50) were added to the solution. After dissolution, this hydrogel precursor was injected into a pre-made mold made of two glass slides and a spacer. The hydrogel precursor was subjected to UV irradiation at 365 nm wavelength for 45 minutes. After fabrication, one glass slide was carefully peeled off, leaving the hybrid hydrogel physically attached to the other piece of glass slide. Hydrogel pieces with certain dimensions were cut from the as-fabricated hydrogel with a razor blade.

6.2.4 Light-triggered shape transformation

An 808 nm laser (MDL-N-808, Changchun New Industries Optoelectronics Technology Co., Ltd, China) was used as the light source and it worked at 5 watts throughout the experiments. During the experiments, the hybrid hydrogel was immersed in 20 mL water in a glass petri dish.

6.2.5 Hydrogel swelling

The swelling property of the hybrid hydrogel sheet was characterized by using the swelling ratio which was measured gravimetrically after wiping off the excess water on the hydrogel's surface with a piece of Kim wipe in the temperature range from 18 to 37 ℃. The hybrid hydrogel sheet was incubated in a water bath for at least 24 h at each temperature. The swelling ratio was calculated by using the following formula,

$$\text{Swelling ratio} = W_s/W_d$$

where W_s was the weight of the swollen hydrogel at the particular temperature and W_d was the dry weight of the hydrogel.

6.2.6 UV-Vis measurement of magnetic nanorod

The optical property of the magnetic nanorod aqueous solution was characterized by measuring its light extinction using UV-Vis spectroscopy (Lambda 40 UV/VIS Spectrometer, PerkinElmer, USA). Magnetic nanorod aqueous solution with different weight percentages of magnetic nanorod were prepared and their UV-Vis spectra were measured. The UV-Vis spectra were taken at a slit width of 1 nm, scanning speed of 480 nm/min and data interval of 1 nm.

6.2.7 Scanning electron microscopy (SEM) of magnetic nanorod and hybrid hydrogel

For magnetic nanorod characterization, a drop of its aqueous solution was dried on silicon wafer and the dried sample was imaged by using scanning electron

microscopy (XL Series-30, Philips, USA). For hybrid hydrogel characterization, the hybrid hydrogel was first freeze-dried and then coated with gold (JFC-1200 Fine Coater, Japan). Following that, scanning electron microscopy was used to characterize its structure.

6.2.8 Photothermal imaging of hybrid hydrogel

The photothermal property of the hybrid hydrogel was studied by photothermal imaging technique. Briefly, the hybrid hydrogel sheet was immersed in 20 mL water in a glass petri dish and was irradiated with an 808 nm laser at a power of 5W for 1 min and then the laser was shut off. The surface temperature of the hybrid hydrogel was monitored by using a FLIR SC300 infrared camera (FLIR, Arlington, VA). Real-time thermal images were captured with frame rate at 60 Hz, and analyzed by FLIR Examiner software. We found that the hybrid hydrogel sheet deformed while its surface temperature increased from 22.5 ℃ to 26.5 ℃ during irradiation process and it went back to its original state when it cooled down.

6.2.9 Cargo loading, transporting and releasing by using self-rolled composite hydrogel tube

A self-rolled composite hydrogel tube was immersed in an aqueous solution consisting of Rhodamine B for 10 minutes. Rhodamine B was loaded in the hydrogel tube via capillary force. Then Rhodamine B-loaded hydrogel tube was transferred to a glass petri dish containing water. A magnet was used to transport the cargo-loaded composite hydrogel tube to a certain place and a NIR laser light was used to irradiate the tube to enhance cargo release from the tube. The amount of released Rhodamine B

during laser irradiation was calculated by using standard fluorescent spectrum of Rhodamine B as a function of its concentration.

6.3 Results and discussion

6.3.1 Self-rolling composite hydrogel sheet

The composite hydrogel sheet was fabricated by photo-polymerization. After releasing from the substrate, the hybrid hydrogel spontaneously curled up. This was probably due to release of the residual stress generated in the fabrication process.[169] The deformation of the hybrid hydrogel includes bending, rolling and helical-twisting (Figure 6.2). We constructed a product diagram for the transformed structures of our hybrid hydrogel with varying length and width (see Figure 6.3). Depending on the length and width of our hybrid hydrogel sheet, the deformed structure (when released from substrate) spanned from bending to helical spring and to singly- and multiply-rolled tube (Figure 6.3). By changing the amount of magnetic nanorod in the hydrogel precursor, we could vary the product diagram of the composite hydrogel sheet (see Figure 6.S1). For example, the parametric domain for producing multiply-rolled tube narrowed when decreasing the amount of magnetic nanorod in the hydrogel precursor. We noted that the hydrogel acquired a planar shape if magnetic nanorod was not in the hydrogel precursor. In addition, by altering geometries of the 2D hybrid hydrogel sheets, we obtained a variety of stable buckled 3D structures (see Figure 6.S2) when the 2D sheets were released from the substrate in water.

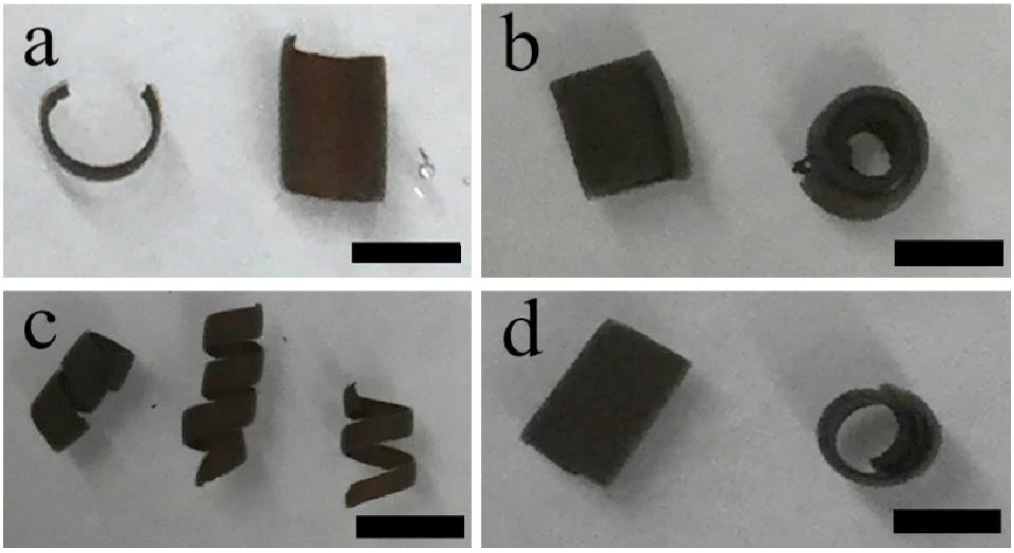

Figure 6.2 Shape deformation of composite hydrogel sheet: a) bending; b) multiply-rolled tube; c) helical spring; d) singly-rolled tube. Scale bar: 0.5 cm.

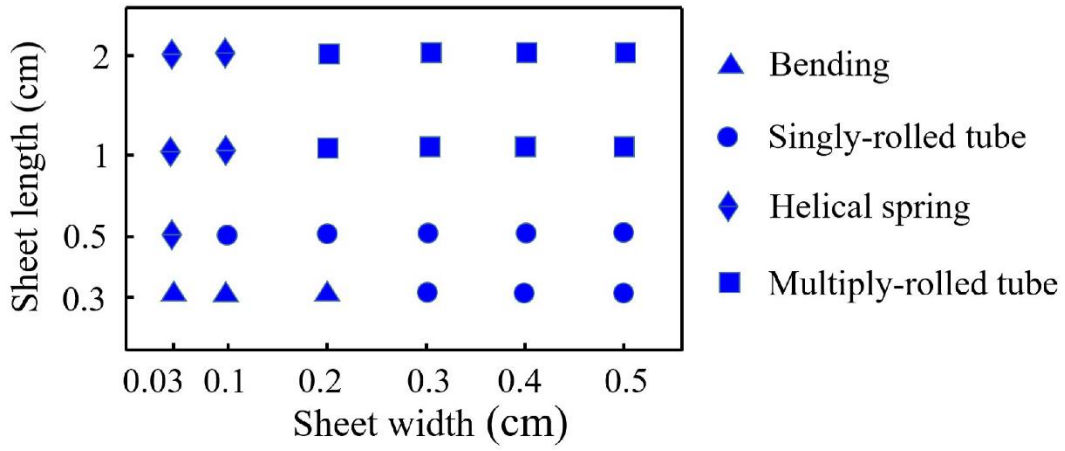

Figure 6.3 Deformation diagram of the hybrid hydrogel sheet. Rectangular strips with varying length and width were cut from the hybrid hydrogel. The thickness of the hydrogel sheet was 125 μm.

6.3.2 Shape transformation of self-rolled composite hydrogel tube under laser irradiation

An interesting phenomenon occurred when light was shed onto the composite hydrogel tube. For example, a self-rolled hydrogel tube opened up when it was irradiated by a near-infrared (NIR) light (wavelength: 808nm) (Figure 6.4a,b). The opening size increased with increase of laser irradiation time (Figure 6.S3). As shown in Figure 6.S4, the magnetic nanorod exhibited a broad absorption in the UV-VIS-NIR wavelength range. When light was cast on the self-rolled hydrogel tube, heat was generated by magnetic nanorod via photo-thermal effect, which was confirmed by the gradual increase of the hybrid tube's surface temperature (Figure 6.5a). Since the swelling experiment (Figure 6.5b) indicated that the hybrid hydrogel gradually lost water with a step-wise increase of temperature, the increase of tube's outer surface temperature (irradiated part) caused the shrinkage of this part. A differential shrinkage in the thickness direction of the hydrogel sheet occurred due to the absorption of the NIR light by the black hydrogel. This asymmetric shrinkage resulted in the tube's opening-up.

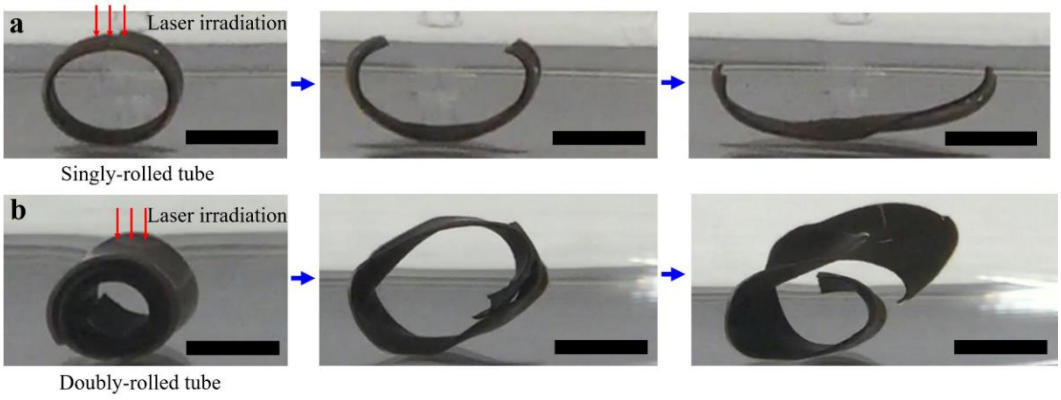

Figure 6.4 Opening of singly- (a) and doubly-rolled (b) tube by NIR light. Scale bar: 0.3cm.

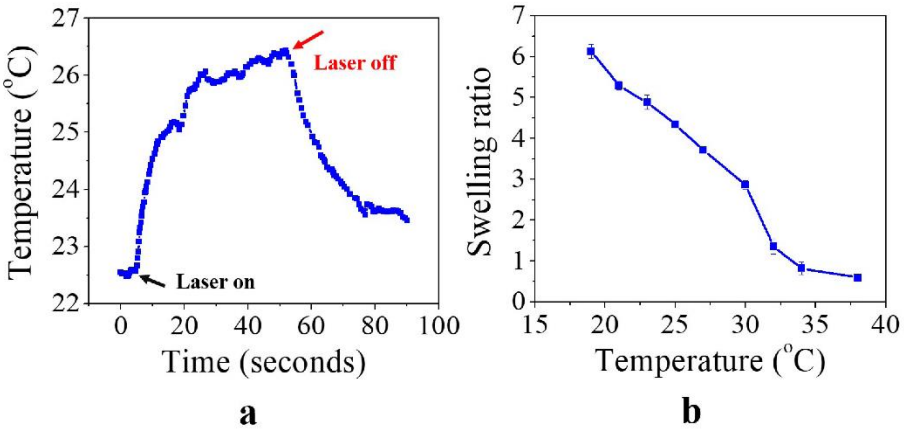

Figure 6.5 Photothermal imaging of the composite hydrogel during NIR light-on-off process (a) and swelling experiment of composite hydrogel (b).

We pointed out that shape deformation of the composite hydrogel was reversible and could be repeated for many times without the need of re-processing the material. This is distinct from light-driven deformation of pre-strained polymer film. The reversibility of the shape deformation made for example the self-rolled tube desirable in application of controlled release of cargos by its cyclic opening (laser on) and closing (laser off). We noted that the response of our composite shape-shifting hydrogel towards light was appealing (on the order of seconds) and could be remarkably enhanced by reducing the thickness of the hydrogel.

6.3.3 Cargo loading, transporting and releasing by using self-rolled composite hydrogel tube

Rhodamine B molecules were loaded in the cavity of the doubly-rolled tube via capillary force. After being transported to the target site using a magnet, the tube was

irradiated by a NIR light which opened the tube and released the cargo (Figure 6.6a). At rest state (Figure 6.6a(i)), Rhodamine B slowly diffused out from the tube into water in its surrounding. When laser was irradiated on the tube (Figure 6.6a(ii)), release of Rhodamine B was greatly accelerated through opening of the tube as well as through heat-induced shrinkage of tube. When laser was switched off (Figure 6.6a(iii)), Rhodamine B was further squeezed out from the cavity due to the recovery effect of the deformed tube. With laser on-off cycles, Rhodamine B was gradually released out from the tube (Figure 6.6a (ii-v)). The tube can be used again to load Rhodamine B by immersing it to aqueous Rhodamine B solution. The released Rhodamine B was quantified by measuring its fluorescence intensity. As shown in Figure 6.6b, the total amount of released Rhodamine B gradually increased during laser on-off cycle till it reached a constant after several laser on-off cycles. In addition to the burst release of the cargo via intense deformation of the multiply-rolled tube, a mild delivery of cargo was achieved by using a tube with a single roll. A cyclic laser-on-off irradiation on the tube resulted in its gradual opening and closing, which gave rise to a mild cargo release. We pointed out that the shrinkage of the hydrogel network caused by light irradiation could also squeeze out the cargo diffused in the hydrogel network which occurred in the cargo-loading process.

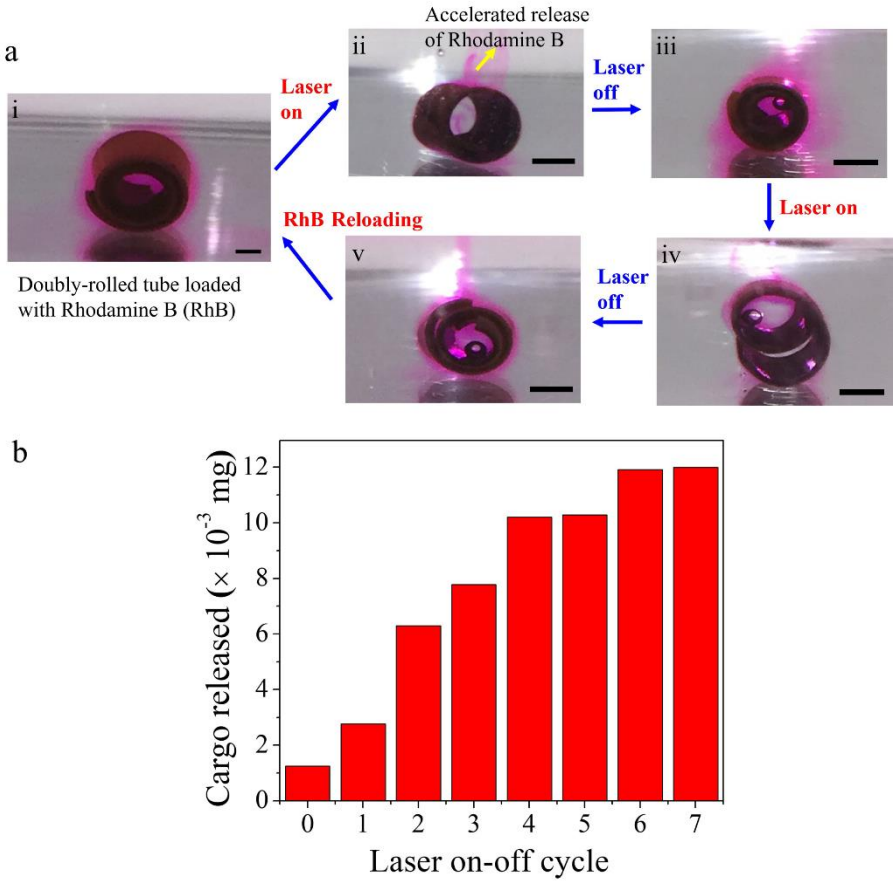

Figure 6.6 a) Cargo (Rhodamine B) release by cyclic opening-and-closing of a multiply-rolled tube mediated by NIR light (wavelength: 808nm) b) quantitative measurement of released cargo (Rhodamine B) during laser on-off cycle. Scale bar: 0.1cm.

6.3.4 Discussion

It is noted that the current approach used to make complex geometries from flat hydrogel sheet using residual stress generated during photopolymerization was not limited to the system using magnetic nanorod as the filler. Instead, it was found that silver nanoparticle (spherical or triangular), gold nanorod, gold bipyramid, magnetic

nanosphere (Fe_3O_4 nanosphere) could also be used as the filler to produce residual stress during UV polymerization. The curvature of the resulted shapes depended on the concentration of the filler in the hydrogel. It is worth noting that surface modification of nanoparticle might be necessary in some cases. For example, the surface chemistry of the as-synthesized gold nanorod or gold bipyramid should be altered, since the as-synthesized CTAB-coated gold nanorod/bipyramid will aggregate when dispersed in PNIPAM hydrogel precursor. The issue can be resolved by modifying the nanoparticles with thiol-terminated polyethylene glycol, thiol-terminated poly(N-isopropylacrylamide), etc.

The above-mentioned nanoparticles can all be used as photo-thermal conversion agents with varying photo-thermal conversion efficiency in the hydrogel. In addition to use light to deform the buckled hydrogel, bulk heating can also deform the residual-stress-induced buckled hydrogel with interesting hydrogel deformation pathway during bulk heating and cooling. While Figure 6.S5 gave some support for the preceding statement, the deformation was richer when the geometry of the starting hydrogel was changed. For example, a ring-shaped hydrogel loaded with magnetic nanosphere (Fe_3O_4 nanosphere) curved up after being heated (Figure 6.7a). During cooling stage, various types of geometry were observed before it finally recovered its original state (Figure 6.7b).

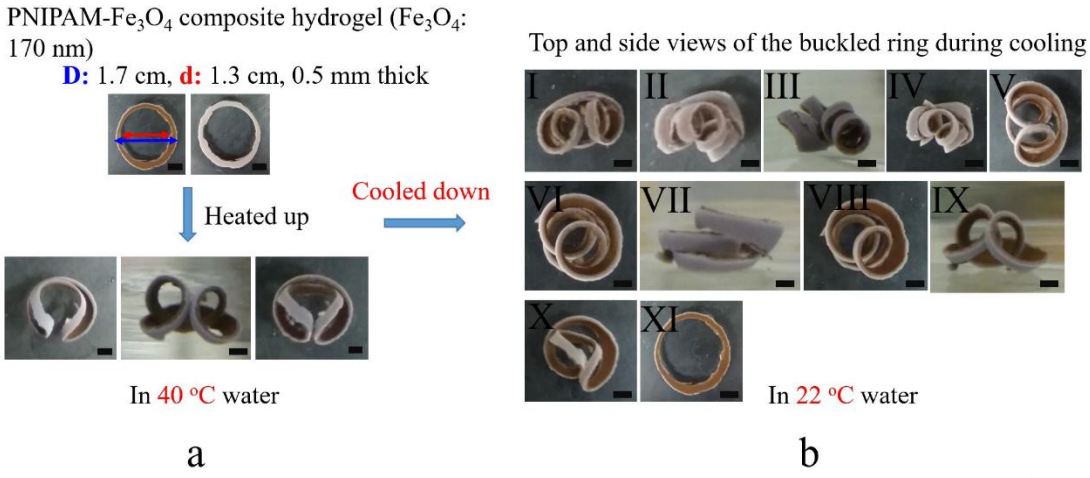

Figure 6.7 a) a ring-shaped composite hydrogel sheet (PNIPAM gel-Fe_3O_4 nanosphere) curved up under bulk heating; b) top (I, II, IV, V, VI, VIII, X, XI) and side (III, VII, IX) views of transformation of the deformed ring during its cooling. Scale bar: 4mm.

In addition to free-standing composite magnetic hydrogel hybrid, the residual stress generated during photo-polymerization could be harnessed to wrinkle hybrid hydrogel surface when the hybrid was covalently attached onto the glass slide during synthesis (Figure 6.8). Compared with the pure PNIPAM hydrogel made by UV polymerization, the hybrid hydrogel surface wrinkled much more appreciably (see Figure 6.8a). It was found that when the thickness of the hybrid hydrogel was 125 μm or below, the hybrid gel did not wrinkle. When the thickness was 250 μm and 500 μm, the hybrid gel wrinkled. The wrinkles were diminished by either bulk heating or by light irradiation (wavelength: 808nm) (Figure 6.8b). The diminished wrinkles recovered after cooling.

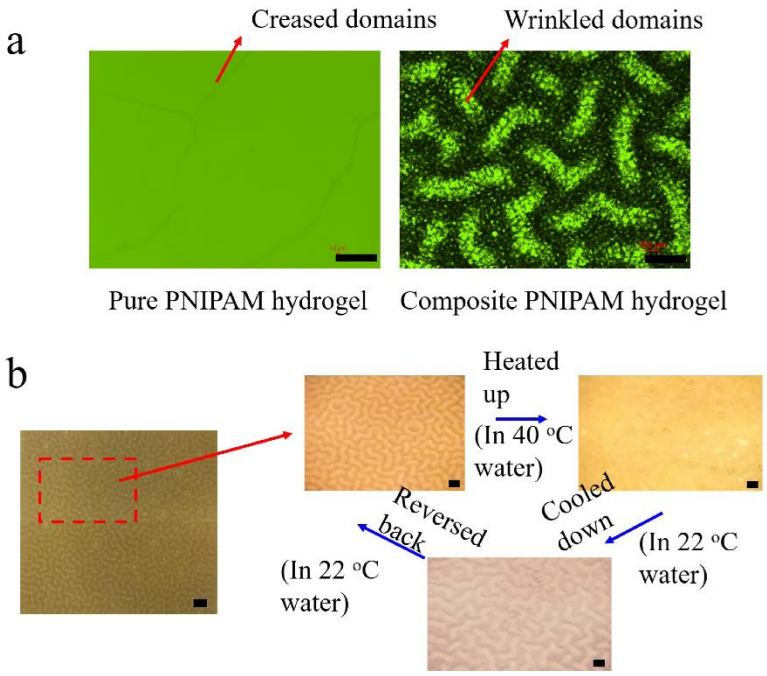

Figure 6.8 a) surface wrinkling of composite hydrogel sheet (PNIPAM-gel-Fe_3O_4 nanorod) covalently attached onto a cover slide after photo-polymerization; b) thermo-responsiveness of surface wrinkles in a). Scale bar: 250 μm.

6.4 Conclusions

In conclusion, we reported a multi-functional self-shaping composite hydrogel which was fabricated by a one-step photopolymerization. The introduction of magnetic nanorods in the poly(N-isopropylacrylamide) hydrogel was the key in bringing in multi-functionality to the hydrogel. The residual stress generated in the composite hydrogel during the one-step photopolymerization produced a variety of stable buckled 3D structures after releasing residual stress generated in the fabrication process. The composite hydrogel could be transported by a magnetic field and it could be largely deformed by using a near-infrared (NIR) light (wavelength: 808nm) via photo-thermal effect of magnetic nanorod. The deformation response of the composite hydrogel

towards light was appealing (on the order of seconds) and could be remarkably enhanced by reducing the thickness of the hydrogel. Self-rolled tubes were used to demonstrate the capability of our shape-shifting composite hydrogel in loading cargoes in the cavity of the tube via capillary force, transporting the cargo by magnetic field and finally opening the tube to release the cargo by using NIR light. It was found that by using the same fabrication approach, self-rolled tubes could also be achieved from other hydrogel monomer materials (Acrylamide, N,N-Diethylacrylamide, N,N-Dimethylacrylamide and their combinations). To conclude, the self-shaping multifunctional composite hydrogel reported here represents an interesting and advanced platform. It has rich scientific phenomena and bears good potentials in a broad range of technological fields such as in biomedicine, microfluidics and soft robotics.

Chapter 7: Conclusions and Future work

7.1 Conclusions

In conclusion, this dissertation develops a new, simple and efficient toolset to program and reprogram photoactive thermo-responsive composite hydrogel material by using near-infrared light through combination of photothermal effect of photoactive filler and thermo-responsiveness of the hydrogel matrix. The dissertation enriches the strategy of using light to control shape transformation of hydrogel material. First, a single composite hydrogel sheet was designed to have multiple distinct shape transformations by manipulating light irradiation patterns. In this case, shape transformation of the composite hydrogel sheet was not pre-determined during fabrication process as usually done previously. On the contrary, shape transformation of composite hydrogel sheet was initiated and altered on demand by using light. Secondly, a simple toolset was developed to pattern nanoparticle in both lateral and thickness-direction of the hydrogel material, which is difficult to be achieved by other approaches. Various type of nanoparticles can be patterned in the hydrogel, such as gold nanoparticle, palladium nanoparticle, platinum nanoparticle, iron oxide nanoparticle, silver nanoparticle through different strategies such as galvanic replacement reaction, selective etching, *in situ* reduction of metal salt, etc. The toolset also allows nanoparticles to be patterned in non-planar (either concave or convex) hydrogel material. Due to presence of nanoparticle gradient in both lateral and z-direction of the hydrogel sheet, the same hydrogel sheet exhibited different shape transformation modes, highly depending on light irradiation direction, which has rarely

been reported. We also constructed a composite hydrogel sheet with erasable and rewritable iron oxide nanoparticle patterns. The same composite hydrogel sheet transformed to various type of geometries under light irradiation by erasing previous nanoparticle patterns and writing new nanoparticle patterns in the hydrogel sheet. Lastly, a simple and general approach was developed to fabricate 3D shape-transforming photoactive composite hydrogel material by releasing the residual stress generated during fabrication process. A self-rolled composite hydrogel tube was used to load cargo via capillary force, transport cargo using magnetic field and finally release cargo by opening up tube under light irradiation.

7.2 Future work

This dissertation has shown an innovative and interesting shape-changing system by using thermo-responsive polymer hydrogel (poly(N-isopropyl acrylamide, PNIPAM)). However, the mechanical property of PNIPAM hydrogel material is weak and it fails to generate large forces under light irradiation. A continuous laser energy input is needed to maintain shape transformation which may not be desirable in applications that need the material to have a permanent shape. The laser energy needed for the shape transformation of hydrogel is large due to requirement of presence of water for PNIPAM hydrogel to work. Therefore, there are several directions for future work to overcome the limitations mentioned above: i) develop approach to sequentially deform hydrogel material by using light to fabricate complex permanent shapes; ii) apply toolset developed in this dissertation to other material such as humidity-responsive polymer film that does not require presence of large amount of water to

have deformation and therefore reduces power cost; iii) improve mechanical property of PNIPAM hydrogel and increase its actuation force for application-oriented research.

Appendices

a b c

Figure 2.S1 Scattering effect of hydrogel network on the deformation. The macroporous hydrogel sheet without AgNPs was irradiated for 1 minute at a laser power density of 0.7 W/cm^2. a) was the hydrogel before irradiation, b) was the hydrogel that has been irradiated for 1 minute, c) was the hydrogel right after switching off the laser after 1 minute irradiation. It can be seen that the contribution of the scattering of the hydrogel network to the deformation was negligible.

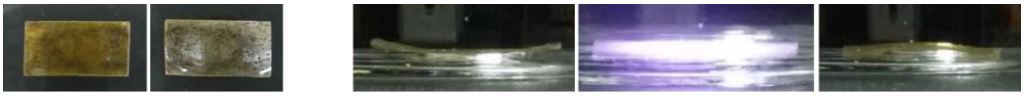

a b

Figure 2.S2 Deformation of non-porous hybrid hydrogel sheet under NIR light irradiation. a) showed the top (left) and bottom (right) surfaces of the non-porous hybrid sheet; b) was the deformation of the non-porous hybrid sheet after NIR irradiation (808nm wavelength) for 3 minutes at a laser power density of 0.7 W/cm^2. Left image in b) was the sheet before irradiation, middle image was the sheet under irradiation for 3 minutes while right image was the non-porous sheet right after switching off the laser.

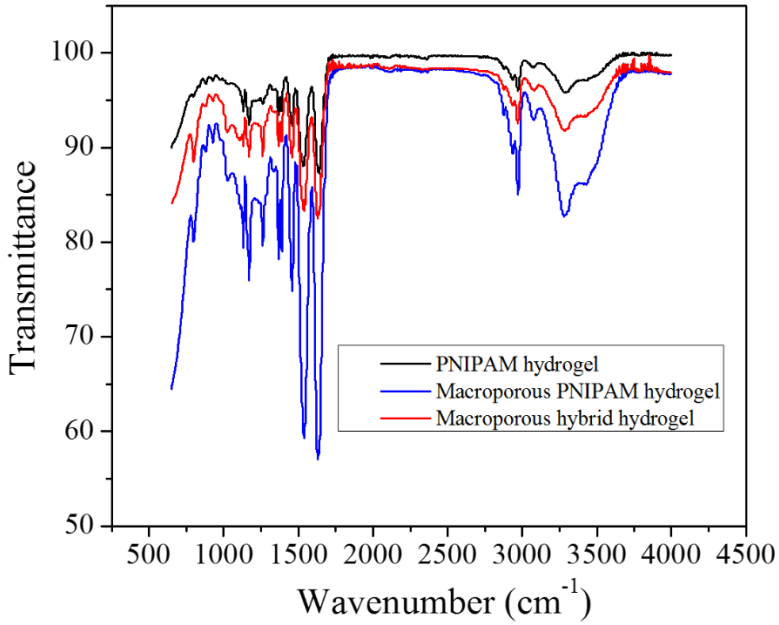

Figure 2.S3 FTIR measurement of PNIPAM hydrogel, macroporous PNIPAM hydrogel and macroporous hybrid PNIPAM-AgNP hydrogel sheet. It indicated the PEG acted as a pore-forming agent in the PNIPAM hydrogel fabrication.

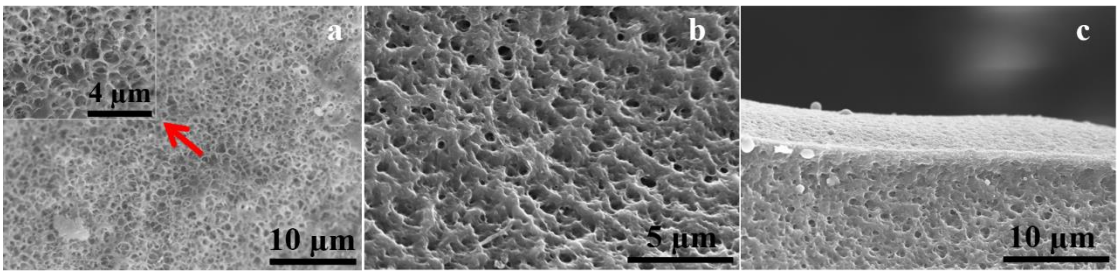

Figure 2.S4 SEM images of the surface morphology of macroporous PNIPAM hydrogel sheet and hybrid hydrogel sheet. a) surface morphology of macroporous PNIPAM hydrogel sheet; b) morphology of the cross-section of the hybrid hydrogel sheet; c) overall morphology of the cross-section of the hybrid hydrogel sheet. Inset: enlarged image of the region denoted by the red arrow.

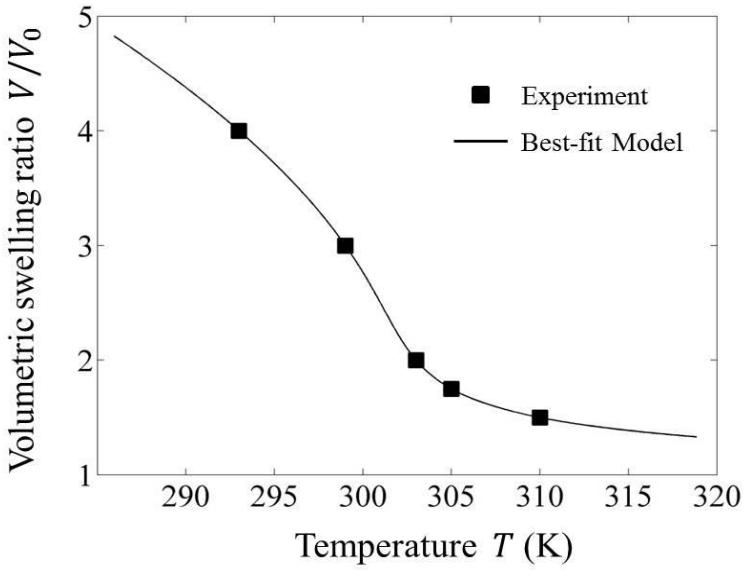

Figure 2.S5 Volumetric swelling ratio of macroporous PNIPAM hydrogel as a function of temperature. This curve was used to determine the parameters used in finite element modeling as described Section 2.2.12

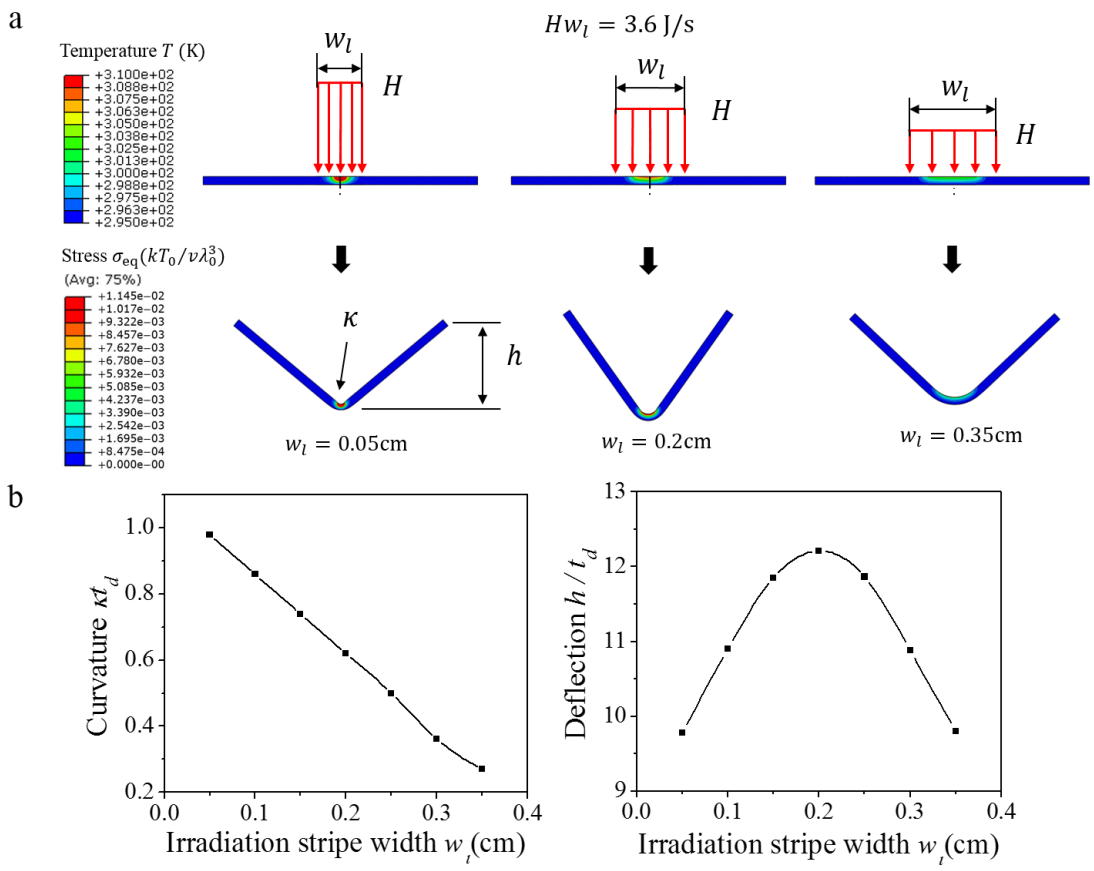

Figure 2.S6 Finite element modeling of the bending of the hybrid hydrogel sheet with respect to laser stripe width at a fixed total input energy. a) The hybrid hydrogel sheet was subject to laser stripes with the light input energy fixed at 3.6 J/s. b) Normalized curvature κt_d and deflection h/t_d as a function of laser stripe width w_l at fixed light input energy of 3.6 J/s. t_d was the thickness of the hybrid sheet which was 0.5 mm. The FEM analyses indicated that at a fixed light input energy, the bending curvature decreased with the increase of laser stripe width, while the overall deflection (h/t_d) reached a maximum when increasing the laser stripe width.

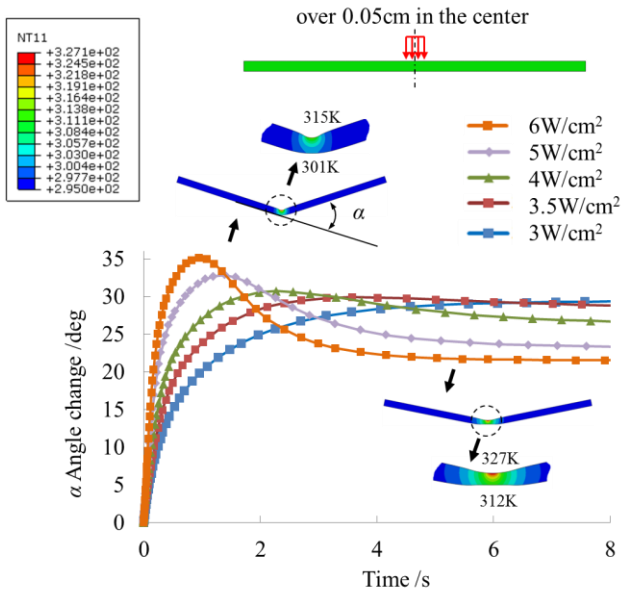

Figure 2.S7 Temporal evolution of the bending angle at various heat fluxes (H) into the center of the hydrogel. The color legend in top left side of the figure showed the temperature distribution at both the peak bending angle state, and at the steady state, when H=6W/cm^2.

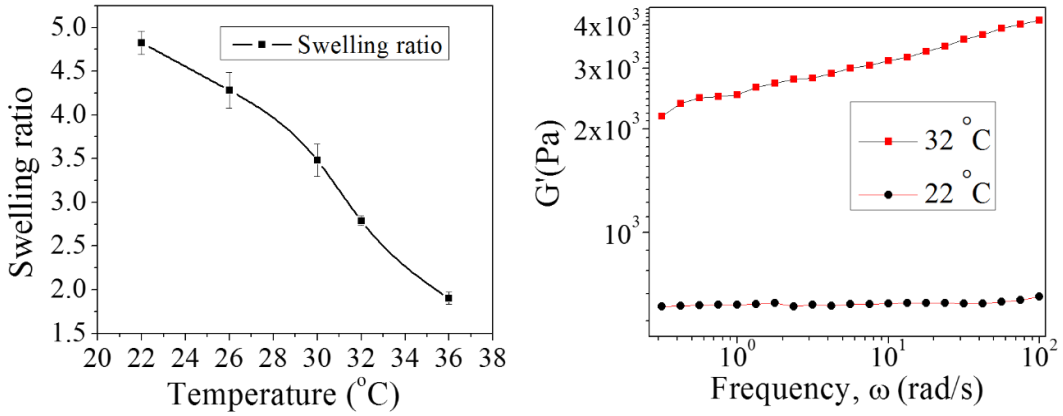

Figure 2.S8 Swelling (a) and shear modulus (b) of hybrid hydrogel sheet at different temperatures. The hybrid sheet had a gradual decrease in swelling when increasing the temperature. It became stiffer with the increase of temperature.

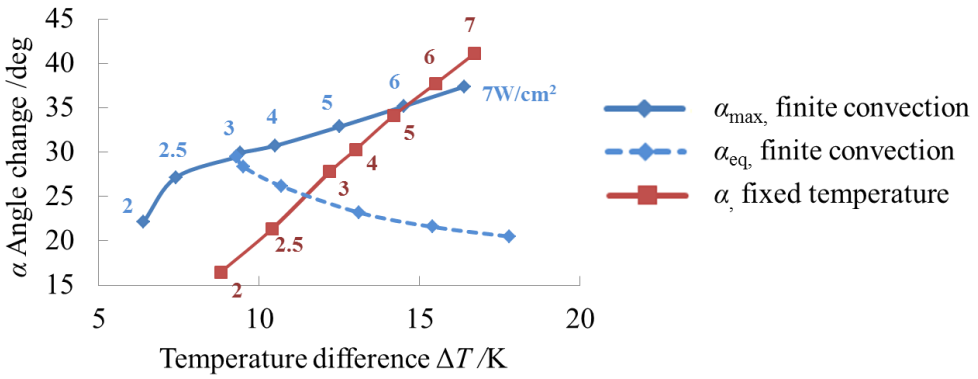

Figure 2.S9 Effect of temperature difference between sheet's top and bottom surface on its bending. The solid blue line showed the maximum bending angle under 700 $Wm^{-2}K^{-1}$ surface convection (finite convection condition), and the dashed line represented α in the steady state under same surface convection condition. The red line showed the bending angle for fixed temperature boundary condition. The number near the lines indicated the heat flux inputs.

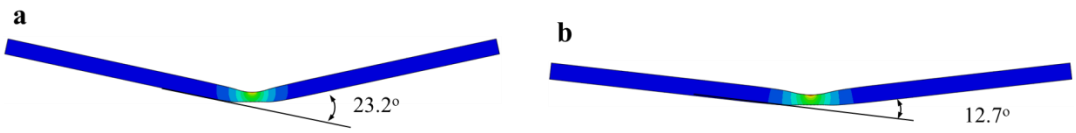

Figure 2.S10 Bending angle reduced from (a) 23.2 °in the baseline case to (b) 12.7 °if the ambience temperature increased to 300K over the center 3.5 mm section of the back surface.

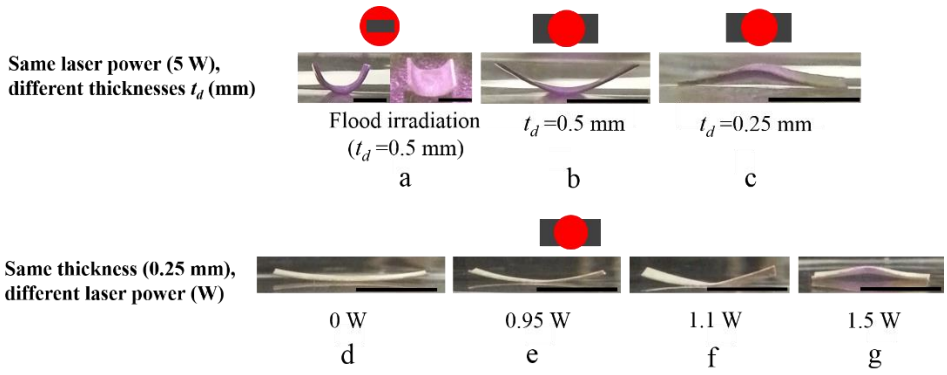

Figure 2.S11 Shape transformation of the hybrid hydrogel sheet under flood irradiation and the bending stability of the hybrid hydrogel sheet with respect to its thickness and the laser power. a) the sheet (length:1cm; width: 0.5cm) bent when its whole surface was subject to NIR irradiation indicating the thermal gradient along the sheet's surface might not play important roles in its shape transformation. b, c) the sheet (length: 1.8 cm; width: 0.9cm) suffered from a bending instability when its thickness reduced from 0.5 mm to 0.25 mm. c) the sheet bent but buckled downwards very quickly to form a saddle-like structure. d,e,f,g) indicated that a thinner sheet had a stable bending at a low laser power. These findings suggested that the thickness-direction thermal gradient was necessary for the hybrid sheet to have a stable shape transformation. The scale bar in a) represents 0.5cm while those in b-g) represent 0.85cm.

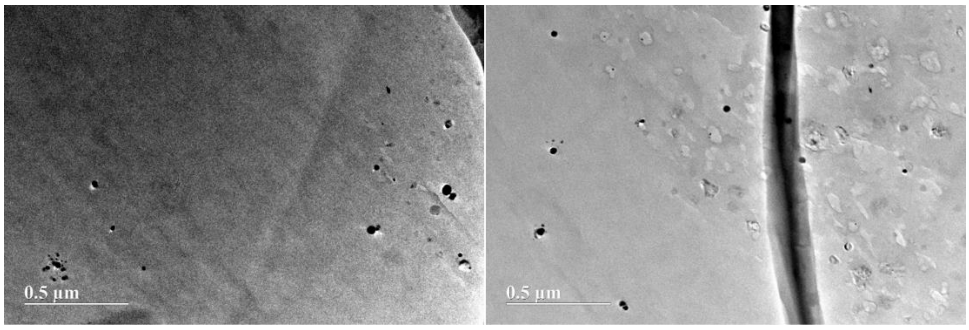

Figure 2.S12 TEM images of AgNPs within the hybrid hydrogel sheet. The AgNPs have a broad size distribution with roughly spherical shapes.

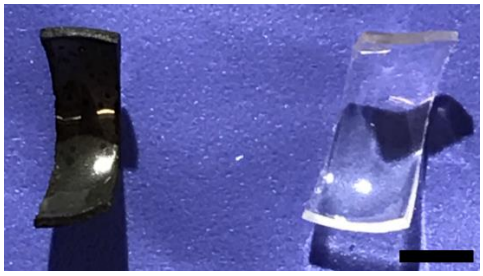

Figure 2.S13 Optical images of macroporous pristine PNIPAM hydrogel sheet (right image) and hybrid hydrogel sheet (left image). It can be seen that the gel surface of the hybrid sheet is dark and shining (rather than transparent as the pristine hydrogel sheet without Ag nanoparticles), indicating the presence of a high-density AgNPs on the sheet's surface. Scale bar: 0.2cm.

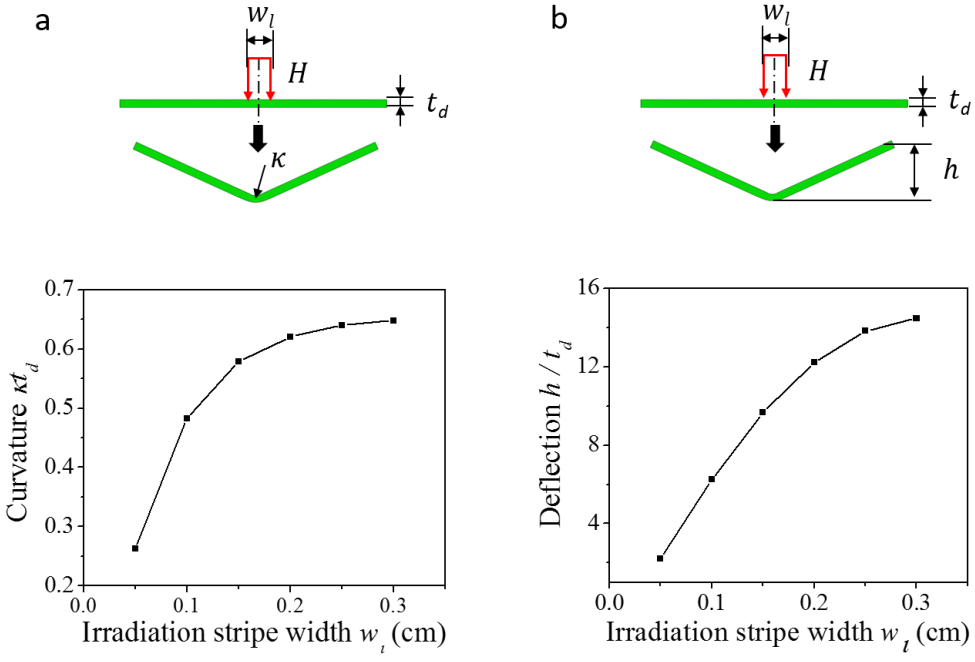

Figure 2.S14 Finite element modeling of effects of supplied light energy and irradiation stripe width on bending of the hybrid sheet. The bending increased with the increase of irradiation stripe width. a) Normalized curvature κt_d ; b) deflection h/t_d as a function of laser stripe width w_l at heat flux intensity H=1.8 J·cm^{-2}·s^{-1}

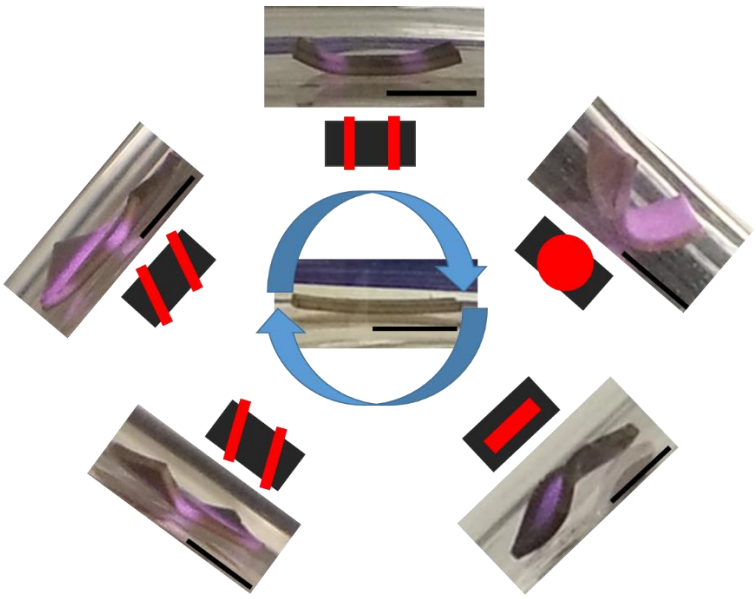

Figure 2.S15 Shape transformations of hybrid hydrogel sheet of reduced overall size (length: 1 cm; width: 0.5 cm; thickness: 0.5 mm). The shape transformations were smaller when reducing the overall size of the hybrid sheet. Scale bar:5mm.

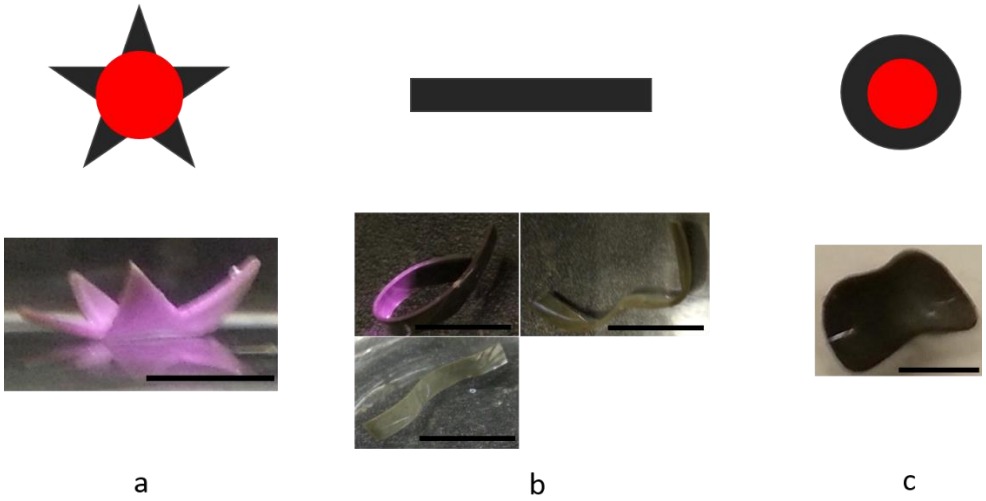

Figure 2.S16 Transformations from hybrid hydrogel sheets with different original shapes. Shapes in a ,c) were directly obtained via irradiation with a circular laser spot when the sheet was in water. Shapes in b) were achieved in water by quickly changing

the irradiated area using a circular laser spot. Scale bar: 8.5mm in a) and c), 20mm in b).

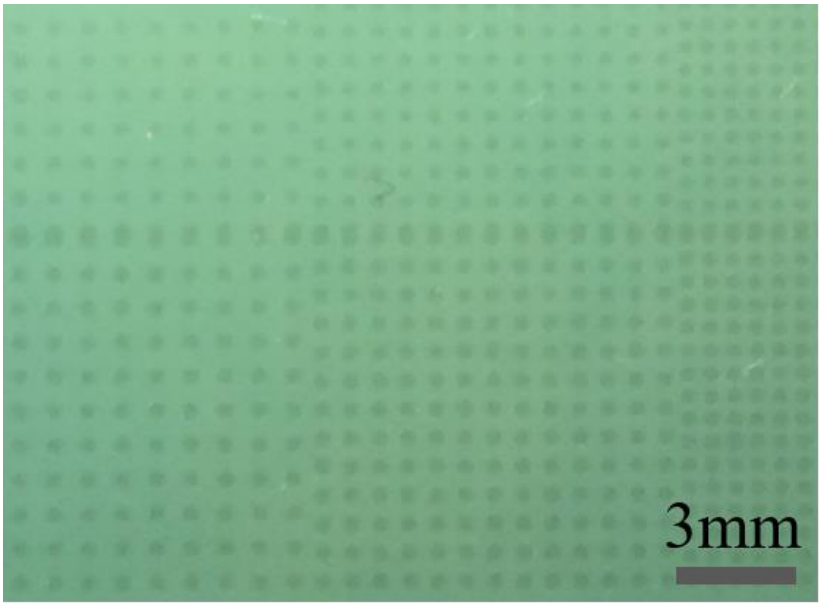

Figure 3.S1 Large-scale patterning of gold nanoparticles via stamping approach

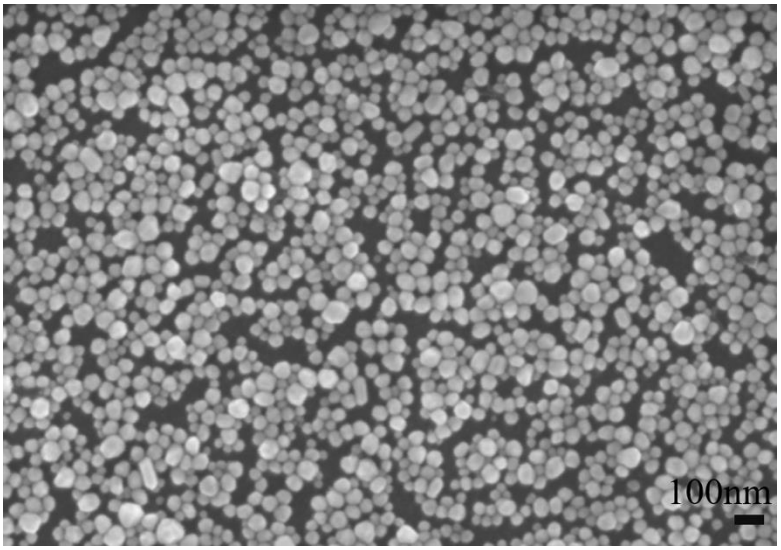

Figure 3.S2 SEM image of AgNP used to generate AuNP during stamping process.

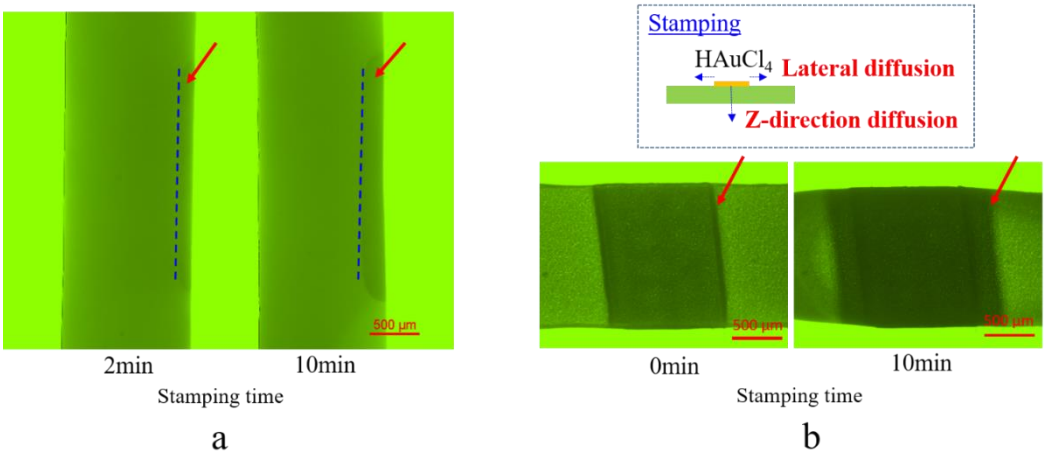

Figure 3.S3 Optical image showing diffusion-reaction process during stamping. The red arrow indicated the front of the gold nanoparticle domain generated during stamping.

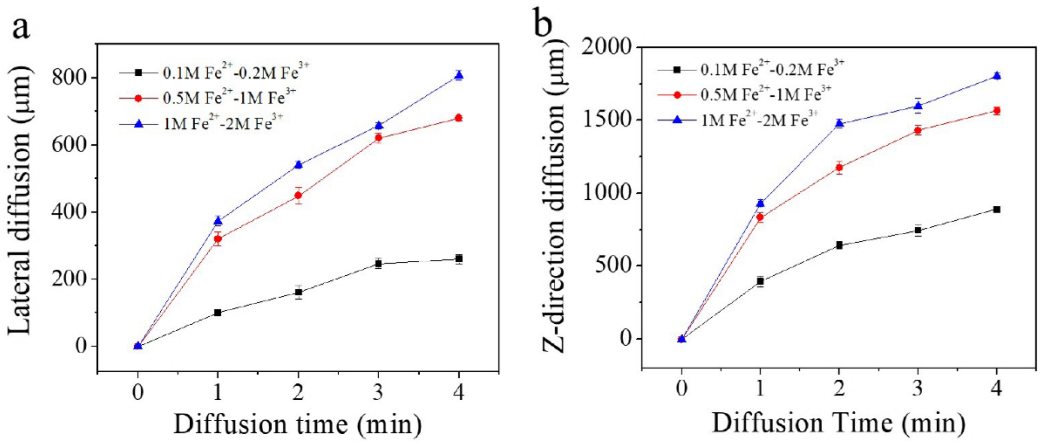

Figure 3.S4 Time-dependent variation of Fe_3O_4 nanoparticle domain size in lateral and z-direction of hydrogel sheet as a function of metal ion concentration in the stamp.

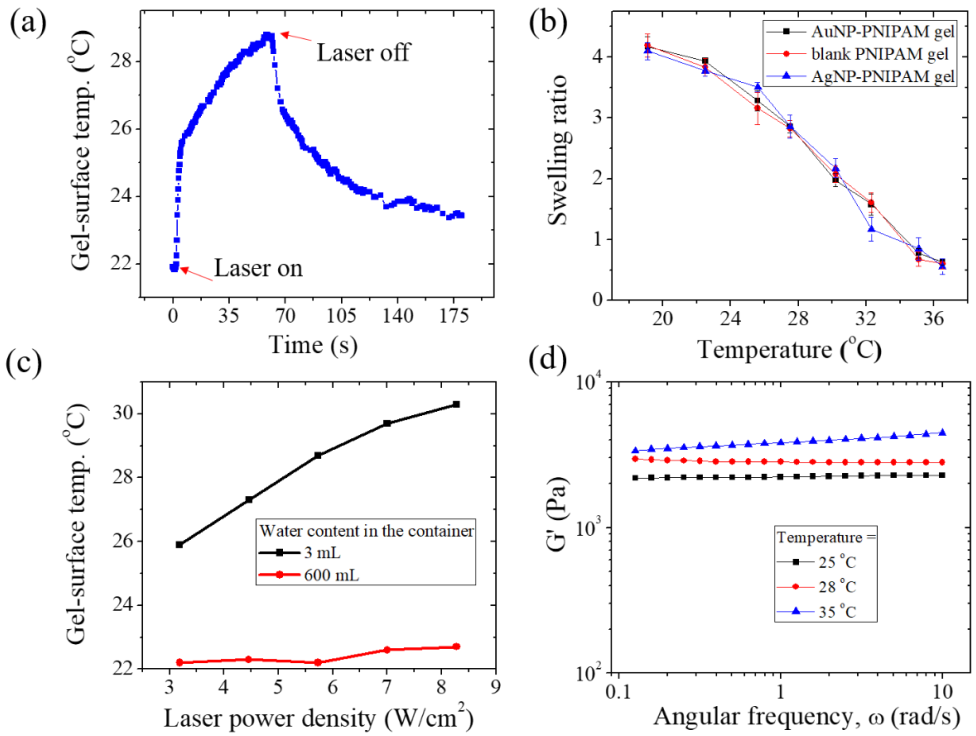

Figure 4.S1 a) Evolution of surface temperature of hydrogel during laser irradiation; b) Swelling of hydrogel as a function of temperature; c) Surface temperature of hydrogel as a function of laser power density; d) Shear modulus of composite hydrogel as a function of temperature.

Figure 4.S2 Bending of composite hydrogel with different thicknesses. The thickness of the composite hydrogel in a) was 0.25mm while it was 0.5mm in b). The gold nanoparticle domain thickness was 0.06mm in a) and 0.12mm in b). Scale bar: 2mm.

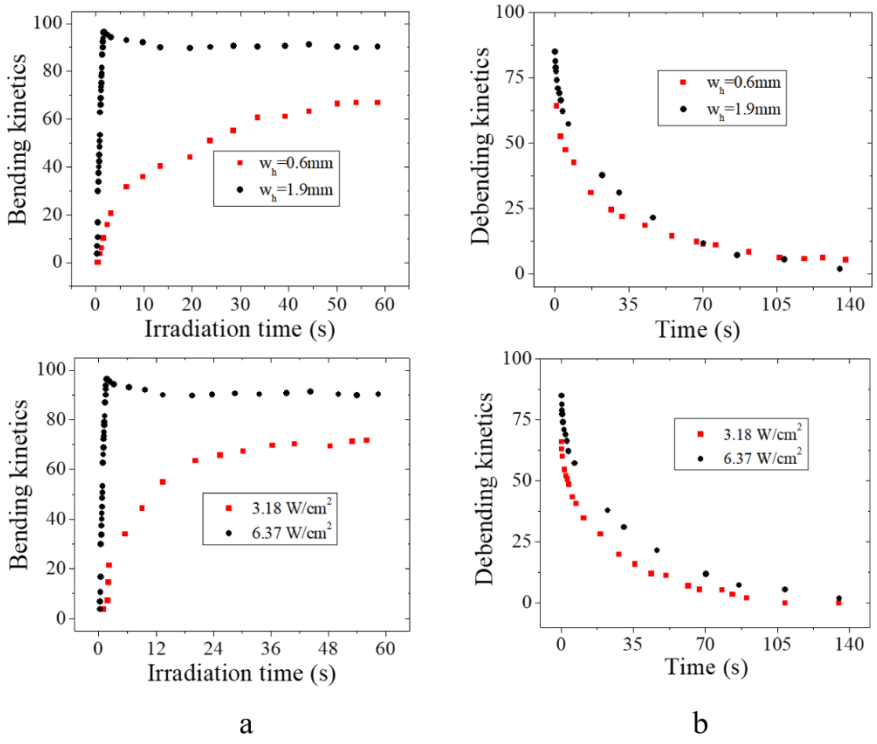

Figure 4.S3 Bending (a) and recovering (b) kinetics of composite hydrogel with time. w_h was the width of gold nanoparticle domain. The length of gold nanoparticle domain was 2.2mm and its depth in z-direction of hydrogel was 0.06mm.

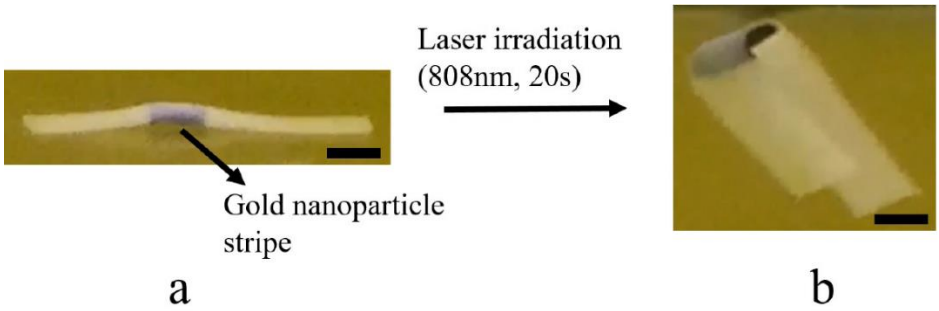

Figure 4.S4 Jumping of composite hydrogel sheet patterned with AuNP strip under laser irradiation. a) composite hydrogel sheet before irradiation; b) the hydrogel sheet jumped towards laser after irradiation for 20s. Scale bar: 3mm.

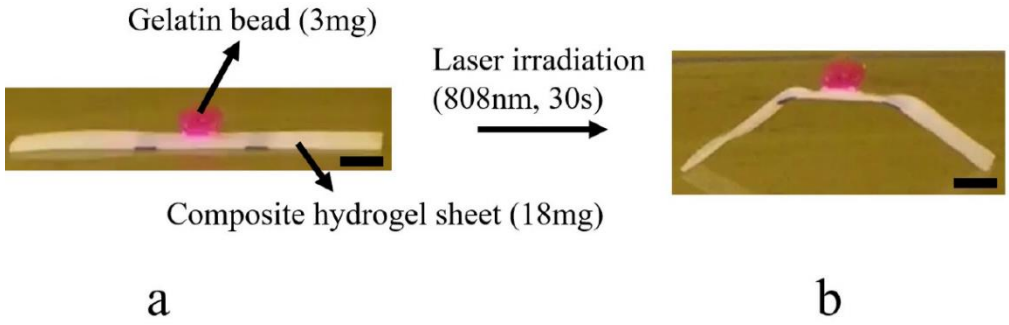

Figure 4.S5 Load-lifting of composite hydrogel sheet under laser irradiation. The composite hydrogel sheet was patterned with two AuNP strips. a) a gelatin bead was glued on the composite sheet before irradiation; b) the gelatin bead was raised to 1 cm high by the sheet after laser irradiation for 30s. Scale bar: 2mm.

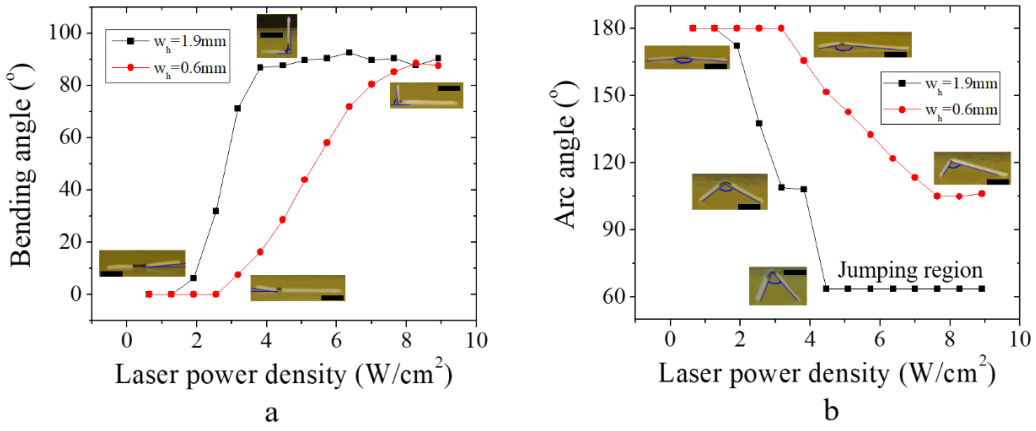

Figure 4.S6 Bending of composite hydrogel as a function of laser power density. w_h was the width of gold nanoparticle domain. The length of gold nanoparticle domain

was 2.2mm. In a) the gold nanoparticle domain faced laser spot while in b) the nanoparticle domain faced away from the laser spot. Scale bar: 5mm.

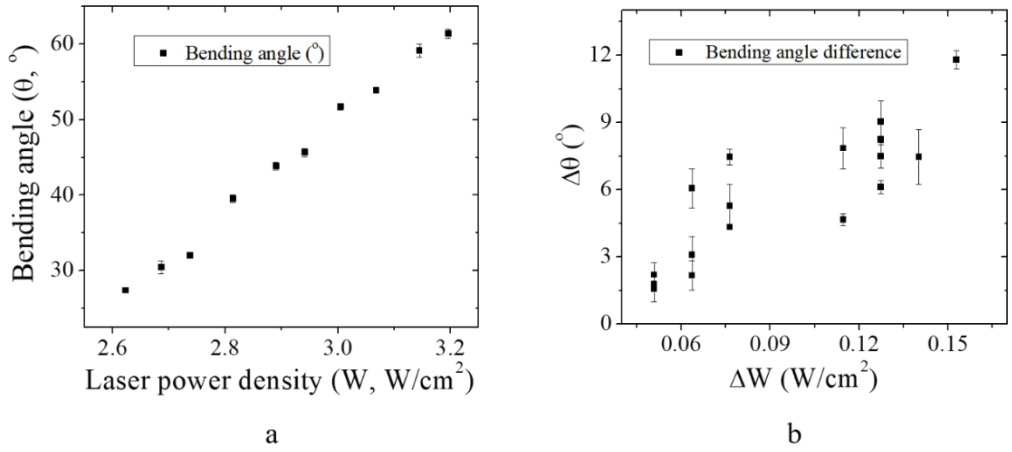

Figure 4.S7 Bending analysis of composite hydrogel as a function of laser power density. The gold nanoparticle domain had a width of 1.9mm, length of 2.2mm and thickness of 0.06mm. The total thickness of the hybrid hydrogel was 0.25mm.

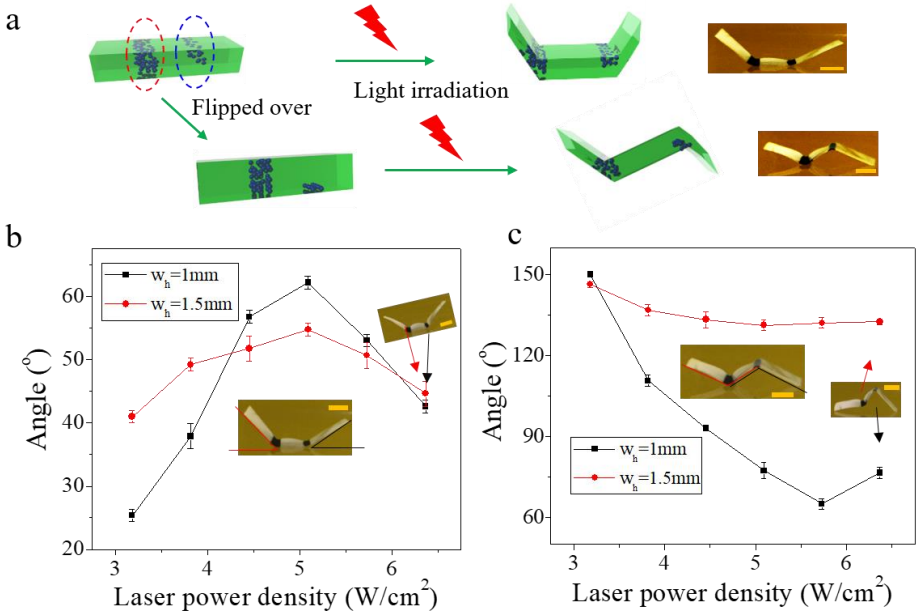

Figure 4.S8 Bending analysis of composite hydrogel with respect to laser irradiation direction. The composite hydrogel had two rectangular gold nanoparticle (AuNP) strips

generated during one-time stamping process. One AuNP strip (w_h=1.5mm) penetrated through gel thickness, while the other one (w_h=1mm) only partially penetrated the gel. Scale bar: 2mm.

Table 4.S1 Analysis of the minimum energy *E* (J) required for bending to occur

Hinge length (*l*, mm)	Hinge width (*w*, mm)	Onset time for bending (*t*, s)	Minimum power density (I_o) needed (W/cm^2)	Minimum energy (E) required (J)
0.6	2.3	19	3.06	0.79
1.0	2.1	20	2.16	0.89
1.9	2.2	10	1.91	0.78
3.4	2.2	6	1.91	0.84

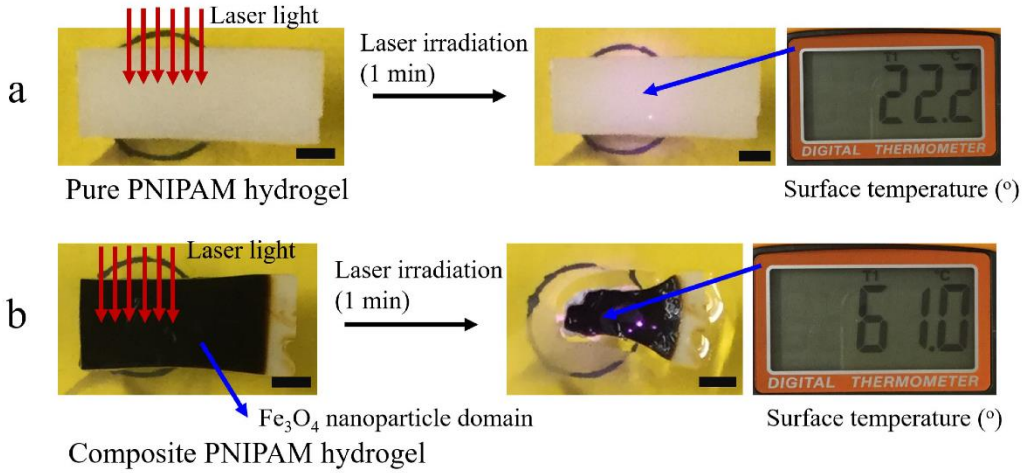

Figure 5.S1 Surface temperature of pure and composite PNIPAM hydrogel under laser irradiation at 6.38W/cm^2 for 1minute. a) For pure PNIPAM hydrogel, its surface temperature slightly increased under laser irradiation; b) For composite PNIPAM hydrogel, its surface temperature increased substantially at same laser irradiation condition. Room temperature was 19.5 °C. Scale bar: 5mm.

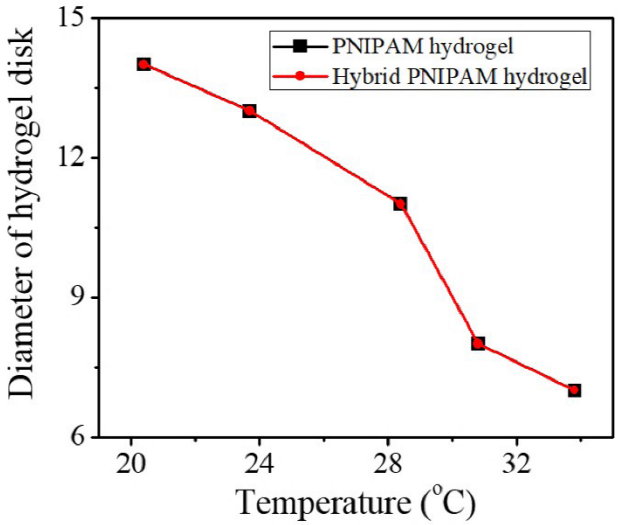

Figure 5.S2 Swelling of disc-shape hydrogel as a function of temperature. The diameter of the hydrogel disc was measured and plotted against temperature.

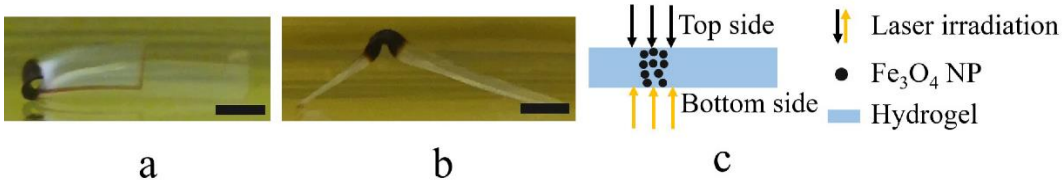

Figure 5.S3 Bending of composite hydrogel sheet under laser irradiation. a) The hydrogel sheet bent upwards when laser was irradiated from top side of hydrogel (black arrows in c). This side was in contact with agarose stamp during ion diffusion; b) the same sheet bent downwards when laser was irradiated onto the bottom side of hydrogel (yellow arrows in c). Scale bar: 3mm.

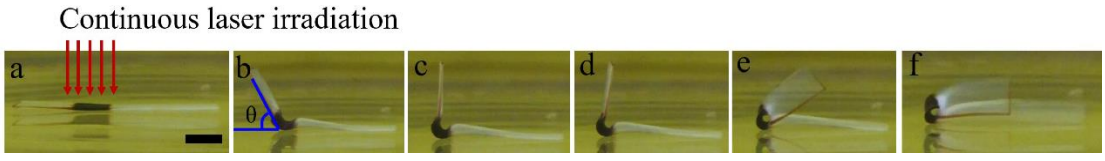

Figure 5.S4 Video snapshot of bending deformation of composite hydrogel sheet patterned with an iron oxide nanoparticle stripe. The deformation of hinge region

brought unexposed side over to laser sight (c), increasing bending angle to 180° (d-f). Scale bar: 3mm.

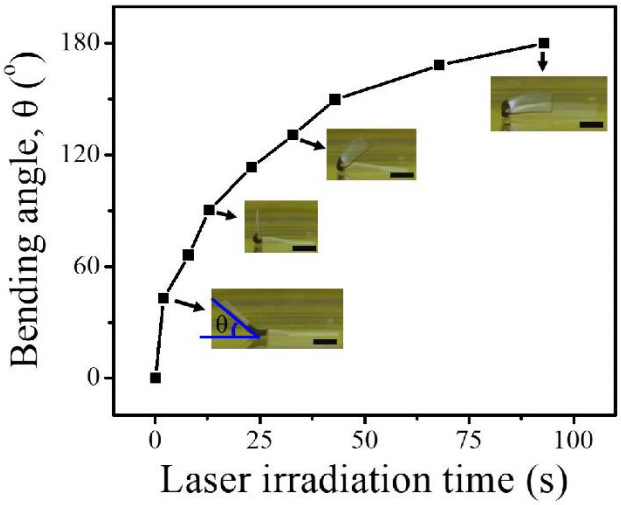

Figure 5.S5 Bending deformation of composite hydrogel sheet with an iron oxide nanoparticle stripe (black domain in the sheet) with respect to laser irradiation time. The bending angle (θ) gradually reached 180° with increase of laser irradiation time. Scale bar: 3mm.

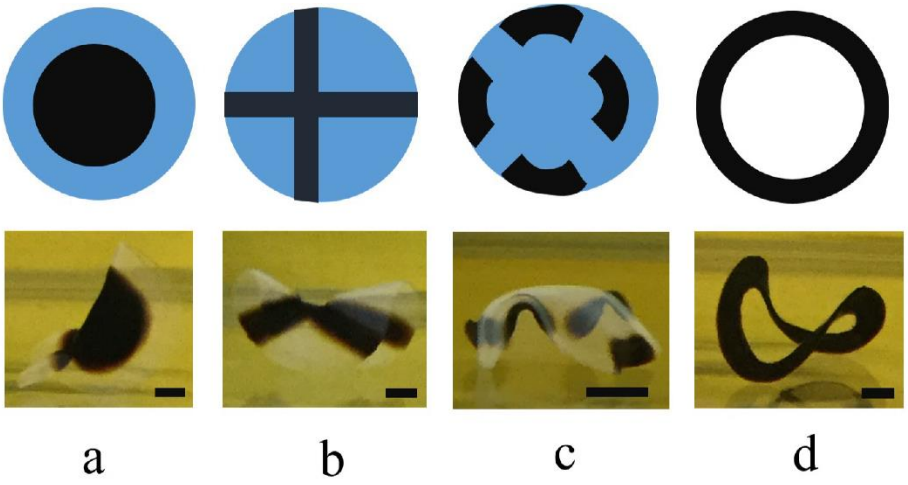

Figure 5.S6 Shape transformation of composite hydrogel sheet with varied Fe_3O_4 nanoparticle patterns (a-c) and varied geometry of sheet patterned with Fe_3O_4

nanoparticle (d). The Fe_3O_4 nanoparticle region was colored black in the hydrogel sheet. Scale bar: 2mm.

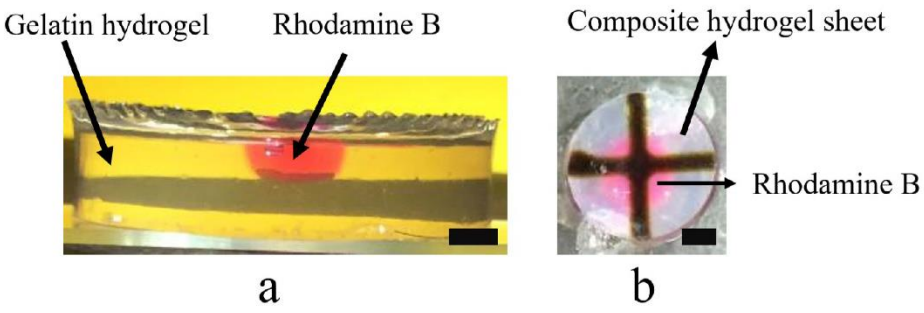

Figure 5.S7 Configuration of hydrogel device for laser-controlled chemical-release. a) Rhodamine B was loaded in the hollow cavity made in the gelatin hydrogel; b) the composite hydrogel sheet was partly glued onto gelatin hydrogel. The composite sheet covered the Rhodamine B-loaded region. Scale bar: 3mm.

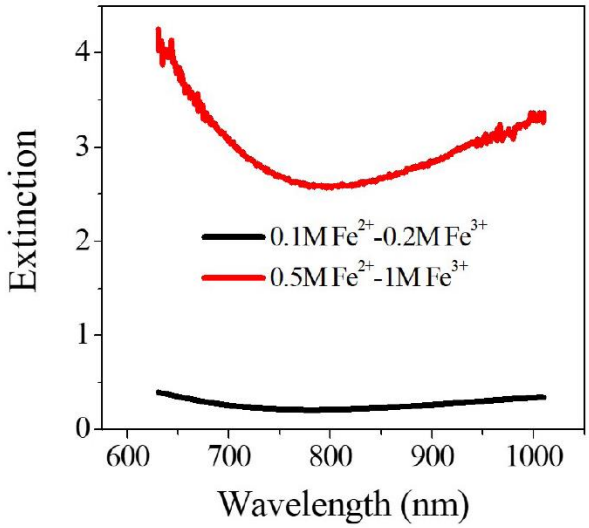

Figure 5.S8 UV-Vis measurement of composite hydrogel sheet with different ion concentrations used during stamping process.

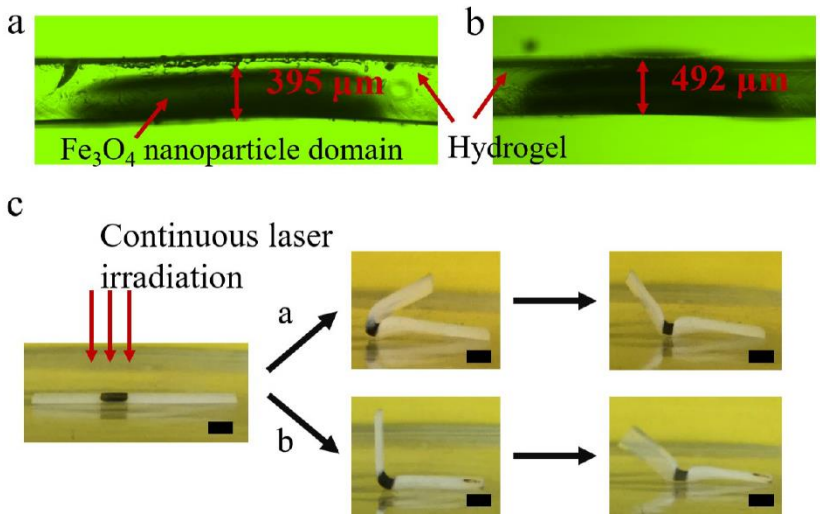

Figure 5.S9. Bending study of a thick hydrogel sheet patterned with an iron oxide nanoparticle stripe with varied penetration depth in thickness-direction of the sheet. Length, width and thickness of hydrogel sheet were 20mm, 4mm and 0.5mm, respectively. a, b) optical image of cross-section of patterned composite hydrogel sheet with varied penetration depth of Fe_3O_4 nanoparticle. The penetration depth of Fe_3O_4 nanoparticle was 395 µm in a) and 492 µm in b). c) Bending deformation of patterned hydrogel sheet with laser irradiation. The hydrogel sheet in a) bent over 90^o and then the bending angle reduced to less than 90^o, while the sheet in b) bent to 90^o as the maximum bending angle which decreased with laser irradiation. Scale bar: 2mm.

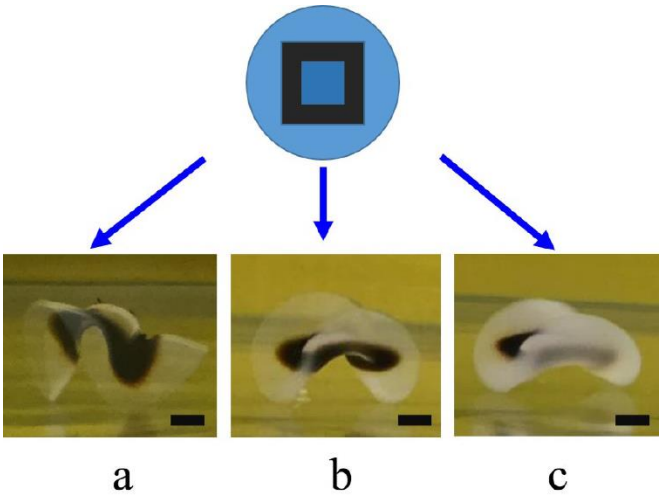

Figure 5.S10 Shape transformation of composite hydrogel sheet with varied thickness. Fe_3O_4 nanoparticle domain was colored black in the hydrogel. The diameter of the hydrogel disc was 13mm. Thickness of hydrogel was: a) 0.25mm; b) 0.5mm; c) 1mm. The composite hydrogel sheet was irradiated for 1min at 6.38W/cm^2. Scale bar: 2mm.

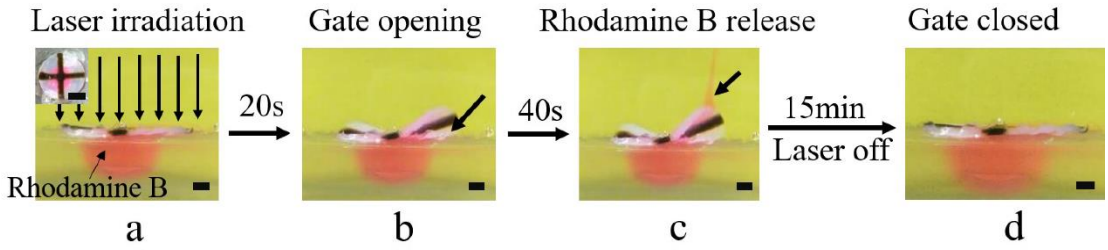

Figure 5.S11 Second-round of laser-controlled chemical release through opening and closing of "gate"-composite hydrogel sheet. Scale bar: 1.5mm. Inset image in a) was top view of the smart gate made of composite hydrogel sheet and the scale bar in it is 3mm.

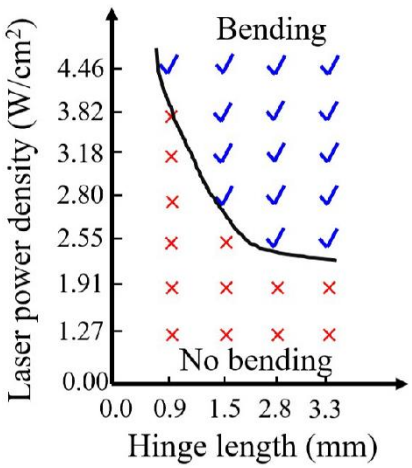

Figure 5.S12 Bending analysis of composite hydrogel sheet patterned with Fe_3O_4 nanoparticle strip as hinge in its bending under laser irradiation. Length, width and thickness of composite hydrogel sheet were 20mm, 2mm and 0.25mm, respectively. The width of Fe_3O_4 nanoparticle strip was 2mm, while its length varied.

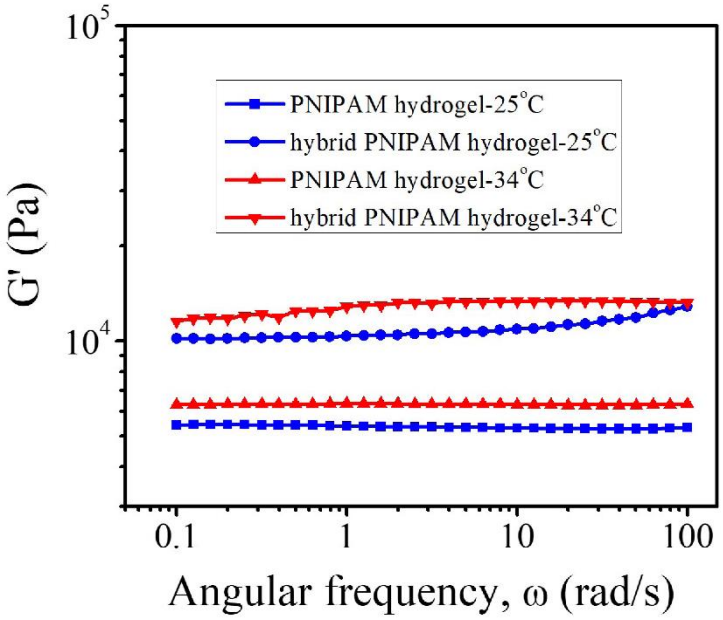

Figure 5.S13 Shear modulus of pure and hybrid PNIPAM hydrogel as a function of temperature.

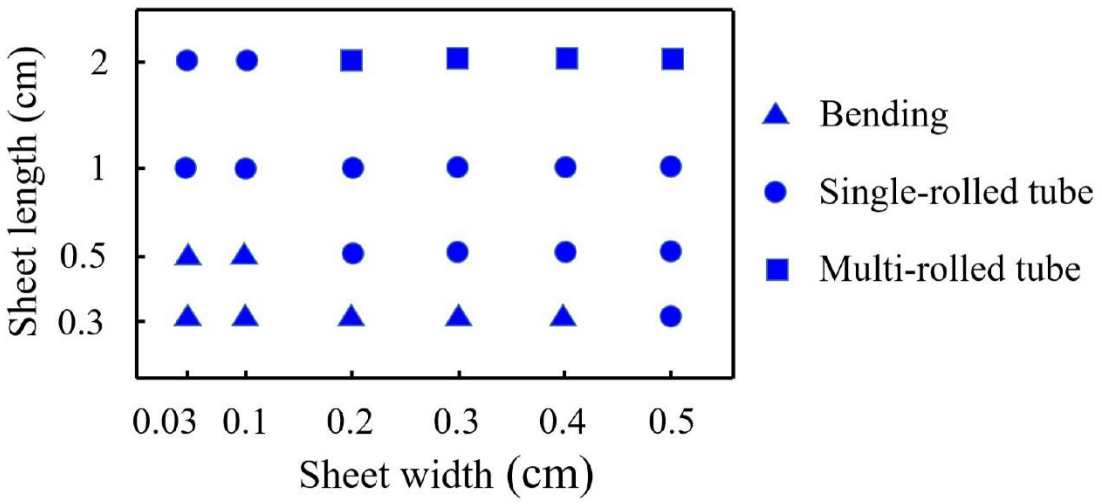

Figure 6.S1 Deformation diagram of composite hydrogel sheet with a smaller magnetic nanorod loading (2% wt). It could be seen that the product diagram was different from that with higher magnetic nanorod loading (Figure 6.2). For example, the parametric domain for producing multiply-rolled tube narrowed when decreasing the amount of magnetic nanorod in the hydrogel precursor.

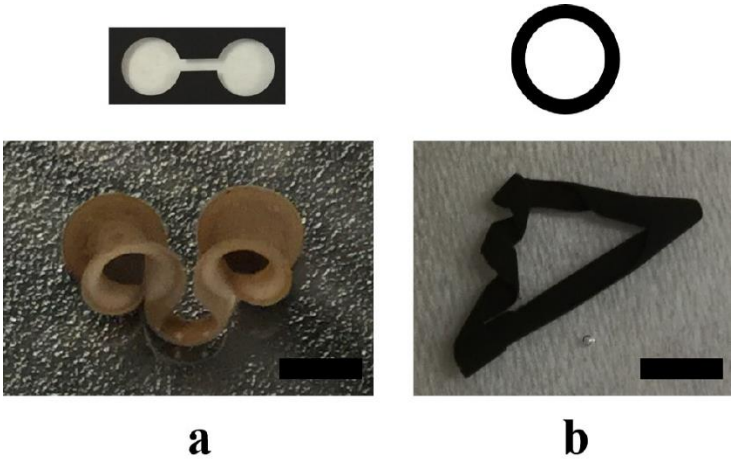

Figure 6.S2 Shape deformation of planar composite hydrogel sheet via altering its geometry by either photo-patterning (a) or manually cutting (b). Scale bar: 0.5 cm.

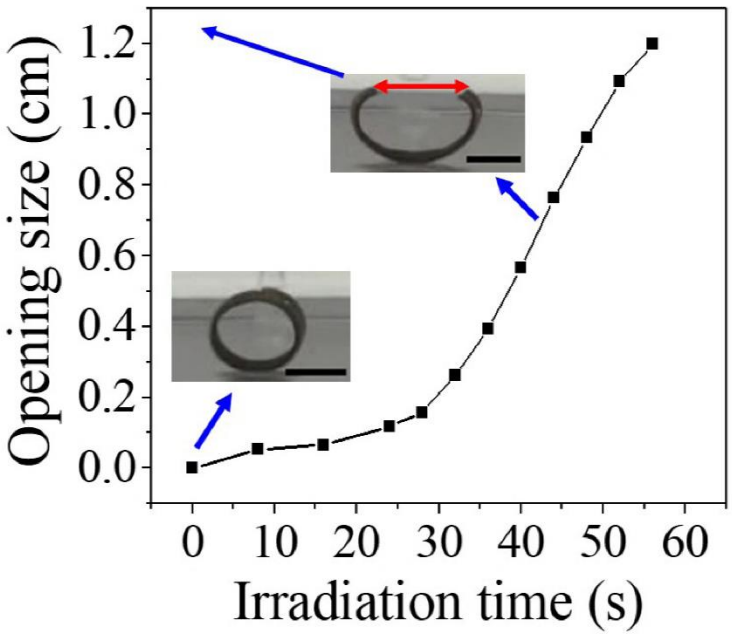

Figure 6.S3 Gradual opening of singly-rolled tube with irradiation time. Scale bar: 0.3cm

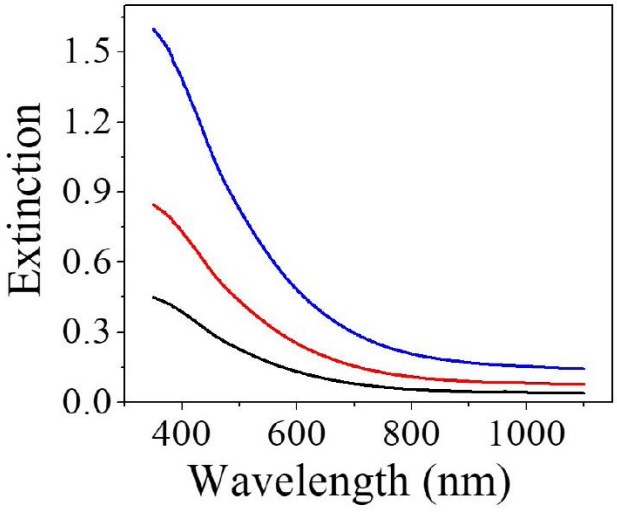

Figure 6.S4 UV-VIS spectrum of magnetic nanorod aqueous solution with different nanorod concentrations. Blue line: 1 mg/mL; red line: 0.5 mg/mL; black line: 0.1 mg/mL.

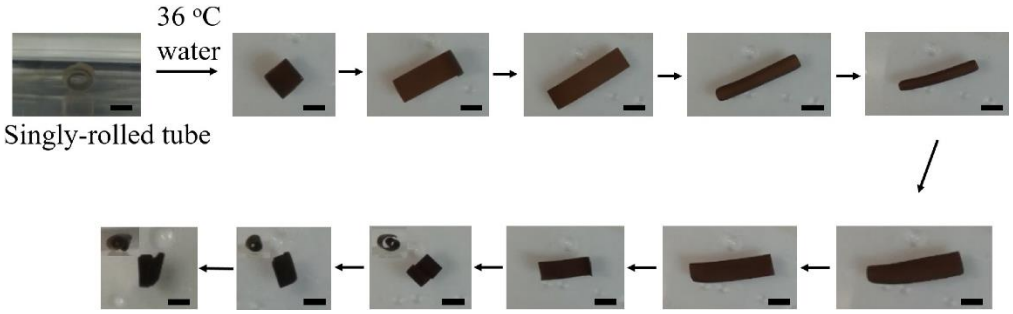

Figure 6.S5 Shape deformation of singly-rolled composite hydrogel tube under bulk heating. The thickness of composite hydrogel tube was 250 μm. Scale bar: 0.2cm.

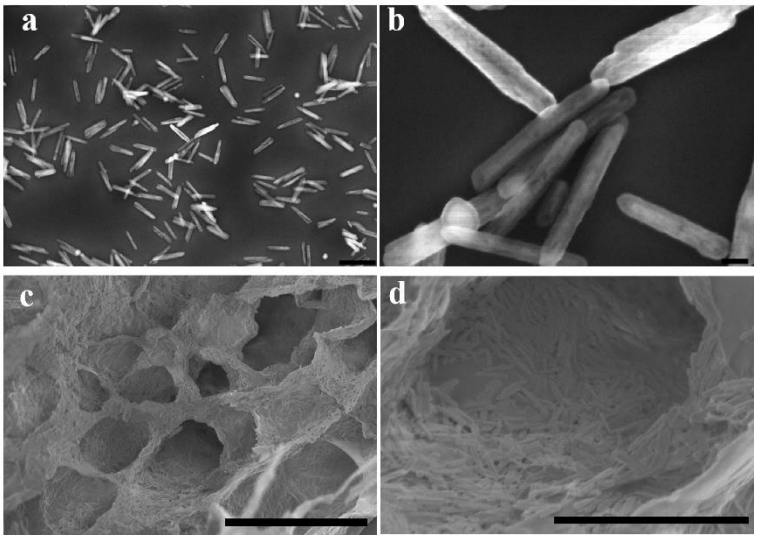

Figure 6.S6 Scanning electron microscopy of as-synthesized magnetic nanorod and nanorod-PNIPAM gel hybrid. The length of magnetic nanorod was about 800 nm and its diameter was around 70nm (a and b). The magnetic nanorod was successfully integrated in the PNIPAM hydrogel (c and d). Scale bar: 1 μm in a); 100nm in b); 10 μm in c); 3 μm in d).

Bibliography

[1] Gerbode, S. J.; Puzey, J. R.; McCormick, A. G.; Mahadevan, L. *Science* **2012,** *337*, 1087-1091.

[2] Forterre, Y.; Skotheim, J. M.; Dumais, J.; Mahadevan, L. *Nature* **2005,** *433*, 421-425.

[3] Harrington, M. J.; Razghandi, K.; Ditsch, F.; Guiducci, L.; Rueggeberg, M.; Dunlop, J. W. C.; Fratzl, P.; Neinhuis, C.; Burgert, I. *Nat. Commun.* **2011,** *2*, 337.

[4] Nath, U.; Crawford, B. C. W.; Carpenter, R.; Coen, E. *Science* **2003,** *299*, 1404-1407.

[5] Liang, H. Y.; Mahadevan, L. *Proc. Natl. Acad. Sci. U. S. A.* **2009,** *106*, 22049-22054.

[6] Burgert, I.; Fratzl, P. *Phil. Trans. R. Soc. A* **2009,** *367*, 1541-1557.

[7] Armon, S.; Efrati, E.; Kupferman, R.; Sharon, E. *Science* **2011,** *333*, 1726-1730.

[8] de Espinosa, L. M.; Meesorn, W.; Moatsou, D.; Weder, C. *Chem. Rev.* **2017,** *117*, 12851-12892.

[9] Liu, Y.; Genzer, J.; Dickey, M. D. *Prog. Polym. Sci.* **2016,** *52*, 79-106.

[10] Li, S. Y.; Wang, K. W. *Bioinspir. Biomim.* **2017,** *12*, 011001.

[11] Studart, A. R.; Erb, R. M. *Soft Matter* **2014,** *10*, 1284-1294.

[12] Shenoy, V. B.; Gracias, D. H. *MRS Bull.* **2012,** *37*, 847-854.

[13] Rogers, J.; Huang, Y. G.; Schmidt, O. G.; Gracias, D. H. *MRS Bull.* **2016,** *41*, 123-129.

[14] Xu, L. Z.; Shyu, T. C.; Kotov, N. A. *Acs Nano* **2017,** *11*, 7587-7599.

[15] Stoychev, G. V.; Ionov, L. *ACS Appl. Mater. Interfaces* **2016,** *8*, 24281-24294.

[16] van Manen, T.; Janbaz, S.; Zadpoor, A. A. *Mater. Today* **2018,** *21*, 144-163.

[17] Smela, E.; Inganas, O.; Lundstrom, I. *Science* **1995,** *268*, 1735-1738.

[18] Carpi, F.; Kornbluh, R.; Sommer-Larsen, P.; Alici, G. *Bioinspir. Biomim.* **2011,** *6*, 045006.

[19] Rogers, J. A. *Science* **2013,** *341*, 968-969.

[20] Hawkes, E.; An, B.; Benbernou, N. M.; Tanaka, H.; Kim, S.; Demaine, E. D.; Rus, D.; Wood, R. J. *Proc. Natl. Acad. Sci. U. S. A.* **2010,** *107*, 12441-12445.

[21] Randhawa, J. S.; Leong, T. G.; Bassik, N.; Benson, B. R.; Jochmans, M. T.; Gracias, D. H. *J. Am. Chem. Soc.* **2008,** *130*, 17238-17239.

[22] Bargardi, F. L.; Le Ferrand, H.; Libanori, R.; Studart, A. R. *Nat. Commun.* **2016,** *7*, 13912.

[23] Kobatake, S.; Takami, S.; Muto, H.; Ishikawa, T.; Irie, M. *Nature* **2007,** *446*, 778-781.

[24] Bushuyev, O. S.; Singleton, T. A.; Barrett, C. J. *Adv. Mater.* **2013,** *25*, 1796-1800.

[25] Zhang, Y. H.; Yan, Z.; Nan, K. W.; Xiao, D. Q.; Liu, Y. H.; Luan, H. W.; Fu, H. R.; Wang, X. Z.; Yang, Q. L.; Wang, J. C.; Ren, W.; Si, H. Z.; Liu, F.; Yang, L. H.; Li, H. J.; Wang, J. T.; Guo, X. L.; Luo, H. Y.; Wang, L.; Huang, Y. G.; Rogers, J. A. *Proc. Natl. Acad. Sci. U. S. A.* **2015,** *112*, 11757-11764.

[26] Xu, S.; Yan, Z.; Jang, K. I.; Huang, W.; Fu, H. R.; Kim, J.; Wei, Z.; Flavin, M.; McCracken, J.; Wang, R.; Badea, A.; Liu, Y.; Xiao, D. Q.; Zhou, G. Y.; Lee, J.;

Chung, H. U.; Cheng, H. Y.; Ren, W.; Banks, A.; Li, X. L.; Paik, U.; Nuzzo, R. G.; Huang, Y. G.; Zhang, Y. H.; Rogers, J. A. *Science* **2015,** *347*, 154-159.
[27] Han, D. D.; Zhang, Y. L.; Liu, Y.; Liu, Y. Q.; Jiang, H. B.; Han, B.; Fu, X. Y.; Ding, H.; Xu, H. L.; Sun, H. B. *Adv. Funct. Mater.* **2015,** *25*, 4548-4557.
[28] Mu, J. K.; Hou, C. Y.; Wang, H. Z.; Li, Y. G.; Zhang, Q. H.; Zhu, M. F. *Sci. Adv.* **2015,** *1*, e1500533.
[29] Xu, W. A.; Qin, Z.; Chen, C. T.; Kwag, H. R.; Ma, Q. L.; Sarkar, A.; Buehler, M. J.; Gracias, D. H. *Sci. Adv.* **2017,** *3*, e1701084.
[30] Cheng, H. H.; Zhao, F.; Xue, J. L.; Shi, G. Q.; Jiang, L.; Qu, L. T. *Acs Nano* **2016,** *10*, 9529-9535.
[31] Felton, S.; Tolley, M.; Demaine, E.; Rus, D.; Wood, R. *Science* **2014,** *345*, 644-646.
[32] Ge, Q.; Dunn, C. K.; Qi, H. J.; Dunn, M. L. *Smart Mater. Struct.* **2014,** *23*, 094007.
[33] Pilate, F.; Toncheva, A.; Dubois, P.; Raquez, J. M. *Eur. Polym. J.* **2016,** *80*, 268-294.
[34] Ube, T.; Ikeda, T. *Angew. Chem. Int. Ed.* **2014,** *53*, 10290-10299.
[35] de Haan, L. T.; Verjans, J. M. N.; Broer, D. J.; Bastiaansen, C. W. M.; Schenning, A. *J. Am. Chem. Soc.* **2014,** *136*, 10585-10588.
[36] Ware, T. H.; McConney, M. E.; Wie, J. J.; Tondiglia, V. P.; White, T. J. *Science* **2015,** *347*, 982-984.
[37] Guin, T.; Settle, M. J.; Kowalski, B. A.; Auguste, A. D.; Beblo, R. V.; Reich, G. W.; White, T. J. *Nat. Commun.* **2018,** *9*, 2531.
[38] Khan, M. K.; Hamad, W. Y.; MacLachlan, M. J. *Adv. Mater.* **2014,** *26*, 2323-2328.
[39] Li, B.; Du, T.; Yu, B.; van der Gucht, J.; Zhou, F. *Small* **2015,** *11*, 3494-3501.
[40] Zhang, L. D.; Chizhik, S.; Wen, Y. Z.; Naumov, P. *Adv. Funct. Mater.* **2016,** *26*, 1040-1053.
[41] Lee, M. R.; Phang, I. Y.; Cui, Y.; Lee, Y. H.; Ling, X. Y. *Small* **2015,** *11*, 740-748.
[42] Yao, C.; Liu, Z.; Yang, C.; Wang, W.; Ju, X. J.; Xie, R.; Chu, L. Y. *ACS Appl. Mater. Interfaces* **2016,** *8*, 21721-21730.
[43] Ma, C. X.; Le, X. X.; Tang, X. L.; He, J.; Xiao, P.; Zheng, J.; Xiao, H.; Lu, W.; Zhang, J. W.; Huang, Y. J.; Chen, T. *Adv. Funct. Mater.* **2016,** *26*, 8670-8676.
[44] Zhao, Q.; Yang, X. X.; Ma, C. X.; Chen, D.; Bai, H.; Li, T. F.; Yang, W.; Xie, T. *Mater. Horiz.* **2016,** *3*, 422-428.
[45] Lowenberg, C.; Balk, M.; Wischke, C.; Behl, M.; Lendlein, A. *Acc. Chem. Res.* **2017,** *50*, 723-732.
[46] Chen, J. W.; Leung, F. K. C.; Stuart, M. C. A.; Kajitani, T.; Fukushima, T.; van der Giessen, E.; Feringa, B. *Nat. Chem.* **2018,** *10*, 132-138.
[47] Adhikari, B.; Yamada, Y.; Yamauchi, M.; Wakita, K.; Lin, X.; Aratsu, K.; Ohba, T.; Karatsu, T.; Hollamby, M. J.; Shimizu, N.; Takagi, H.; Haruki, R.; Adachi, S.; Yagai, S. *Nat. Commun.* **2017,** *8*, 15254.
[48] Evans, J. S.; Sun, Y. R.; Senyuk, B.; Keller, P.; Pergamenshchik, V. M.; Lee, T.; Smalyukh, II *Phys. Rev. Lett.* **2013,** *110*, 187802.

[49] Keber, F. C.; Loiseau, E.; Sanchez, T.; DeCamp, S. J.; Giomi, L.; Bowick, M. J.; Marchetti, M. C.; Dogic, Z.; Bausch, A. R. *Science* **2014,** *345*, 1135-1139.
[50] Schlicke, H.; Battista, D.; Kunze, S.; Schroter, C. J.; Eich, M.; Vossmeyer, T. *ACS Appl. Mater. Interfaces* **2015,** *7*, 15123-15128.
[51] Shim, T. S.; Estephan, Z. G.; Qian, Z. X.; Prosser, J. H.; Lee, S. Y.; Chenoweth, D. M.; Lee, D.; Park, S. J.; Crocker, J. C. *Nat. Nanotechnol.* **2017,** *12*, 41-47.
[52] Si, K. J.; Sikdar, D.; Chen, Y.; Eftekhari, F.; Xu, Z. Q.; Tang, Y.; Xiong, W.; Guo, P. Z.; Zhang, S.; Lu, Y. R.; Bao, Q. L.; Zhu, W. R.; Premaratne, M.; Cheng, W. L. *Acs Nano* **2014,** *8*, 11086-11093.
[53] Ionov, L. *Adv. Funct. Mater.* **2013,** *23*, 4555-4570.
[54] Ionov, L. *Mater. Today* **2014,** *17*, 494-503.
[55] Kempaiah, R.; Nie, Z. H. *J. Mater. Chem. B* **2014,** *2*, 2357-2368.
[56] Jeon, S. J.; Hauser, A. W.; Hayward, R. C. *Acc. Chem. Res.* **2017,** *50*, 161-169.
[57] Keplinger, C.; Sun, J. Y.; Foo, C. C.; Rothemund, P.; Whitesides, G. M.; Suo, Z. G. *Science* **2013,** *341*, 984-987.
[58] Malachowski, K.; Jamal, M.; Jin, Q. R.; Polat, B.; Morris, C. J.; Gracias, D. H. *Nano Lett.* **2014,** *14*, 4164-4170.
[59] Lendlein, A.; Langer, R. *Science* **2002,** *296*, 1673-1676.
[60] Kopecek, J. *Biomaterials* **2007,** *28*, 5185-5192.
[61] Zhang, Y. S.; Khademhosseini, A. *Science* **2017,** *356*, 500-+.
[62] Malachowski, K.; Breger, J.; Kwag, H. R.; Wang, M. O.; Fisher, J. P.; Selaru, F. M.; Gracias, D. H. *Angew. Chem. Int. Ed.* **2014,** *53*, 8045-8049.
[63] Wei, Z. J.; Jia, Z.; Athas, J. M.; Wang, C. Y.; Raghavan, S. R.; Li, T.; Nie, Z. H. *Soft Matter* **2014,** *10*, 8157-8162.
[64] Jiang, S. H.; Liu, F. Y.; Lerch, A.; Ionov, L.; Agarwal, S. *Adv. Mater.* **2015,** *27*, 4865-4870.
[65] Ma, C.; Li, T.; Zhao, Q.; Yang, X.; Wu, J.; Luo, Y.; Xie, T. *Adv. Mater.* **2014,** *26*, 5665-5669.
[66] Wu, Z. L.; Moshe, M.; Greener, J.; Therien-Aubin, H.; Nie, Z. H.; Sharon, E.; Kumacheva, E. *Nat. Commun.* **2013,** *4*, 1586.
[67] Athas, J. C.; Nguyen, C. P.; Zarkett, B. C.; Gargava, A.; Nie, Z. H.; Raghavan, S. R. *ACS Appl. Mater. Interfaces* **2016,** *8*, 19066-19074.
[68] Cangialosi, A.; Yoon, C.; Liu, J.; Huang, Q.; Guo, J. K.; Nguyen, T. D.; Gracias, D. H.; Schulman, R. *Science* **2017,** *357*, 1126-1129.
[69] Palleau, E.; Morales, D.; Dickey, M. D.; Velev, O. D. *Nat. Commun.* **2013,** *4*, 2257.
[70] Arazoe, H.; Miyajima, D.; Akaike, K.; Araoka, F.; Sato, E.; Hikima, T.; Kawamoto, M.; Aida, T. *Nat. Mater.* **2016,** *15*, 1084-1089.
[71] Ma, M. M.; Guo, L.; Anderson, D. G.; Langer, R. *Science* **2013,** *339*, 186-189.
[72] Luo, R.; Wu, J.; Dinh, N.-D.; Chen, C.-H. *Adv. Funct. Mater.* **2015,** *25*, 7272-7279.
[73] Wang, E.; Desai, M. S.; Lee, S. W. *Nano Lett.* **2013,** *13*, 2826-2830.
[74] Han, D.; Farino, C.; Yang, C.; Scott, T.; Browe, D.; Choi, W.; Freeman, J. W.; Lee, H. *ACS Appl. Mater. Interfaces* **2018,** *10*, 17512-17518.

[75] Morales, D.; Palleau, E.; Dickey, M. D.; Velev, O. D. *Soft Matter* **2014,** *10*, 1337-1348.
[76] Hu, Z. B.; Zhang, X. M.; Li, Y. *Science* **1995,** *269*, 525-527.
[77] Zhao, L.; Huang, J. H.; Zhang, Y. C.; Wang, T.; Sun, W. X.; Tong, Z. *ACS Appl. Mater. Interfaces* **2017,** *9*, 11866-11873.
[78] Stoychev, G.; Zakharchenko, S.; Turcaud, S.; Dunlop, J. W. C.; Ionov, L. *Acs Nano* **2012,** *6*, 3925-3934.
[79] Stoychev, G.; Puretskiy, N.; Ionov, L. *Soft Matter* **2011,** *7*, 3277-3279.
[80] Breger, J. C.; Yoon, C.; Xiao, R.; Kwag, H. R.; Wang, M. O.; Fisher, J. P.; Nguyen, T. D.; Gracias, D. H. *ACS Appl. Mater. Interfaces* **2015,** *7*, 3398-3405.
[81] Hu, Y. W.; Kahn, J. S.; Guo, W. W.; Huang, F. J.; Fadeev, M.; Harries, D.; Willner, I. *J. Am. Chem. Soc.* **2016,** *138*, 16112-16119.
[82] Wang, L.; Jian, Y. K.; Le, X. X.; Lu, W.; Ma, C. X.; Zhang, J. W.; Huang, Y. J.; Huang, C. F.; Chen, T. *Chem. Comm.* **2018,** *54*, 1229-1232.
[83] Duan, J. J.; Liang, X. C.; Zhu, K. K.; Guo, J. H.; Zhang, L. N. *Soft Matter* **2017,** *13*, 345-354.
[84] Athas, J. C.; Nguyen, C. P.; Kummar, S.; Raghavan, S. R. *Soft Matter* **2018,** *14*, 2735-2743.
[85] Na, J. H.; Evans, A. A.; Bae, J.; Chiappelli, M. C.; Santangelo, C. D.; Lang, R. J.; Hull, T. C.; Hayward, R. C. *Adv. Mater.* **2015,** *27*, 79-85.
[86] Erb, R. M.; Sander, J. S.; Grisch, R.; Studart, A. R. *Nat. Commun.* **2013,** *4*, 1712.
[87] Gladman, A. S.; Matsumoto, E. A.; Nuzzo, R. G.; Mahadevan, L.; Lewis, J. A. *Nat. Mater.* **2016,** *15*, 413-418.
[88] Lee, B. P.; Konst, S. *Advanced Materials* **2014,** *26*, 3415-3419.
[89] Shang, J.; Shao, Z. Z.; Chen, X. *Biomacromolecules* **2008,** *9*, 1208-1213.
[90] Yang, C.; Wang, W.; Yao, C.; Xie, R.; Ju, X. J.; Liu, Z.; Chu, L. Y. *Sci. Rep.* **2015,** *5*, 13622
[91] Takashima, Y.; Hatanaka, S.; Otsubo, M.; Nakahata, M.; Kakuta, T.; Hashidzume, A.; Yamaguchi, H.; Harada, A. *Nat. Commun.* **2012,** *3*, 1270.
[92] Lv, C.; Xia, H.; Shi, Q.; Wang, G.; Wang, Y. S.; Chen, Q. D.; Zhang, Y. L.; Liu, L. Q.; Sun, H. B. *Adv. Mater. Interfaces.* **2017,** *4*, 1601002.
[93] Zhang, L. D.; Liang, H. R.; Jacob, J.; Naumov, P. *Nat. Commun.* **2015,** *6*, 7429.
[94] Klein, Y.; Efrati, E.; Sharon, E. *Science* **2007,** *315*, 1116-1120.
[95] Kim, J.; Hanna, J. A.; Byun, M.; Santangelo, C. D.; Hayward, R. C. *Science* **2012,** *335*, 1201-1205.
[96] Therien-Aubin, H.; Wu, Z. L.; Nie, Z. H.; Kumacheva, E. *J. Am. Chem. Soc.* **2013,** *135*, 4834-4839.
[97] Han, D. D.; Zhang, Y. L.; Ma, J. N.; Liu, Y. Q.; Han, B.; Sun, H. B. *Adv. Mater.* **2016,** *28*, 8328-8343.
[98] Jiang, H. Y.; Kelch, S.; Lendlein, A. *Adv. Mater.* **2006,** *18*, 1471-1475.
[99] Wie, J. J.; Shankar, M. R.; White, T. J. *Nat. Commun.* **2016,** *7*, 13260.
[100] Jiang, W. T.; Niu, D.; Liu, H. Z.; Wang, C. H.; Zhao, T. T.; Yin, L.; Shi, Y. S.; Chen, B. D.; Ding, Y. C.; Lu, B. H. *Adv. Funct. Mater.* **2014,** *24*, 7598-7604.

[101] Yang, Y.; Pei, Z. Q.; Li, Z.; Wei, Y.; Ji, Y. *J. Am. Chem. Soc.* **2016,** *138*, 2118-2121.
[102] Zhang, L. D.; Naumov, P. *Angew. Chem. Int. Ed.* **2015,** *54*, 8642-8647.
[103] Lendlein, A.; Jiang, H. Y.; Junger, O.; Langer, R. *Nature* **2005,** *434*, 879-882.
[104] Xie, H.; He, M. J.; Deng, X. Y.; Du, L.; Fan, C. J.; Yang, K. K.; Wang, Y. Z. *ACS Appl. Mater. Interfaces* **2016,** *8*, 9431-9439.
[105] Ikegami, T.; Kageyama, Y.; Obara, K.; Takeda, S. *Angew. Chem. Int. Ed.* **2016,** *55*, 8239-8243.
[106] Gelebart, A. H.; Mc Bride, M.; Schenning, A.; Bowman, C. N.; Broer, D. J. *Adv. Funct. Mater.* **2016,** *26*, 5322-5327.
[107] Iamsaard, S.; Anger, E.; Asshoff, S. J.; Depauw, A.; Fletcher, S. P.; Katsonis, N. *Angew. Chem. Int. Ed.* **2016,** *55*, 9908-9912.
[108] Li, C.; Yun, J. H.; Kim, H.; Cho, M. *Macromolecules* **2016,** *49*, 6012-6020.
[109] Wu, W.; Yao, L. M.; Yang, T. S.; Yin, R. Y.; Li, F. Y.; Yu, Y. L. *J. Am. Chem. Soc.* **2011,** *133*, 15810-15813.
[110] Zhou, Y.; Hauser, A. W.; Bende, N. P.; Kuzyk, M. G.; Hayward, R. C. *Adv. Funct. Mater.* **2016,** *26*, 5447-5452.
[111] Zhang, J. Y.; Du, P.; Xu, D. Y.; Li, Y.; Peng, W. C.; Zhang, G. L.; Zhang, F. B.; Fan, X. B. *Ind. Eng. Chem. Res.* **2016,** *55*, 4526-4531.
[112] Kim, D.; Lee, H. S.; Yoon, J. *Sci. Rep.* **2016,** *6*, 20921.
[113] Kuksenok, O.; Balazs, A. C. *Adv. Funct. Mater.* **2013,** *23*, 4601-4610.
[114] Kuksenok, O.; Balazs, A. C. *Mater. Horiz.* **2016,** *3*, 53-62.
[115] Francis, W.; Dunne, A.; Delaney, C.; Florea, L.; Diamond, D. *Sens. Actuators B Chem.* **2017,** *250*, 608-616.
[116] Zong, L.; Li, X. K.; Han, X. S.; Lv, L. L.; Li, M. J.; You, J.; Wu, X. C.; Li, C. X. *ACS Appl. Mater. Interfaces* **2017,** *9*, 32280-32289.
[117] Iamsaard, S.; Asshoff, S. J.; Matt, B.; Kudernac, T.; Cornelissen, J.; Fletcher, S. P.; Katsonis, N. *Nat. Chem.* **2014,** *6*, 229-235.
[118] Huang, H. W.; Sakar, M. S.; Petruska, A. J.; Pane, S.; Nelson, B. J. *Nat. Commun.* **2016,** *7*, 12263.
[119] Zhu, Z. C.; Senses, E.; Akcora, P.; Sukhishvili, S. A. *Acs Nano* **2012,** *6*, 3152-3162.
[120] Shim, T. S.; Kim, S. H.; Heo, C. J.; Jeon, H. C.; Yang, S. M. *Angew. Chem. Int. Ed.* **2012,** *51*, 1420-1423.
[121] Kapyla, E.; Delgado, S. M.; Kasko, A. M. *ACS Appl. Mater. Interfaces* **2016,** *8*, 17885-17893.
[122] Kim, Y. S.; Liu, M. J.; Ishida, Y.; Ebina, Y.; Osada, M.; Sasaki, T.; Hikima, T.; Takata, M.; Aida, T. *Nat. Mater.* **2015,** *14*, 1002-1007.
[123] Maeda, S.; Hara, Y.; Sakai, T.; Yoshida, R.; Hashimoto, S. *Adv. Mater.* **2007,** *19*, 3480-3484.
[124] Kwon, G. H.; Park, J. Y.; Kim, J. Y.; Frisk, M. L.; Beebe, D. J.; Lee, S. H. *Small* **2008,** *4*, 2148-2153.
[125] Wehner, M.; Truby, R. L.; Fitzgerald, D. J.; Mosadegh, B.; Whitesides, G. M.; Lewis, J. A.; Wood, R. J. *Nature* **2016,** *536*, 451-455.
[126] Eddington, D. T.; Beebe, D. J. *Adv. Drug Deliv. Rev.* **2004,** *56*, 199-210.

[127] Yu, Q.; Bauer, J. M.; Moore, J. S.; Beebe, D. J. *Appl. Phys. Lett.* **2001,** *78*, 2589-2591.
[128] Jamal, M.; Zarafshar, A. M.; Gracias, D. H. *Nat. Commun.* **2011,** *2*, 527.
[129] Gracias, D. H. *Curr. Opin. Chem. Eng.* **2013,** *2*, 112-119.
[130] Hu, Y.; Wu, G.; Lan, T.; Zhao, J. J.; Liu, Y.; Chen, W. *Adv. Mater.* **2015,** *27*, 7867-7873.
[131] Deng, J.; Li, J. F.; Chen, P. N.; Fang, X.; Sun, X. M.; Jiang, Y. S.; Weng, W.; Wang, B. J.; Peng, H. S. *J. Am. Chem. Soc.* **2016,** *138*, 225-230.
[132] Hauser, A. W.; Liu, D. Q.; Bryson, K. C.; Hayward, R. C.; Broer, D. J. *Macromolecules* **2016,** *49*, 1575-1581.
[133] Tai, Y. L.; Lubineau, G.; Yang, Z. G. *Adv. Mater.* **2016,** *28*, 4665-4670.
[134] Norman, M. D.; Finn, J.; Tregenza, T. *Proc. R. Soc. B* **2001,** *268*, 1755-1758.
[135] Hauser, A. W.; Evans, A. A.; Na, J. H.; Hayward, R. C. *Angew. Chem. Int. Ed.* **2015,** *54*, 5434-5437.
[136] Zhang, X. Z.; Yang, Y. Y.; Chung, T. S.; Ma, K. X. *Langmuir* **2001,** *17*, 6094-6099.
[137] Cai, S.; Suo, Z. *Journal of the Mechanics and Physics of Solids* **2011,** *59*, 2259-2278.
[138] Huggins, M. L. *J.Chem.Phys.* **1941,** *9*, 440.
[139] Hong, W.; Liu, Z.; Suo, Z. *International Journal of Solids and Structures* **2009,** *46*, 3282-3289.
[140] Ding, Z.; Liu, Z.; Hu, J.; Swaddiwudhipong, S.; Yang, Z. *International Journal of Solids and Structures* **2013,** *50*, 2610-2619.
[141] Binkert, T.; Oberreich, J.; Meewes, M.; Nyffenegger, R.; Ricka, J. *Macromolecules* **1991,** *24*, 5806-5810.
[142] Shibayama, M.; Tanaka, T.; Han, C. C. *J. Chem. Phys.* **1992,** *97*, 6829-6841.
[143] Afroze, F.; Nies, E.; Berghmans, H. *J. Mol. Struct.* **2000,** *554*, 55-68.
[144] Yuan, B.; Jin, Y.; Sun, Y.; Wang, D.; Sun, J. S.; Wang, Z.; Zhang, W.; Jiang, X. Y. *Adv. Mater.* **2012,** *24*, 890-896.
[145] Morales, D.; Bharti, B.; Dickey, M. D.; Velev, O. D. *Small* **2016,** *12*, 2283-2290.
[146] Santhanam, V.; Andres, R. P. *Nano Lett.* **2004,** *4*, 41-44.
[147] Shukla, S.; Vidal, X.; Furlani, E. P.; Swihart, M. T.; Kim, K. T.; Yoon, Y. K.; Urbas, A.; Prasad, P. N. *Acs Nano* **2011,** *5*, 1947-1957.
[148] Rodrigues, T. S.; da Silva, A. G. M.; Goncalves, M. C.; Fajardo, H. V.; Balzer, R.; Probst, L. F. D.; da Silva, A. H. M.; Assaf, J. M.; Camargo, P. H. C. *Langmuir* **2016,** *32*, 9371-9379.
[149] Chen, Q.; Zhu, L.; Zhao, C.; Wang, Q. M.; Zheng, J. *Adv. Mater.* **2013,** *25*, 4171-4176.
[150] Au, L.; Lu, X. M.; Xia, Y. N. *Adv. Mater.* **2008,** *20*, 2517-2522.
[151] Sun, Y. G.; Xia, Y. N. *Science* **2002,** *298*, 2176-2179.
[152] Metraux, G. S.; Mirkin, C. A. *Adv. Mater.* **2005,** *17*, 412-415.
[153] Gelebart, A. H.; Mulder, D. J.; Vantomme, G.; Schenning, A.; Broer, D. J. *Angew. Chem. Int. Ed.* **2017,** *56*, 13436-13439.
[154] He, J.; Wei, Z. J.; Wang, L.; Tomova, Z.; Babu, T.; Wang, C. Y.; Han, X. J.; Fourkas, J. T.; Nie, Z. H. *Angew. Chem. Int. Ed.* **2013,** *52*, 2463-2468.

[155] Niidome, T.; Yamagata, M.; Okamoto, Y.; Akiyama, Y.; Takahashi, H.; Kawano, T.; Katayama, Y.; Niidome, Y. *J. Control. Release* **2006,** *114*, 343-347.
[156] Sun, S. S.; Gao, M. X.; Lei, G.; Zou, H. Y.; Ma, J.; Huang, C. Z. *Nano Res.* **2016,** *9*, 1125-1134.
[157] Grzelczak, M.; Perez-Juste, J.; Mulvaney, P.; Liz-Marzan, L. M. *Chem. Soc. Rev.* **2008,** *37*, 1783-1791.
[158] Ahn, T.; Kim, J. H.; Yang, H. M.; Lee, J. W.; Kim, J. D. *J. Phys. Chem. C* **2012,** *116*, 6069-6076.
[159] Zhou, J.; Sheiko, S. S. *J. Polym. Sci. Poly. Phys.* **2016,** *54*, 1365-1380.
[160] Zhao, Q.; Qi, H. J.; Xie, T. *Prog. Polym. Sci.* **2015,** *49-50*, 79-120.
[161] White, T. J.; Broer, D. J. *Nat. Mater.* **2015,** *14*, 1087-1098.
[162] Ge, F. J.; Lu, X. L.; Xiang, J.; Tong, X.; Zhao, Y. *Angew. Chem. Int. Ed.* **2017,** *56*, 6126-6130.
[163] Liu, Y.; Shaw, B.; Dickey, M. D.; Genzer, J. *Sci. Adv.* **2017,** *3*, e1602417.
[164] Guo, H. Y.; Cheng, J.; Wang, J. Y.; Huang, P.; Liu, Y. J.; Jia, Z.; Chen, X. Y.; Sui, K. Y.; Li, T.; Nie, Z. H. *J. Mater. Chem. B* **2017,** *5*, 2883-2887.
[165] Gelebart, A. H.; Jan Mulder, D.; Varga, M.; Konya, A.; Vantomme, G.; Meijer, E. W.; Selinger, R. L. B.; Broer, D. J. *Nature* **2017,** *546*, 632-636.
[166] Freund, L. B.; Floro, J. A.; Chason, E. *Appl. Phys. Lett.* **1999,** *74*, 1987-1989.
[167] Timoshenko, S. *J. Opt. Soc. Am.* **1925,** *11*, 233-255.
[168] Li, Z.; Zhang, X. Y.; Wang, S. Q.; Yang, Y.; Qin, B. Y.; Wang, K.; Xie, T.; Wei, Y.; Ji, Y. *Chem. Sci.* **2016,** *7*, 4741-4747.
[169] Zhao, Z.; Wu, J. T.; Mu, X. M.; Chen, H. S.; Qi, H. J.; Fang, D. N. *Sci. Adv.* **2017,** *3*, e1602326.